

1  
2  
3  
4  
5  
6  
7

# a Coriolis tutorial, Part 4:

## wind-driven circulation and the Sverdrup relation

James F. Price

Woods Hole Oceanographic Institution,  
Woods Hole, Massachusetts, 02543

<https://www2.whoi.edu/staff/jprice/>    [jprice@whoi.edu](mailto:jprice@whoi.edu)

Version 5.6

May 23, 2019

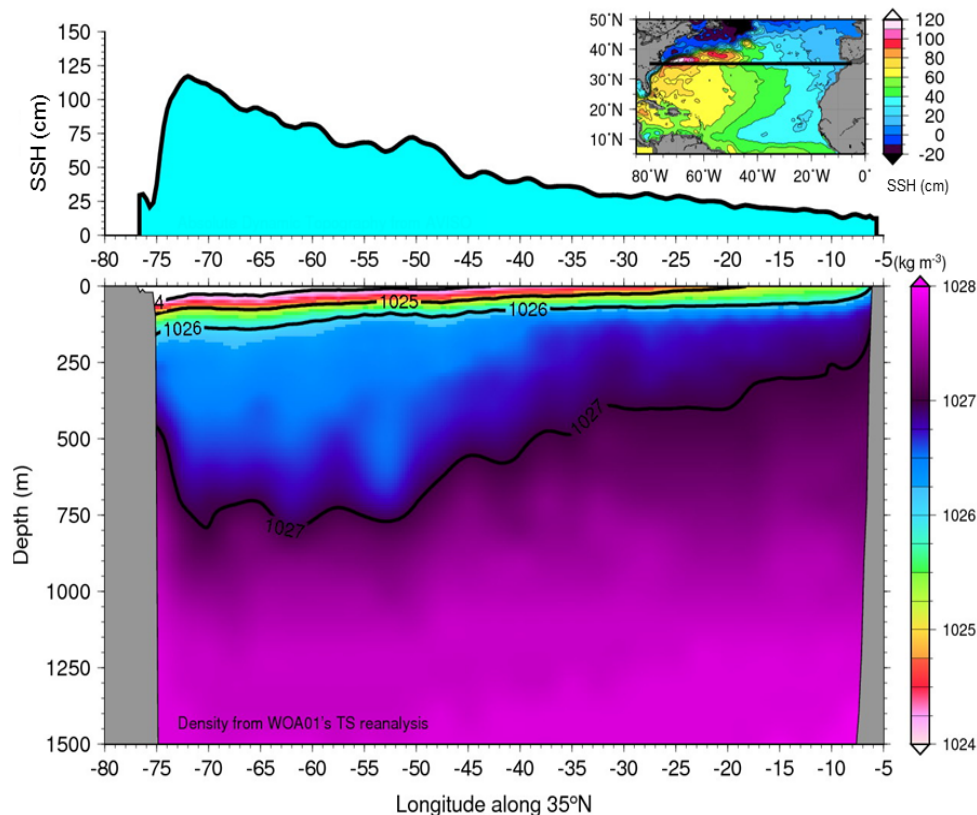


Figure 1: A zonal section through the North Atlantic thermocline at 35°N, viewed toward the north. **(upper)** Sea surface height (SSH) from satellite altimetry. **(lower)** Potential density from in situ observations. This section shows the remarkable zonal asymmetry that is characteristic of the major ocean gyres. Within a narrow western boundary region, the SSH slope is positive and comparatively very large. The inferred geostrophic current, the Gulf Stream, is northward and fast. Over the rest of the basin, the SSH slope is negative and much smaller, and the inferred geostrophic flow is southward and very slow. This broadly distributed southerly flow is wind-driven Sverdrup flow, mainly, and is the central topic of this essay.

8 **Abstract:** This essay is the fourth of a four part introduction to the effects of Earth's rotation on the  
9 fluid dynamics of the atmosphere and ocean. The theme is wind-driven ocean circulation, and the central  
10 topic is the Sverdrup relation between meridional transport and the curl of the wind stress. The goal is to  
11 develop some insight for several features of the observed ocean circulation, *viz.* western intensification of  
12 upper ocean gyres and the geography of seasonal variability. To that end, a shallow water model is solved  
13 for the circulation of a model ocean that is started from rest by a specified wind stress field that includes  
14 westerlies at mid-latitudes and easterlies in the lower subtropics. This gives three regions of stress curl,  
15 negative over the subtropical gyre and positive over subpolar and tropical gyres.

16 The developing circulation can be described in terms of four stages. Stage 1 is the direct, local  
17 response to the imposed wind stress and includes inertia-gravity oscillations and boundary waves. These  
18 die out over several weeks and leave a steady Ekman transport that persists for the rest of the experiment.  
19 The Ekman transport varies spatially on account of the latitudinal variation of the wind stress and of the  
20 Coriolis parameter,  $f$ . The resulting divergence of Ekman transport modifies the layer thickness  
21 (stratification) and thus the circulation: over the subtropics, where wind stress curl is negative, the  
22 convergence of Ekman transport leads to an initially steady increase in layer thickness (Stage 2) and thus  
23 a steady increase of sea surface height and hydrostatic pressure. The zonal geostrophic currents that  
24 develop along with the pressure are proportional to  $1/f^2$  and thus comparatively large at lower latitudes.  
25 These zonal currents are blocked by the basin's meridional boundaries, and near the eastern boundary of  
26 the nascent subtropical gyre the flow is turned equatorward. This eastern boundary blocking propagates  
27 westward across the basin at the speed of a long Rossby wave,  $-\beta C^2/f^2$ , about  $3 \text{ km day}^{-1}$  in the  
28 subtropics, and greater at lower latitudes. Within several hundreds of days after the passage of this  
29 so-called eastern boundary wave, the meridional flow reaches an approximate steady state consistent with  
30 the Sverdrup relation, here dubbed Stage 3. The central subtropical gyre reaches steady-state Sverdrup  
31 flow in about five years, but the layer thickness continues to increase slowly over the next several decades  
32 as the subtropical gyre absorbs water expelled from the subpolar region where the wind stress curl is  
33 positive and the wind-driven layer becomes dramatically thinner. A basin-wide steady state, Stage 4,  
34 follows after the subpolar gyre has also been swept by a slowly moving long Rossby wave along the  
35 northern boundary, requiring about 30 years.

36 The observed, basin-scale horizontal structure of the wind-driven ocean circulation, including  
37 western intensification and several of the qualitative differences between tropical, subtropical and  
38 subpolar gyres, have a plausible analog in solutions of the shallow water model. In particular, the  
39 Sverdrup relation plus the wind stress curl provide a concise and convincing explanation of the sense of  
40 the circulation over the majority of an ocean basin, e.g., equatorward (southward) meridional flow in the  
41 subtropics of the North Atlantic where the wind stress curl is negative. The Sverdrup relation is valid  
42 where the dominant terms of the potential vorticity balance are just two: the beta effect acting on a slow  
43 meridional flow, and the curl of the wind stress. In practice, this holds in the interior of a basin, where the  
44 currents and the friction are both very weak, and well away from zonal or meridional boundaries. The

45 meridional transport must vanish on zonal boundaries, and in the present model the affected zonal  
46 boundary regions are fairly wide, up to 1000 km in north-south extent. Within these wide zonal boundary  
47 regions, the meridional transport is considerably less than the expected Sverdrup transport.

48 The net transport through any given basin-wide zonal section must vanish in steady state, and the  
49 meridional Sverdrup transport in the interior of the basin is balanced in this volumetric sense by a very  
50 intense western boundary current (wbc) having a width of order the baroclinic radius of deformation,  
51  $O(100 \text{ km})$  in the subtropics. The transport of a wbc reaches approximate steady state after the ocean  
52 interior to the east has reached steady state Sverdrup flow, about five years in the subtropical gyre as  
53 noted before. In that sense, the wbc follows the interior circulation, despite that it is far more energetic.

54 Experiments with an annually-varying zonal wind stress show that wbc transport responds only  
55 weakly to even a large,  $\pm 50\%$  annual cycle of the wind stress. In the subtropical gyre, the resulting  
56 annual cycle of wbc transport is only about  $\pm 4\%$  of the mean transport. The annual cycle of wbc  
57 transport is even less in the subpolar gyre, and somewhat greater though still not prominent in the tropical  
58 gyre. There are some specific aspects of the circulation that do respond appreciably to an annually  
59 varying wind stress, most notably within the interior, eastern half of the tropical gyre. There the annual  
60 cycle of zonal currents is about  $\pm 50\%$  of the mean, or roughly proportional to the wind stress variation.  
61 This vigorous seasonal cycle of zonal currents is mainly a local (Stage 2) response to the seasonal  
62 variation of stress curl, but includes an annual period eastern boundary Rossby wave.

63 **More on Fig. 1** The SSH data in the upper panel are the monthly average for September over about  
64 twenty years of measurement compiled by the AVISO Project (<https://www.aviso.altimetry.fr>). The lower  
65 panel is the long-term, September average of density along  $35^\circ\text{N}$  from the World Ocean Atlas 2001  
66 ([http://www.nodc.noaa.gov/OC5/WOA01/pr\\_woa01.html](http://www.nodc.noaa.gov/OC5/WOA01/pr_woa01.html)). Notice that the tilt of the thermocline mirrors  
67 the tilt of SSH so that high SSH corresponds to a thick, low density upper layer (this holds also within the  
68 western boundary region, though not resolved in this climatology). The net result of this mass  
69 distribution is a comparatively small horizontal gradient of hydrostatic pressure at depths of about 1500  
70 meters. This is suggestive of a reduced gravity approximation that will be utilized in the numerical  
71 experiments to follow. At still greater depths, there are cold, mainly southward flowing currents that  
72 constitute the lower limb of the meridional overturning circulation. This figure was kindly provided by  
73 Iam-Fei Pun of WHOI.

74 **Contents**

75 **1 Earth’s rotation and its effects upon large-scale flows** **5**

76 1.1 Two observations on the wind-driven circulation . . . . . 6

77 1.1.1 O1, Space scales: Wind-driven gyres are markedly asymmetric east to west . . . . . 6

78 1.1.2 O2, Time scales: Mean and annual period variability depends strongly upon latitude 7

79 1.2 The plan for this essay . . . . . 9

80 1.3 A brief review of the Coriolis force, and the beta effect\* . . . . . 11

81 1.4 Aspects of depth-dependence\* . . . . . 15

82 1.5 Learning and understanding\* . . . . . 19

83 **2 A shallow water model of wind-driven circulation** **20**

84 2.1 Boundary and initial conditions . . . . . 20

85 2.2 Wind stress and its curl . . . . . 21

86 2.3 An expedient parameterization of drag on ocean currents\* . . . . . 23

87 2.4 A forced, dissipative shallow water model . . . . . 24

88 **3 The transient circulation develops in four stages** **26**

89 3.1 Stage 1: Short time, local response to the wind . . . . . 26

90 3.1.1 Inertial oscillations\* . . . . . 29

91 3.1.2 Ekman currents and Ekman transport . . . . . 30

92 3.1.3 Fast and slow time scales\* . . . . . 31

93 3.1.4 Latitudinal dependence, scaling, and the equator\* . . . . . 32

94 3.2 Stage 2: Long time, local response to wind stress curl . . . . . 34

95 3.2.1 Divergent Ekman transport changes the stratification . . . . . 34

96 3.2.2 Geostrophic currents accompany the changing stratification . . . . . 35

97 3.3 Stage 3: Blocking by the meridional boundaries and the onset of meridional flow . . . . . 39

98 3.3.1 Sverdrup flow in the basin interior . . . . . 39

99 3.3.2 Western boundary currents . . . . . 41

100 3.3.3 Changing stratification\* . . . . . 45

101 3.3.4 A simple model of transport in a time-dependent wbc\* . . . . . 47

102 3.4 Stage 4: Intra- and inter-gyre exchange, and basin-wide steady state . . . . . 48

103 **4 The (almost) steady circulation** **49**

104 4.1 A streamfunction depiction of the circulation . . . . . 50

	<b>1</b>	<b><i>EARTH'S ROTATION AND ITS EFFECTS UPON LARGE-SCALE FLOWS</i></b>	<b>5</b>
105	4.2	Dynamics of the steady circulation: the balance of potential vorticity . . . . .	52
106	4.2.1	Sverdrup interior . . . . .	53
107	4.2.2	Western boundary currents . . . . .	55
108	4.2.3	Zonal boundary regions . . . . .	57
109	4.3	A trip around the subtropical gyre . . . . .	59
110	4.3.1	Momentum balance and energy exchanges . . . . .	61
111	4.3.2	Potential vorticity balance . . . . .	63
112	4.3.3	Depth dependence* . . . . .	63
113	4.4	Another way to view the Sverdrup relation . . . . .	65
114	<b>5</b>	<b>Experiments with other wind fields and basin configurations</b>	<b>66</b>
115	5.1	Annually-varying winds and circulation . . . . .	67
116	5.2	A stress field with no curl* . . . . .	70
117	5.3	Meridional winds over a basin without sidewalls (a channel)* . . . . .	71
118	<b>6</b>	<b>Summary and closing remarks</b>	<b>74</b>
119	6.1	O1: East-west asymmetry of the subtropical and subpolar gyres . . . . .	74
120	6.2	O2: Time scales of the wind-driven circulation . . . . .	76
121	6.3	What's gone missing? . . . . .	77
122	<b>7</b>	<b>Supplemental material</b>	<b>78</b>
123	7.1	Links to models and updated manuscripts . . . . .	78
124	7.2	Homework problems . . . . .	79
125		Index . . . . .	81

126 **1 Earth's rotation and its effects upon large-scale flows**

127 This essay is the fourth in a four-part introduction to fluid dynamics on a rotating Earth. These essays  
128 were written for students who have some background in classical fluid dynamics, and who are beginning  
129 a study of geophysical fluid dynamics (GFD).

130 Some of the most important, subtle and distinctive phenomena of GFD are those that result from

131 Earth's rotation. The first three of these essays introduced three of these — the Coriolis force,  
 132 geostrophic adjustment, and westward propagation — topics that are about equally relevant for students  
 133 of atmospheric and oceanographic science.

## 134 1.1 Two observations on the wind-driven circulation

135 The present essay continues the study of rotation, but with a more avowedly oceanic theme, wind-driven  
 136 ocean circulation. The wind-driven phenomenon evident in Figs. (1) and (2) include gyres that fill the  
 137 subpolar and subtropical basins, and zonally elongated SSH features that span the tropics (Fig. 2). The  
 138 goal of this essay is to develop insight for two of the most important, observed characteristics of these  
 139 phenomena.

### 140 1.1.1 O1, Space scales: Wind-driven gyres are markedly asymmetric east to west

141 SSH sampled along  $35^\circ$  N across the subtropical gyre in Fig. (1) shows two distinctly different regions of  
 142 SSH zonal slope,  $\partial\eta/\partial x$  (Fig. 1, upper and Fig. 2). Going from the western boundary toward the east,  
 143 there is a narrow region adjacent to the western boundary of width  $L_{wb}$  that is  $O(100 \text{ km})$  within which  
 144 the SSH increases eastward to a maximum  $\delta\eta \approx 1 \text{ m}$ . The inferred geostrophic current in this western  
 145 boundary current, the Gulf Stream, is poleward (northward) and comparatively swift,  $U_{wb} \approx g\delta\eta/(L_{wb}f)$   
 146 is  $O(1 \text{ m sec}^{-1})$ . To the east, there is a broad interior region, essentially all the rest of the basin, width  
 147  $L_i \approx 7000 \text{ km}$ , over which there is a gradual decrease of  $\eta$  to approx. zero on the eastern boundary. The  
 148 inferred geostrophic current in the interior is equatorward (southward) and very slow compared to the  
 149 western boundary current,  $U_i \approx U_{wb}L_{wb}/L_i$  is  $O(0.01 \text{ m sec}^{-1})$  when averaged over zonal scales of  
 150  $O(1000 \text{ km})$ . This slow southward flow is mainly wind-driven Sverdrup flow, about which much more  
 151 below. A similar structure of rapid western boundary current and much slower interior flow is found also  
 152 in the subpolar gyre, though with the sense of the SSH anomaly and the circulation reversed. From this it  
 153 is evident that the east-west asymmetry of wind-driven circulation, often called western intensification, is  
 154 very pronounced,  $L_i/L_{wb} \approx U_{wb}/U_i$  is  $O(50)$ , which is typical of all of the major ocean gyres.

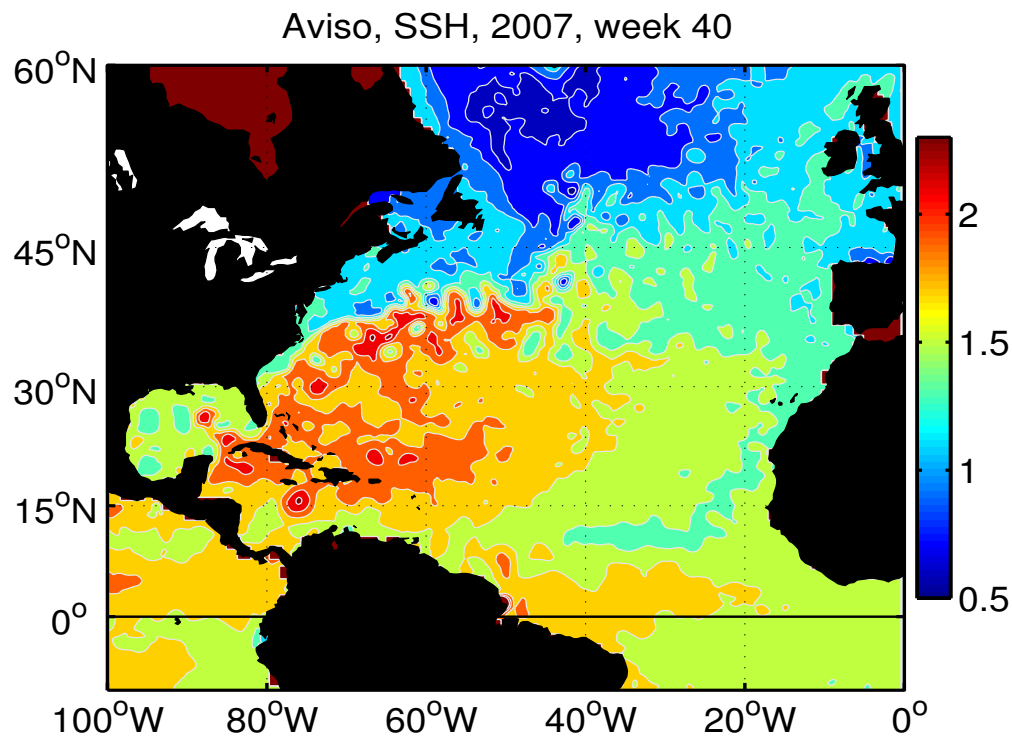


Figure 2: A snapshot of sea surface height (SSH) over the North Atlantic (repeats Fig. 1 of Part 3). The color scale at right is in meters. The largest SSH variability occurs primarily on two spatial scales — basin scale gyres (thousands of kilometers), a clockwise rotating high in the subtropics and a counter clockwise rotating low in the subpolar basin — and mesoscale eddies (several hundred kilometers) that are both highs and lows. The subtropical and subpolar gyres are clearly present in both instantaneous and time-averaged views, while mesoscale eddies are significantly time-dependent, including marked westward propagation. An animation of a year of this data is available at [www.whoi.edu/jpweb/Aviso-NA2007.flv](http://www.whoi.edu/jpweb/Aviso-NA2007.flv) and see also the AVISO homepage: <https://www.aviso.altimetry.fr>

### 155 1.1.2 O2, Time scales: Mean and annual period variability depends strongly upon latitude

156 The subtropical gyre is always present in the sense that every basin-wide snapshot of SSH (as in Fig. 2)  
 157 and every across-basin hydrographic section (as in Fig. 1 lower) will show an easily recognizable,  
 158 poleward-flowing Gulf Stream near the western boundary and an equatorward Sverdrup flow over most  
 159 of the rest of the basin. Said a little differently, the subtropical gyre and its wbc are present on long-term  
 160 average and instantaneously. This holds just as well for the subpolar gyre (with signs reversed). The  
 161 systematic, annual variation of the subtropical gyre, often represented by the Gulf Stream transport, is

162 only about 5% of the time-mean.<sup>1</sup> Such a small annual variation is somewhat surprising, given that the  
163 wind stress and air-sea heat flux over the North Atlantic exhibit a substantial annual variation, up to  
164  $\pm 50\%$  in the northern North Atlantic. This implies that the response time of the gyre-scale circulation of  
165 the subtropical and higher latitudes to a time-changing wind stress is considerably longer than a year.<sup>2</sup>

166 Lower latitude circulation appears to be quite different in these respects. Tropical ocean SSH is  
167 characterized by one or several narrow, zonally elongated ridges and troughs that vary seasonally. The  
168 associated, zonal geostrophic currents have alternate signs, e.g., between about 20 °N and 10 °N a  
169 westward flowing North Equatorial Current, a little further south an eastward flowing North Equatorial  
170 Countercurrent, and still further south, a westward flowing South Equatorial Current that spans the  
171 equator.<sup>3</sup> The amplitude of these tropical currents is comparable to that found in the subtropical and  
172 subpolar gyres, but the SSH amplitude evident in Fig. (1) is considerably less, a straightforward  
173 consequence of the  $f$ -dependence of geostrophy. In marked contrast to the quasi-steady subtropical and  
174 subpolar gyres noted above, some of these tropical circulation features exhibit systematic, large  
175 amplitude seasonality, e.g., the North Equatorial Counter Current is strongest in summer and disappears  
176 in winter, while the South Equatorial Current fluctuates annually by about  $\pm 50\%$  (to see this, you will  
177 need to follow the links to animations noted with Fig. 2, and see also the references in footnote 3).

---

<sup>1</sup>Rosby, T, C. Flagg and K. Donohue, 2010, 'On the variability of Gulf Stream transport from seasonal to decadal', *J. Mar. Res.*, 68, 503-522.

<sup>2</sup>Mesoscale eddies are ubiquitous, and impose large amplitude, but comparatively short time (periods of several months) and space (several hundred kilometers) scale variations on the gyre-scale SSH and currents, Fig. 2. For example, the SSH slope in the interior, if measured on scales of  $O(100 \text{ km})$ , will be dominated by mesoscale eddy variability. Thus the instantaneous (time and space) meridional geostrophic current in the basin interior is just about as likely to be northward as southward. Similarly, any single estimate of the instantaneous Gulf Stream transport may vary by  $\pm 15\%$  around the long term mean due to superimposed, apparently random mesoscale eddy variability.<sup>1</sup>

<sup>3</sup>The connection of these zonal currents with a western boundary current is not clear from observations. There does appear to be a northward-flowing western boundary current in Fig. 2 that crosses the equator and continues northwestward along the coast of South America. This North Brazil Current is thought to be the shallow side of the the global-scale, overturning circulation that imports warm South Atlantic water into the North Atlantic basin and returns cold water at great depth. The meandering North Brazil Current frequently sheds large (several hundred kilometer diameter) eddies that transport a significant part of the warm water flow. The presence of the strong and highly variable North Brazil Current makes it difficult to discern a relationship between the western boundary current and the mainly zonal currents to the east. A concise discussion of equatorial ocean circulation including the annual variability of winds and currents is by Philander, S. G., 2001, 'Atlantic ocean equatorial currents', Academic Press, doi:10.1006/rwos.2001.0361. An excellent depiction of surface currents generally is provided by <http://oceancurrents.rsmas.miami.edu/atlantic/north-brazil.html>

178 **1.2 The plan for this essay**

179 Wind-driven circulation encompasses a wide array of interesting phenomena and challenging problems.  
 180 To help keep us on a course toward O1 and O2, our pole star will be the Sverdrup relation,

$$181 \quad M_{Sv}^y = \frac{1}{\rho_o \beta} \nabla \times \tau \quad (1)$$

182 which is one of the bedrocks of ocean circulation theory. The righthand side of (1) is the curl of the wind  
 183 stress,  $\tau(x, y)$ , a vector field that has to be given from observations (if taking an ocean-only perspective as  
 184 here). The left hand side of (1) is the meridional (north-south) volume transport per unit width. In  
 185 general, transport per unit width is

$$186 \quad M^y(x, y) = \int_{-d}^0 v(x, y, z) dz, \quad (2)$$

187 where the meaning or significance is determined by the lower limit of the integral,  $-d$ . If  $M^y$  is meant to  
 188 be the Sverdrup transport of (1), then the depth  $d$  has to be sufficiently deep to encompass all of the  
 189 wind-driven meridional velocity: in the real ocean,  $d$  is not an obvious quantity, but is expected to be  
 190  $O(1000 \text{ m})$ . The Sverdrup relation gives the depth-integrated volume transport, and thus no clue to  
 191 depth-dependence, and it gives only the meridional component of the transport. There is a brief review of  
 192 the Sverdrup relation in the remainder of this section that will help set the stage for what follows, and a  
 193 somewhat deeper dive into other important but somewhat peripheral aspects in Sec. 1.4.<sup>4</sup>

194 The Sverdrup relation is extraordinarily concise: the wind-driven meridional transport per unit width  
 195 (hereafter understood) has the sign of the wind stress curl and a magnitude proportional to the curl divided  
 196 by  $\beta$ . Thus, if the wind stress curl is known, then so is the Sverdrup transport (notwithstanding that the  
 197 meridional transport in the ocean may include a contribution from, e.g., the global-scale, meridional

---

<sup>4</sup>Sverdrup's pioneering paper that introduced the equivalent of Eqn. (1) is unfortunately not easily read or appreciated, but nevertheless: Sverdrup, H. U., 1947, 'Wind-driven currents in a baroclinic ocean, with application to the eastern Pacific', *Proc. Natl. Acad. Sci. U. S. A.*, **33**, 318-326, which is available online at <http://www.pnas.org/content/33/11/318> The first model of a western-intensified wind-driven gyre was by Stommel, H., 1948, and the time-dependent, gyre spin-up problem was discussed by Stommel, H., 1957, 'A survey of ocean current theory', *Deep Sea Res.*, **4**, 149-184. Be sure to see also Stommel's masterpiece, 'The Gulf Stream', 1966, Univ. of California Press. Time-dependence was treated in greater detail by Anderson, D. L. T. and Gill A. E., 1975, 'Spin-up of a stratified ocean with applications to upwelling', *Deep-Sea Research* **22**. These classic research papers are highly readable and may be found at <http://www.aos.princeton.edu/WWWPUBLIC/gkv/history/oceanic.html> The GFD texts noted in Part 1 each have very good discussion of the Sverdrup interior. Ch. 1 of Pedlosky, J., 1998, 'Ocean Circulation Theory', and Ch. 10 of Marshall, J. and R. A. Plumb, 2008, 'Atmosphere, Ocean and Climate Dynamics', and Ch. 14 of Vallis, G., 2006, 'Atmospheric and Oceanic Fluid Dynamics', are all highly recommended.

198 overturning circulation noted in the discussion of Fig. 1). The physical content of the Sverdrup relation is  
199 also clear insofar as it is the forced, steady, linear version of potential vorticity balance (Sec. 1.4).

200 What is not at all clear from (1) standing alone is its range of validity. The Sverdrup relation makes  
201 no reference to time; either it holds instantaneously (no), or it applies to steady flows and wind stress  
202 (steady conditions seldom if ever occur in the oceans or atmosphere), or, it applies to a time-average of  
203 the wind stress and circulation. Wind stress varies significantly on time scales of hours to seasons, and in  
204 some important cases, year-to-year. The wind stress appropriate to (1) should then be a time-average over  
205 an interval that is consistent with the ocean's response to a fluctuating stress curl. In a similar way, the  
206 Sverdrup relation is local in space; the Sverdrup transport at a given point depends only upon the stress  
207 curl and the  $\beta$  at that point, regardless of the surroundings, e.g., even a nearby landmass. This can not be  
208 true of real ocean currents, which are, of course, blocked by land masses. The conclusion from this first  
209 look at the Sverdrup relation is that there must be important qualifications on the time and the space  
210 scales over which Eqn. (1) may be valid. The premise of this essay is that when we understand what  
211 those are, we will have gone a considerable distance toward an understanding of O1 and O2. The specific  
212 objectives of this essay are then to:

213 i) Observe how the Sverdrup relation arises when the circulation of a model ocean is started  
214 from rest, and so gain a sense of the time scales and mechanisms implicit in the  
215 time-independent Sverdrup relation (relevant to O2).

216 ii) Show that the Sverdrup relation holds over most of the interior of a model ocean basin and  
217 thus the sign of the wind stress curl determines the sense (clockwise, anti-clockwise) of  
218 wind-driven gyres (relevant to O1).

219 iii) Learn how the Sverdrup relation necessarily fails near solid boundaries and is supplanted  
220 by western or zonal boundary current dynamics (relevant to O1).

221 These are among the foundational problems of physical oceanography and they have been addressed  
222 many times over, and from many perspectives. Most notably, modern observational methods applied to  
223 both the atmosphere and the ocean have made possible detailed analyses of the Sverdrup relation over the  
224 global ocean.<sup>5</sup> In a nutshell, these studies concur that the Sverdrup relation is reasonably accurate (is  
225 valid) over most of the interior of the North Atlantic and North Pacific subtropical gyres, provided that  
226 winds and currents are averaged over multi year periods and horizontal scales of O(500 km) or greater.

---

<sup>5</sup>Three excellent, observation-based studies of the Sverdrup relation are by Gray, A. R. and Riser, S. C., 2014, 'A global analysis of Sverdrup balance using absolute geostrophic velocities from Argo', *J. Phys. Oceanogr.*, 1213-1229, doi: 10.1175/JPO-D-12-0206.1, and by Wunsch, C., 2011, 'The decadal mean ocean circulation and Sverdrup balance', *J. Mar. Res.*, **69**, 417-434, online at [dspace.mit.edu/openaccess-disseminate/1721.1/74048](https://dspace.mit.edu/openaccess-disseminate/1721.1/74048) and by Thomas, M. D. et al., 2014, 'Spatial and temporal scales of Sverdrup balance', *J. Phys. Oceanogr.*, **44**, 2644-2660. doi: 10.1175/JPO-D-13-0192.1

227 The Sverdrup relation is not valid near western boundary currents (wbc), which is no surprise, nor is it  
 228 valid in the eastward extension of the subtropical wbc (Gulf Stream) into the North Atlantic Current. The  
 229 subpolar gyres of the North Pacific and North Atlantic have a sense of circulation (counterclockwise) that  
 230 is consistent with the Sverdrup relation, but there is only a rather poor correlation in the magnitude of the  
 231 observed and Sverdrup-inferred transport. The difference is especially marked in the northerly half,  
 232 roughly, of the subpolar gyres, where the observed meridional transport is considerably less than the  
 233 expected Sverdrup transport.

234 The plan here is to address these objectives by the analysis of a comparatively simple wind-driven  
 235 circulation computed by a shallow water model that may be familiar from Parts 2 and 3. For most of the  
 236 problems studied here the domain will be a closed ocean basin that is about the size of the North Atlantic,  
 237 but otherwise highly idealized. The shallow water model is necessarily extended to include wind forcing  
 238 and dissipation. These new features are described in Section 2, which may be skipped by readers not  
 239 interested in the fine details (who should nevertheless take a look at the wind stress fields in Figs. 4 and  
 240 5). The integration is started from a state of rest and continues until the circulation reaches a basin-wide  
 241 steady state, requiring about 30 years. The transient circulation is described in Section 3 in terms of four  
 242 overlapping stages, and e.g., Stage 3 begins with the onset of Sverdrup flow. The steady circulation varies  
 243 a great deal over the basin. Over the majority of the basin, the steady potential vorticity balance is that of  
 244 the Sverdrup relation. However, near the western boundary, the balance includes a significant torque due  
 245 to drag on an energetic western boundary current, discussed in Section 4. Section 5 considers several  
 246 experiments with other wind fields including one with an annual cycle, especially relevant to the annual  
 247 variation of tropical ocean circulation noted in O2 above. Closing remarks are in Section 6, and links to  
 248 the shallow water model and a few homework problems are in Section 7.<sup>6</sup>

### 249 1.3 A brief review of the Coriolis force, and the beta effect\*

250 The Part 1 essay of this series examined the classical dynamics of moving parcels observed from a  
 251 steadily rotating coordinate frame.<sup>7</sup> An immediate consequence of Earth's rotation is the Coriolis force,

$$252 \text{Coriolis force} = -2\boldsymbol{\Omega} \times \mathbf{V},$$

253 where  $\boldsymbol{\Omega}$  is Earth's rotation vector which has a magnitude  $7.292 \times 10^{-5} \text{ sec}^{-1}$  and  $\mathbf{V}$  is the parcel velocity  
 254 having (east, north, up) components  $(u, v, w)$ . The Coriolis force is, like gravity, an inertial force, that is

---

<sup>6</sup>Sections that are mainly a review of earlier material, or that may be skipped over with little loss of continuity toward O1 and O2 are noted by a title having a trailing asterisk, starting with the next subsection.

<sup>7</sup>These essays, including the most recent version of this essay, are available online from <https://www2.who.edu/staff/jprice/>

255 exactly proportional to the mass of an object (and hence it might be more appropriate to call it the  
 256 Coriolis acceleration). The Coriolis force deflects all moving objects, without doing work. For most  
 257 everyday objects and motions, the Coriolis force is small to the point of being negligible. It is, however,  
 258 of first importance for the horizontal motions of the atmosphere and oceans, i.e., winds and currents, in  
 259 large part because all of the other possible horizontal forces are also small. The horizontal component of  
 260 the Coriolis force acting on a horizontal velocity  $V$  is

$$261 \quad -f e_z \times V = f v e_x - f u e_y \quad (3)$$

262 where  $e_x, e_y$  and  $e_z$  are the usual east, north and up unit vectors, and

$$263 \quad f = 2\Omega \sin(lat) \quad (4)$$

264 is the all-important Coriolis parameter evaluated at a latitude  $lat$ . (Homework problem 1, Sec. 7.2.)

265 Part 2 went on to consider geostrophic balance, the defining property of large scale, low frequency  
 266 (extra-equatorial) geophysical flows of the atmosphere and ocean. In a geostrophic balance, the  
 267 horizontal component of the Coriolis force is balanced by a pressure (or geophysical height) gradient,

$$268 \quad f v_{geo} = g' \frac{\partial h}{\partial x} \quad \text{and} \quad f u_{geo} = -g' \frac{\partial u}{\partial x} \quad (5)$$

269 where  $g' \partial h / \partial x$  is the hydrostatic pressure gradient of a reduced gravity, shallow water model.  
 270 Geostrophic balance may be understood using an  $f$ -plane approximation in which the latitudinal  
 271 dependence of the Coriolis parameter (4) is, purely for convenience, represented by a constant evaluated  
 272 at the central latitude of a model domain,  $lat_o$ ,

$$273 \quad f\text{-plane approximation: } f_o = 2\Omega \sin(lat_o) = const., \quad (6)$$

274 and the coordinates are rectangular. For this to be appropriate to a given flow, the horizontal scale of the  
 275 motion should be limited to  $O(100 \text{ km})$ . The dynamics of an  $f$ -plane model are isotropic, having no  
 276 favored direction (recall the isotropic dispersion relation of inertia-gravity waves and geostrophic motion  
 277 of Part 2, Sec. 2.3).

278 In contrast to the isotropy of the  $f$ -plane, observations of the atmosphere and ocean show that  
 279 large-scale, low frequency, nearly geostrophic phenomena are often markedly anisotropic in one or more  
 280 properties. Part 3 studied the striking example offered by mid-latitude, mesoscale eddies, which are  
 281 observed to propagate westward, slowly but relentlessly, at a speed that depends upon latitude: at  $30^\circ \text{ N}$ ,  
 282 the propagation speed is about  $-3 \text{ km per day}$ . In an  $f$ -plane model, an isolated, geostrophically balanced  
 283 mesoscale eddy may be exactly stationary in the sense of being unmoving in space and unchanging in

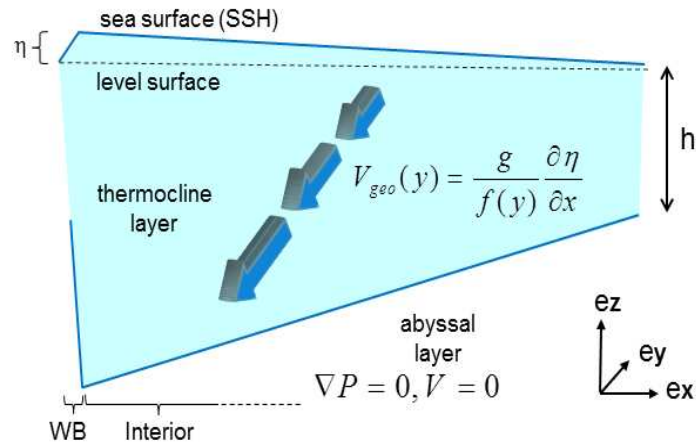


Figure 3: A schematic cross section of the North Atlantic subtropical thermocline, sliced east-west and viewed looking toward the north as in Fig. (1). The thermocline is modeled as a single active layer. The tilt of the thermocline compensates the tilted sea surface so that the pressure gradient and velocity vanish (approximately) in the very thick abyssal layer. The comparatively narrow western boundary region is noted at lower left, and the much wider interior region is all of the rest. The meridional geostrophic current in the interior is equatorward; the three bold arrows are meant to depict the geostrophic current amplitude at three latitudes and assuming constant zonal gradient of the SSH. The meridional geostrophic current increases toward the equator, simple because because  $f$  decreases toward the equator. A meridional geostrophic current is thus divergent, the beta effect. In this case the layer thickness tendency is thinning,  $\partial h / \partial t < 0$ .

284 time. However, when the northward increase of  $f$  is acknowledged, the same eddy will propagate  
 285 westward much like observed mesoscale eddies. In Part 3 and here, the northward increase of  $f$  is  
 286 represented by the  $\beta$ -plane approximation, a linear expansion of (1) around a central latitude,

$$287 \quad \beta - \text{plane approximation: } f_1 = f_o + \beta(y - y_o), \quad (7)$$

288 with  $y$  the north coordinate and

$$289 \quad \beta = (2\Omega/R_e) \cos(\text{lat}_o)$$

290 and a constant. For this study,  $\text{lat}_o = 30^\circ \text{ N}$  and hence  $f_o = 7.29 \times 10^{-5} \text{ sec}^{-1}$ , and  
 291  $\beta = 1.98 \times 10^{-11} \text{ sec}^{-1} \text{ m}^{-1}$ . A  $\beta$ -plane model is sufficient to reveal some of the most important  
 292 consequences of the northward variation of  $f$ , but once again the spatial scale of the phenomena should  
 293 be somewhat limited, say  $O(1000 \text{ km})$ , or less than fully global.

294 The mechanism of westward propagation by mesoscale eddies may be understood as a consequence

295 of geostrophic momentum balance, (5), in combination with continuity (volume balance),

$$296 \quad \frac{\partial h}{\partial t} = -\left(\frac{\partial hu}{\partial x} + \frac{\partial hv}{\partial y}\right) \quad (8)$$

297 and presuming  $f(y)$  via Eqn. (13). Assuming that the motion has small enough amplitude that variations  
298 of  $h$  are small compared to the nominal  $h$ , and that the velocity is geostrophic, then Eqns. (5) and (8) may  
299 be combined in a way that reveals the very important beta effect,

$$300 \quad \boxed{\frac{\partial h}{\partial t} = \frac{\beta h}{f} v_{geo}} \quad (9)$$

301 that meridional geostrophic motion is divergent on account of the equatorward increase of geostrophic  
302 motion (Fig. 3). Something is going to happen, either the stratification is going to change with time, or, if  
303 the flow is steady, then something more has to be involved.<sup>8</sup> Consider the former case: Eqn. (9) may be  
304 rewritten as the first order wave/advection equation (Sec. 7.2, Problem 3),

$$305 \quad \frac{\partial h}{\partial t} = \beta R_d^2 \frac{\partial h}{\partial x}, \quad (10)$$

306 where

$$307 \quad R_d = \frac{\sqrt{g'h}}{f} = \frac{C}{f}$$

308 is the radius of deformation.  $C$  is the gravity wave speed; in the subtropics,  $C \approx 3 \text{ m sec}^{-1}$ , and at  $30^\circ \text{ N}$ ,  
309  $R_d \approx 40 \text{ km}$ .

310 Eqn. (13) is appropriate for free motions, e.g., elementary waves  $h(x,t) \propto \sin(kx - \omega t)$ , and so may  
311 be characterized by a dispersion relation that connects the wavenumber,  $k = 2\pi/\lambda$ , and the frequency,  $\omega$ ,

$$312 \quad \omega = -k\beta R_d^2. \quad (11)$$

313 This is the long wave limit of baroclinic Rossby waves (Part 3, Sec. 2.3). In this limit, phase and group  
314 speeds are equal, and dubbed the long Rossby wave speed,

$$315 \quad \boxed{C_{longRo} = \frac{\omega}{k} = \frac{\partial \omega}{\partial k} = -\beta R_d^2 \leq 0.} \quad (12)$$

---

<sup>8</sup>There does not appear to be a wide consensus on the meaning of 'beta effect'. Many authors, including the Glossary of the American Meteorological Society, use the term to signify anything that happens on a beta plane that would not have happened on an otherwise similar  $f$ -plane. That sort of beta effect may thus be a different thing in every different setting.

316  $C_{longRo}$  is independent of  $k$  and  $\omega$ , and so this propagation is nondispersive and westward ( $\beta \geq 0$ ). Eqn.  
 317 (10) is thus a first order wave/advection equation,

$$318 \quad \boxed{\frac{\partial h}{\partial t} = -C_{longRo} \frac{\partial h}{\partial x}} \quad (13)$$

319  $C_{longRo}$  varies quite a lot with  $f$ , but at a fixed cite,  $C_{longRo}$  is, insofar as  $h$  is concerned, a constant,  
 320 westward advection velocity. Using values from  $30^\circ$  N,  $C_{longRo} \approx -3 \text{ km day}^{-1}$ , which is about 1% of  
 321 the gravity wave speed,  $C$ , and consistent with the observed propagation of mesoscale eddies noted above.

322 What is most important is that all free (unforced) large scale ( $\lambda \gg R_d$ ), low frequency ( $\omega \ll f$ )  
 323 phenomena that share (5), (8) and (13) will propagate westward, regardless of planform. If there are  
 324 indeed no small horizontal scales involved, then the planform will be conserved and will appear to be  
 325 shifted steadily westward, as if by advection, at the constant rate,  $C_{longRo}$ . It seems appropriate to call  
 326 such westward propagating phenomena 'Rossby waves', even if the planform may look nothing like an  
 327 elementary wave.<sup>9</sup> As we will see in Sec. 3.1.3, an appreciation for this generalized Rossby wave  
 328 propagation is a key concept needed to understand the response of an ocean circulation to a transient  
 329 wind. (For a little more on this see Homework problem 3, Sec. 7.2.)

#### 330 1.4 Aspects of depth-dependence\*

331 The shallow water model used here (modified as described in Sec. 2) is simplified considerably compared  
 332 to the real ocean or a comprehensive general circulation model in that it represents ocean currents by  
 333 means of only one active layer. Thus the shallow water horizontal velocity is, *per force*,  
 334 depth-independent; east and north velocity components are  $u$  and  $v$ , and e.g.,  $u$  is  $u(x, y, t)$ , but not  
 335  $u(x, y, z, t)$ .

336 As a prelude to a shallow water model, it is helpful to consider briefly what amounts to its  
 337 complement, a three-dimensional system that is presumed to be steady, linear and inviscid and that does  
 338 admit depth-dependence. The three dimensional velocity components of this system are  $u$ ,  $v$ , and  $w$ , and  
 339 e.g.,  $u$  is  $u(x, y, z)$  (note that this holds for the present section only). The three dimensional continuity and

---

<sup>9</sup>Much of the pioneering research on the topics discussed in this essay appeared in a series of classic papers by Carl G. Rossby and colleagues published in the late 1930s. A collection of Rossby's highly readable papers is available online at <http://www.aos.princeton.edu/WWWPUBLIC/gkv/history/general.html>

340 momentum equations of this system are

$$341 \quad 0 = \frac{\partial u}{\partial x} + \frac{\partial v}{\partial y} + \frac{\partial w}{\partial z}, \quad (14)$$

$$343 \quad 0 = -fv - \frac{1}{\rho_o} \frac{\partial p}{\partial x} + \frac{1}{\rho_o} \frac{\partial \tau^x}{\partial z}, \quad (15)$$

$$344 \quad 0 = fu - \frac{1}{\rho_o} \frac{\partial p}{\partial y} + \frac{1}{\rho_o} \frac{\partial \tau^y}{\partial z}. \quad (16)$$

346 The Coriolis parameter  $f$  is  $f(y)$  via the  $\beta$ -plane approximation, Eqn. (7), and  $\beta$  effects are crucially  
 347 important in what follows. There are two steady forces recognized here, the horizontal gradient of the  
 348 hydrostatic pressure,  $p$ ,

$$349 \quad p(x, y, z) = \int_{-z}^{\eta(x, y)} g \rho(x, y, z) dz,$$

350 which, like the velocity components, is an unknown. In principle, the density field and the SSH anomaly  
 351  $\eta$  that contribute to the hydrostatic pressure are within the scope of a comprehensive ocean circulation  
 352 model, though we are not claiming that here. A second important force is the vertical gradient of a  
 353 turbulent momentum flux,

$$354 \quad \tau^x(x, y, z) = \rho_o \langle u'(x, y, z, t) w'(x, y, z, t) \rangle$$

355 where the brackets  $\langle \rangle$  indicate a time average over tens of minutes. The small scale,  
 356 three-dimensional motions  $u'$ ,  $w'$  that propagate a turbulent momentum flux are far outside the scope of  
 357 large scale circulation model. We will, however, claim to know the surface value,  $\tau_o = \tau(x, y, z = 0)$ ,  
 358 which may be estimated from observations of wind over the oceans, i.e.,  $\tau_o$  is said to be the wind stress.  
 359 And we also know something about the vertical scale over which the stress is divergent, discussed below.

360 Given that the balances are steady and linear, we can rewrite the force terms on the right hand side of  
 361 (15) and (16) in terms of geostrophic and Ekman velocity components, say for the meridional component,

$$362 \quad v_{geo} = \frac{1}{\rho_o f} \frac{\partial p}{\partial x} \quad \text{and} \quad v_{Ek} = -\frac{1}{\rho_o f} \frac{\partial \tau^x}{\partial z}$$

363 with no loss of generality. Thus, in this steady, linear model

$$364 \quad v = v_{geo} + v_{Ek}.$$

365 Similarly, the meridional transports associated with these velocities may be written

$$366 \quad M^y = M_{geo}^y + M_{Ek}^y \quad (17)$$

367 where

$$368 \quad M_{geo}^y = \int_{-d_{geo}}^0 v_{geo} dz, \quad (18)$$

369 and

$$370 \quad M_{Ek}^y = \int_{-d_{Ek}}^0 v_{Ek} dz = -\frac{1}{\rho_o} \frac{\tau_o^x}{f}. \quad (19)$$

371 The lower limit of depth in these transport integrals is significant. The wind-driven geostrophic velocity  
 372 of the major ocean gyres is appreciable to at least the depth of the lower main thermocline,  $d_{geo}$  is  
 373 O(1000 m), and geostrophic currents associated with the global-scale overturning circulation extend over  
 374 the full depth water column, noted in the discussion of Fig. (1). The Ekman velocity will be significant  
 375 within an upper ocean surface layer that is mixed and stirred by the turbulent stress imposed at the  
 376 surface by the wind, and so is quasi-homogeneous with respect to density. In density-stratified regions,  
 377 such as the subtropical gyre, this Ekman layer may be as deep as the top of the seasonal thermocline,  $d_{Ek}$   
 378 is O(100 m), and hence almost always much less than  $d_{geo}$ . This important effect of stratification is  
 379 something we will come back to when it is time to consider what is missing from a shallow water model  
 380 (Secs. 4.3.2 and 6.3).

381 Assuming that the wind stress on the sea surface is known, then the Ekman transport Eq. (19) is also  
 382 known. The geostrophic transport (18) remains completely unconstrained, however, and so we can't go  
 383 any further with momentum balance and continuity alone. To find out what we can learn about this  
 384 system, it is very helpful to form the vorticity balance: take the partial  $x$  derivative of (16) and subtract  
 385 the  $y$  derivative of (15); then eliminate the horizontal divergence  $\partial u/\partial x + \partial v/\partial y$  using the continuity  
 386 equation (14). This has the effect of eliminating pressure and yields the (steady, linear) vorticity balance,

$$387 \quad \beta v = f \frac{\partial w}{\partial z} + \frac{1}{\rho_o} \frac{\partial}{\partial z} \left( \frac{\partial \tau^y}{\partial x} - \frac{\partial \tau^x}{\partial y} \right), \quad (20)$$

388 that holds at all  $z$  where (15) - (14) are valid. The depth-dependence of  $w$  and of the wind stress-induced  
 389 momentum flux are not knowable within this system alone, and so it is very helpful to depth-integrate  
 390 (20) from some great depth  $z = -d$  where the wind stress may be presumed to vanish, up to the sea  
 391 surface where the wind stress is presumed known and the vertical velocity must vanish, *to wit*, the depth  
 392 integral of (20) is

$$393 \quad \beta \int_{-d}^0 v dz = \beta M_{-d}^y = -fw(-d) + \frac{1}{\rho_o} \left( \frac{\partial \tau_o^y}{\partial x} - \frac{\partial \tau_o^x}{\partial y} \right). \quad (21)$$

394 While this depth-integrated vorticity equation (21) has given up on depth-dependence, the transport that it  
 395 helps uncover is of great interest. The first term on the right is the vortex stretching effect of the vertical  
 396 velocity at  $z = -d$ ,  $fw(-d)$ . With this term included, (21) is as general as Eqns. (15) - (14), and  $M_{-d}^y$  of  
 397 (21) is the meridional transport regardless of what the ultimate cause may be, i.e., whether wind-driven in

398 the Ekman or Sverdrup sense or geostrophic flow associated with the global-scale, overturning  
399 circulation.

400 The depth-integrated vorticity equation (21) is still not closed as there are two unknowns, the  
401 transport above  $z = -d$ ,  $M_{-d}^y$ , and the vortex stretching term,  $fw(-d)$ . To make a closed estimate of the  
402 transport we have to evaluate the latter. The simplest assumption is that  $w(-d)$  vanishes under one of  
403 three possible scenarios: If the sea floor was both flat and frictionless, then  $w$  at the sea floor would  
404 vanish. However, the sea floor is only rarely flat, and in any event, not truly frictionless so that a bottom  
405 Ekman layer may provide a form of Ekman pumping or suction near the bottom (Ekman pumping is  
406 discussed in Sec. 3.1.2). Another argument for dropping the  $w(-d)$  term is that the wind-driven  
407 circulation of a density-stratified ocean should be somewhat surface intensified, and may be negligible at  
408 some depth below the thermocline, typically 1000 - 2000 m, implying that  $w(-d) = 0$  at that depth as  
409 well. The almost flat isopycnal surfaces at approx. 1500 m in Fig. (1) suggest that this could be  
410 appropriate for much of the subtropical gyre in the North Atlantic. An important exception, already  
411 noted, is that the western basin shows evidence of significant deep flows associated with the global-scale,  
412 meridional overturning circulation and so clearly,  $d = 1500$  m is not valid generally. Finally, the best  
413 rationale for dealing with the deep vortex stretching term is that since the balances have already been  
414 presumed to be linear, the meridional transport may be imagined to be a superposition from more than  
415 one source, i.e., wind-driven, Sverdrup transport plus overturning transport which is not related to the  
416 local wind. To get at the former, we can assert that  $w(-d) = 0$  for a plausibly deep  $d$ , and then Eqn. (21)  
417 reduces to the Sverdrup relation, Eqn. (1),

$$418 \quad \boxed{\beta M_{-d}^y = \frac{1}{\rho_o} \nabla \times \tau_o} \quad (22)$$

419 We could just as well write the transport on the left side as  $M_{Sv}^y$  since that is what we have defined the  
420 Sverdrup transport to be. Setting aside questions of the appropriate  $d$ , this last result shows that Sverdrup  
421 transport is the total meridional transport, regardless of the momentum balance. In the present system, the  
422 transport is just geostrophic plus Ekman, Eqn. (17) and so

$$423 \quad \boxed{\beta M_{Sv}^y = \beta (M_{geo}^y + M_{Ek}^y) = \frac{1}{\rho_o} \nabla \times \tau_o} \quad (23)$$

424 (The superscript  $y$  on  $M_{Sv}^y$  is redundant since Sverdrup transport is solely meridional.) Said a little  
425 differently, the Sverdrup relation can be seen as a mode, i.e., a two term balance, of the steady, linear  
426 vorticity balance (21) in which deep vortex stretching is argued to be negligible. Geostrophic and Ekman  
427 balances are modes of the *momentum* balance and hence they come from a different class than does the  
428 Sverdrup relation. Geostrophic and Ekman flows are important in virtually all large scale ocean

429 circulation problems. However, other forces and processes are possible too, e.g., horizontal eddy fluxes  
 430 of potential vorticity may also contribute to the mean vorticity balance and to meridional transport.<sup>10</sup>

431 The meridional Ekman transport (19) may be subtracted from (23) to yield the geostrophic  
 432 component of the Sverdrup transport,

$$433 \quad M_{Svgeo}^y = \frac{f}{\rho_o \beta} \nabla \times \left( \frac{\tau_o}{f} \right) \quad (24)$$

434 Notice that the geostrophic transport, which is generally appreciable at depths well below the Ekman  
 435 layer that is driven directly by a turbulent wind stress, can nevertheless be written in terms of the curl of  
 436 the wind stress at the sea surface if the assumptions behind the Sverdrup relation are valid. This implies a  
 437 connection between the Ekman layer and the deeper ocean via vortex stretching that will be discussed in  
 438 Section 4.3.

## 439 1.5 Learning and understanding\*

440 The goal/plan of this essay is to develop insight for two concrete, observed facts, O1 and O2, by  
 441 reference to a fairly abstract concept, the Sverdrup relation. In other words, we aim to understand the  
 442 Sverdrup relation and its context in an ocean circulation. What would it mean to 'understand' something  
 443 like the Sverdrup relation, and, how would you know if you have gotten there? Four progressive stages of  
 444 learning and levels of understanding might be as follows: 1) To begin, you should be able to write down  
 445 the Sverdrup relation and define the terms in some detail. Then describe the parameter dependence and  
 446 the geographic variation that follows. 2) Replay a derivation of the Sverdrup relation beginning from a  
 447 fairly general framework, the time-mean balance of potential vorticity say, and explain the  
 448 approximations that are appropriate for the basin interior vs. boundary regions. 3) Explain when and  
 449 where the Sverdrup relation fails, and what else happens instead, at least qualitatively. 4) Understanding  
 450 derives from models that are idealizations that will not mimic everything that may happen in nature. A  
 451 deep and secure understanding will include an appropriate skepticism of model-dependent knowledge.

---

<sup>10</sup>Holland, W. R. and P. B. Rhines, 1980, 'An example of eddy-induced ocean circulation', *J. Phys. Oceanogr.*, **10**, 1010-1031.

## 2 A shallow water model of wind-driven circulation

The shallow water model introduced in the Part 2 essay can be made into a useful tool for studying some important facets of the large scale, wind-driven circulation by defining an appropriate domain and boundary conditions, and by adding new terms that represent wind forcing and dissipation.

### 2.1 Boundary and initial conditions

The ocean domain is taken to be a square basin with sides of length  $2L$  centered on  $30^\circ\text{N}$ . Rotation is treated by a  $\beta$ -plane approximation and the basin size is then chosen so that the southern boundary will correspond to the equator,  $f = 0$ . Given  $\beta(30^\circ)$ , this requires  $L = 3600$  km. The resulting basin width,  $2L = 7200$  km, is roughly comparable to the average width of the North Atlantic Ocean, but is only about half the width of the mighty Pacific Ocean. The intention is to model a self-contained circulation, and so the boundaries of the model domain are made impermeable by setting the normal component of velocity to zero,

$$\mathbf{V} \cdot \mathbf{n} = 0, \quad (25)$$

on all of the boundaries.

The initial condition on velocity is taken to be a state of rest, and the initial stratification is as before in Parts 2 and 3 but with no initial eddy,

$$\mathbf{V}(x, y) = 0 \quad \text{and} \quad h(x, y) = h_o \quad \text{at} \quad t = 0 \quad \text{and for all} \quad (x, y). \quad (26)$$

The initial thickness is chosen to be fairly large,  $h_o = 500$  m, and the density difference fairly small,  $\delta\rho = 2 \text{ kg m}^{-3}$ . The nominal gravity wave speed is thus  $= \sqrt{g\delta\rho h_o/\rho} = 3 \text{ m sec}^{-1}$ , which is realistic for most of the ocean. The initial radius of deformation at  $30^\circ$  is  $R_d = 42$  km, and the equatorial radius of deformation is  $R_{deq} = \sqrt{C/\beta} = 400$  km. The layer thickness changes quite a lot during the experiments that follow, especially in the subpolar region, and so  $R_d$  changes as well.

## 474 2.2 Wind stress and its curl

475 The energy source in these experiments is a wind stress,  $\tau(x, y)$ , a tangential force per unit area imposed  
 476 on the sea surface (the subscript  $o$  needed in Sec. 1.3 has been dropped since only the surface value of  
 477 wind stress will be relevant from here on). The wind stress field has to be specified from outside the  
 478 model, and here it will be represented by an idealization of the time-mean wind stress that has been  
 479 computed from observed winds over the oceans, Fig. (4).<sup>11</sup> So far as the Sverdrup relation is concerned,  
 480 the crucial property of the wind stress field is the curl,  $\nabla \times \tau(x, y)$ . The shallow water model requires the  
 481 wind stress itself, and here, just to keep it simple, we will specify the zonal component  $\tau^x$  only, and  
 482 assume that  $\tau^x$  is independent of  $x$ , thus

$$483 \tau^x(y) = \xi \sin(n\pi y/L), \quad (27)$$

484 where the amplitude  $\xi$  is a positive constant. For the standard case of Sec. 3,  $n = 1$ , and the wind stress  
 485 is eastward over the northern half of the basin, which mimics westerly winds, and westward on the  
 486 southern half of the basin, i.e., easterlies (Fig. (5). The amplitude is taken to be  $\xi = 0.1$  Pa, or about what  
 487 is estimated for the mean wind stress by the westerlies. In the experiment of Sec. 3, this wind stress field  
 488 is assumed to be constant in time once it is switched on. (In Sec. 5.1, the amplitude,  $\xi$ , will be made to  
 489 oscillate with an annual cycle, and in Sec. 5.3 the wind stress will be made meridional.)

490 A very important parameter of (27) is

491 the meridional length scale of the wind field; for  $n = 1$ ,  $L_\tau = L/n\pi \approx 1200$  km.

492 This is comparable to though a little less than two other important horizontal scales in this problem,

493 the basin scale,  $L = 3600$  km, and,

494  
 495 the planetary scale on which  $f$  varies,  $R_f = R_E/2 \approx 3300$  km,

496 where  $R_E$  is the radius of the Earth. All of these length scales are much greater than the natural horizontal  
 497 length scale of the baroclinic ocean,

498 the radius of deformation at  $30^\circ$  latitude,  $R_d \approx 40$  km.

---

<sup>11</sup>A particularly handy reference for such climate data is by Peixoto and Oort, 1992, *Physics of Climate*, American Inst. of Physics, New York, NY. There are now more than a dozen wind stress climatologies that are consistent at the semi-quantitative level needed here (see Townsend, T. L., H. E. Hurlburt and P. J. Hogan, 2000, 'Modeled Sverdrup flow in the North Atlantic from 11 different wind stress climatologies', *Dyn. Atmos. Oceans*, **32**, 373-417.) The differences in detail between the various wind stress climatologies make an easily detectable and in some ways important difference in the computed Sverdrup flow, as does the basin topography.

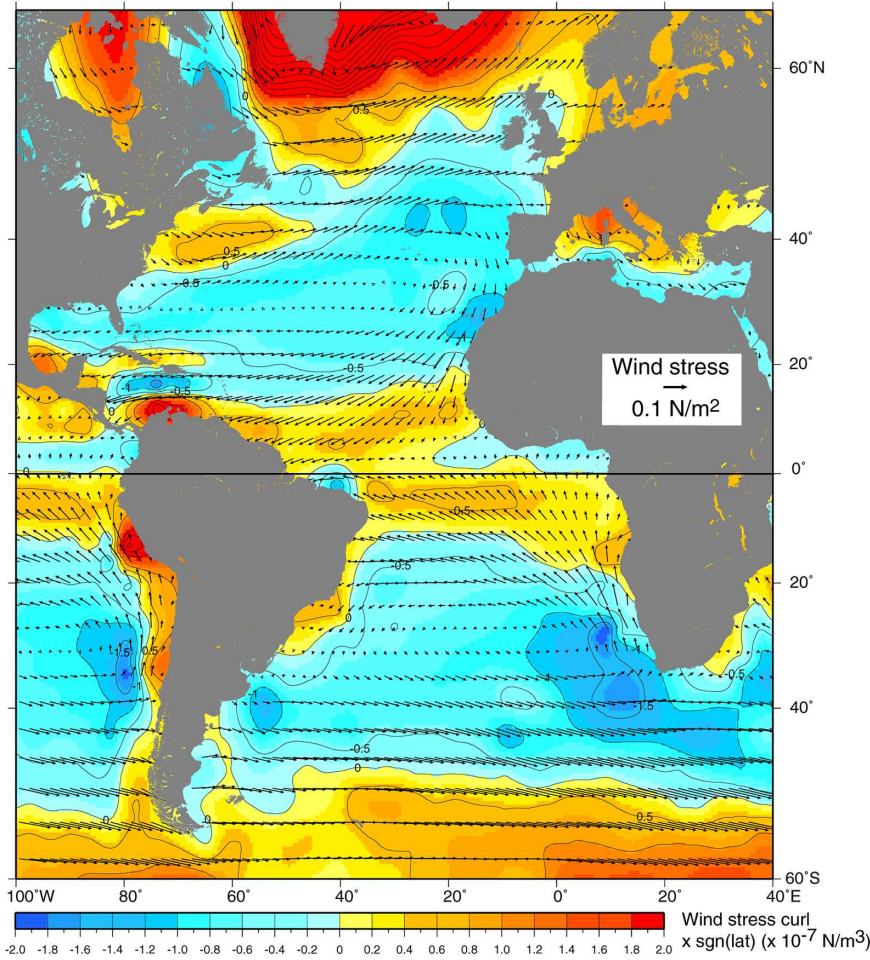


Figure 4: The vector field is the climatological mean wind stress (scale at center right), the color contours are proportional to the wind stress curl (scale at the bottom). These data were computed from a reanalysis of observed wind compiled by the National Center for Environmental Prediction. Over both the North Atlantic and South Atlantic basins the broad pattern includes westerly winds from roughly  $35^\circ$  to  $50^\circ$ , and easterly winds in tropical regions, latitude less than  $20^\circ$ , and also in subpolar regions, latitude greater than roughly  $55^\circ$ . The stress curl is thus negative over the subtropics and positive over the equatorial and subpolar regions. This beautiful and informative figure is thanks to L. D. Talley et al., *Descriptive Physical Oceanography*, Elsevier, Fig. S09.3, <http://booksite.elsevier.com/DPO/chapterS09.html>

499 Given that our shallow water model has only a single active layer of thickness  $h$ , the wind stress is  
 500 necessarily modeled as a body force that is distributed evenly throughout that layer and hence the  
 501 acceleration due solely to wind stress alone is just

$$502 \quad \frac{D\mathbf{v}}{Dt} = \frac{\boldsymbol{\tau}}{\rho_0 h}, \quad (28)$$

503 which is a valid approximation of the full momentum balance for very short times,  $t \ll 1/f$ , a few hours  
 504 or less. In a shallow water model,  $d_{Ek} = h$ , and here we have chosen  $h \approx 500$  m, in order to have a  
 505 realistic baroclinic wave speed. In the real, stratified ocean,  $d_{Ek}$  is much less, typically  $O(100$  m). We  
 506 will consider some of the implications of this as we go along, but for now note that the Ekman current in  
 507 this model is considerably weaker than in the real ocean, but the Ekman transport and the Sverdrup  
 508 transport are the same whether the wind stress is absorbed in a comparatively thin surface layer (as  
 509 actually occurs) or over the entire upper ocean layer that is wind-driven in the Sverdrup sense, as happens  
 510 in a shallow water model.

511 The curl of the wind stress given by (27) is

$$512 \quad \nabla \times \boldsymbol{\tau}(x, y) = -\frac{\partial \tau^x}{\partial y} = -\frac{n\pi\xi}{L} \cos(\pi y/L), \quad (29)$$

513 which has an amplitude  $\xi/L_\tau \simeq 0.8 \times 10^{-7} \text{ N m}^{-3}$  ( $n = 1$ ). This is comparable to typical values of  
 514 stress curl seen in Fig. (4), but less than the maximum values, which are roughly  $2 \times 10^{-7} \text{ N m}^{-3}$ . The  
 515 sign of the wind stress curl defines three regions: a central subtropical region where the stress curl is  
 516 negative (clockwise turning), and tropical and subpolar regions where the curl is positive  
 517 (anti-clockwise), Fig. (5).

518 This idealized stress field is least realistic for the tropical region insofar as it omits a secondary  
 519 maximum of the easterly winds often present near the equator (most pronounced in the Pacific). This  
 520 gives a narrow region of negative stress curl within a few degrees of the equator that, if included here,  
 521 would give two smaller tropical gyres vs. one rather large tropical gyre that results from (27). This error  
 522 in the tropical winds is left in place because the goal is not so much a realistic simulation of the observed  
 523 ocean circulation — which would require much more than just a better wind field — but rather to  
 524 investigate how the wind-driven circulation varies with latitude. The idealized stress field Eqn. (27) is  
 525 appropriate to this goal since the wind stress curl magnitude of (27) is the same over the three regions  
 526 (tropical, subtropical and subpolar).  $\beta$  is also the same, and hence so too is the Sverdrup transport. The  
 527 *actual* transport is, *not* the same, however, because of zonal boundary effects that extend many hundreds  
 528 of kilometers into the tropical and subpolar gyres and reduce the transport to values below that expected  
 529 from the Sverdrup relation (Sec. 4.2.3).

### 530 **2.3 An expedient parameterization of drag on ocean currents\***

531 With a wind stress included, and if we intend to compute up to a possible steady state, then there has to  
 532 be some mechanism to dissipate the energy and potential vorticity that are supplied by the wind. The  
 533 present model follows the classic treatment by Stommel (1948)<sup>4</sup> in choosing a linear drag that is  
 534 proportional to and anti-parallel to the velocity,

$$535 \quad \text{drag} = -r h_o \mathbf{V}, \quad (30)$$

536 sometimes called Stokes drag. This has the dimensions of a stress/density, and the resulting acceleration  
 537 is  $-r h_o \mathbf{V}/h$  (as in the single particle model of Part 1, Section 5, aside from varying layer thickness). The  
 538 coefficient  $r$  is taken to be  $r = 1/(15 \text{ days})$ , the smallest value of  $r$  that will allow the ocean circulation in  
 539 this system (wind stress included) to reach a near steady state. Given a nominal layer thickness,  $h \approx h_o$ ,

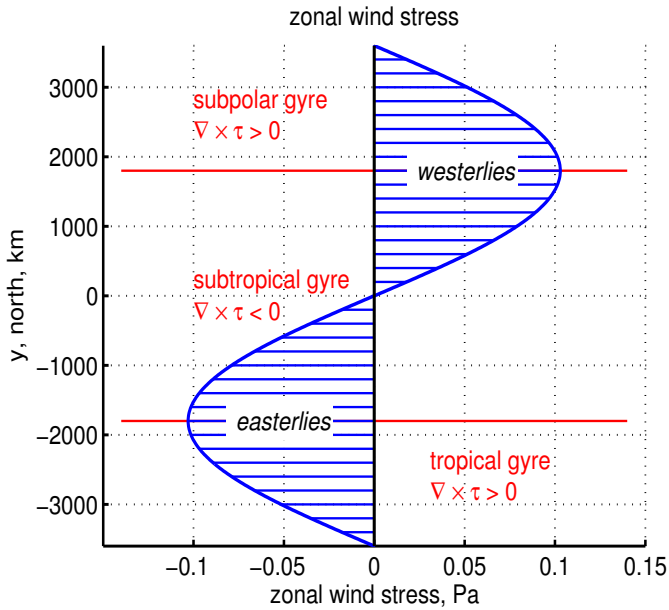


Figure 5: An idealized, zonal wind stress field that is applied to the shallow water model. The horizontal red lines appear in subsequent figures to show the axes of the easterly and westerly wind maxima, and thus the boundaries of the stress curl — negative (clockwise) in the large subtropical region between the westerly and easterly axes, and positive (anti-clockwise) over the smaller tropical and subpolar regions. These red lines correspond closely to the gyre boundaries.

540 the Ekman number at  $30^\circ\text{N}$  is  $E = r/f \approx 0.01$ . This  $E$  may seem quite small, but nevertheless, the  
 541 model dynamics are almost certainly more viscous overall than is the real ocean. In Secs. 3 and 4 we will  
 542 find out how this value of  $r$  is related to the natural width of the western boundary current, the radius of  
 543 deformation.

544 In some contexts it might be argued that the Stokes drag represented by Eqn. (30) is a crude  
 545 treatment of bottom drag. However, that is not plausible here since the active layer is not imagined to be  
 546 in contact with a sea floor. It is probably better to think of the Stokes drag as nothing more than the  
 547 simplest form of a drag or dissipation process that permits a steady state in this model. Given this *ad hoc*  
 548 basis for (30), we will have to be careful not to over interpret those aspects of the solution that depend  
 549 sensitively upon the value of  $r$ , most notably the zonal boundary current width of Sec. 4.3.

## 550 2.4 A forced, dissipative shallow water model

551 With wind stress and drag included, the shallow water continuity (thickness balance) and momentum  
 552 equations (derived in Part 2) are

$$553 \quad \frac{Dh}{Dt} = \frac{\partial h}{\partial t} + \mathbf{V} \cdot \nabla h = -h \nabla \cdot \mathbf{V}, \quad (31)$$

$$\frac{D\mathbf{V}}{Dt} = \frac{\partial\mathbf{V}}{\partial t} + \mathbf{V} \cdot \nabla \mathbf{V} = -g\nabla\eta - f\mathbf{k} \times \mathbf{V} + \frac{\tau}{\rho_o h} - \frac{rh_o}{h}\mathbf{V}. \quad (32)$$

The  $\eta$  of the hydrostatic pressure term of (32) is the SSH anomaly computed from the layer thickness  $h$  via the reduced gravity approximation,

$$\eta = \frac{\delta\rho}{\rho_o}(h - h_o). \quad (33)$$

Notice that the thickness balance (31) is adiabatic in the sense that the thickness can change only by way of a divergent thickness flux, and hence the net (basin integral) thickness is conserved.<sup>12</sup> This is not true for the momentum balance because of the wind stress source term and the Stokes drag dissipation term.

The shallow water potential vorticity is

$$q = \frac{\nabla \times \mathbf{V} + f}{h}, \quad (34)$$

and the  $q$ -balance is

$$\frac{Dq}{Dt} = \frac{\partial q}{\partial t} + \mathbf{V} \cdot \nabla q = \frac{1}{\rho_o h} \nabla \times \frac{\tau}{h} - \frac{rh_o}{h} \nabla \times \frac{\mathbf{V}}{h}. \quad (35)$$

Part 3 studied free Rossby waves that could be described via the mechanisms of  $q$  conservation,  $Dq/Dt = 0$ . Rossby wave-like motions are possible also in (35) and are a crucial part of the time-dependent dynamics discussed in Sec. 3.3.

What can we expect to learn from such an idealized model? And just as important, how can we avoid being misled by the omissions and inadequacies of this model? The shallow water dynamics (31) - (35) are a subset of the processes known to be important comprehensive general circulation models and in the real ocean, and so we can not expect a high fidelity reproduction of all aspects of the observations pictured of Sec. 1.1. Some physical processes are inaccessible by virtue of the single active layer assumption, *viz.* baroclinicity and the effects of topography, and other processes are represented crudely, especially dissipation by Stokes drag. Nevertheless, the analysis will seek to describe and understand the solutions as they are, warts and all, and then draw a bright line distinction between aspects of the shallow water solutions that are in common with comprehensive models — time-dependence and the pattern of Sverdrup transport, especially, and those that are not — anything dependent upon vertical structure and the details of the dissipation process. In reaching these judgments we can rely upon results from comprehensive ocean general circulation models, along with data-based studies of the Sverdrup relation.<sup>6</sup>

<sup>12</sup>This adiabatic property is especially convenient for some diagnostics of the time-changing stratification. However, it is also a liability, insofar as the layer thickness given by (31) can vanish under some plausible forcing regimes, especially at high latitudes. Vanishing layer thickness means instant death for a numerical integration. A partial remedy is to start with a fairly thick initial layer, 500 m, as is done here. Better would be the inclusion of a vertical mixing process that kept the upper layer thickness finite at all times, but which is not attempted here.

### 581 3 The transient circulation develops in four stages

582 Now, finally, we are ready to integrate and find a solution. The wind stress field Eqn. (27) is switched on  
 583 at time = 0 and held constant for a little more than 10,000 days. This long time is necessary to allow the  
 584 solution to reach a (nearly) basin-wide steady state, (Fig. 6, bottom panel).

585 The resulting circulation is fully three dimensional,  $(x, y, t)$  and includes several variables, and so it  
 586 is helpful to organize the description along the lines of geography and time. In most of what follows we  
 587 will start with a description of the subtropical gyre and then note the differences observed in the tropical  
 588 and subpolar gyres. These differences are in some respects quite pronounced and are a very important  
 589 part of the narrative. Nevertheless these differences are quantitative rather than qualitative. (There can  
 590 arise distinctly different phenomena in the near-equatorial region, but which are not prominent in these  
 591 solutions.) As well, the transient circulation develops in four more or less distinct, temporal stages. These  
 592 are not necessarily non-overlapping, but they are characterized by quite different processes.

#### 593 3.1 Stage 1: Short time, local response to the wind

594 For the first few weeks, and away from the boundaries and the equator, the momentum balance of the  
 595 wind-driven current may be approximated by the linearized subset of Eqn. (32) in which all the terms  
 596 involving horizontal spatial derivatives are omitted,

$$597 \quad \frac{\partial h}{\partial t} = 0, \quad (36)$$

$$598 \quad \frac{\partial u}{\partial t} = fv - ru + \frac{\tau^x}{\rho_0 h}, \quad (37)$$

$$599 \quad \frac{\partial v}{\partial t} = -fu - rv.$$

600 You may notice that these equations are exactly the form used to model the motion of a dense parcel  
 601 released onto a slope (Part 1, Sec. 5), though of course here the external force is a wind stress rather than  
 602 a buoyancy force. These equations are local in the sense that they apply to what amounts to a single  
 603 parcel, or since the equations are linear, a single position, and that does not interact in any way with its  
 604 surroundings, i.e., pressure gradients and advection are not admitted. these very important *non*-local  
 605 processes will come soon.

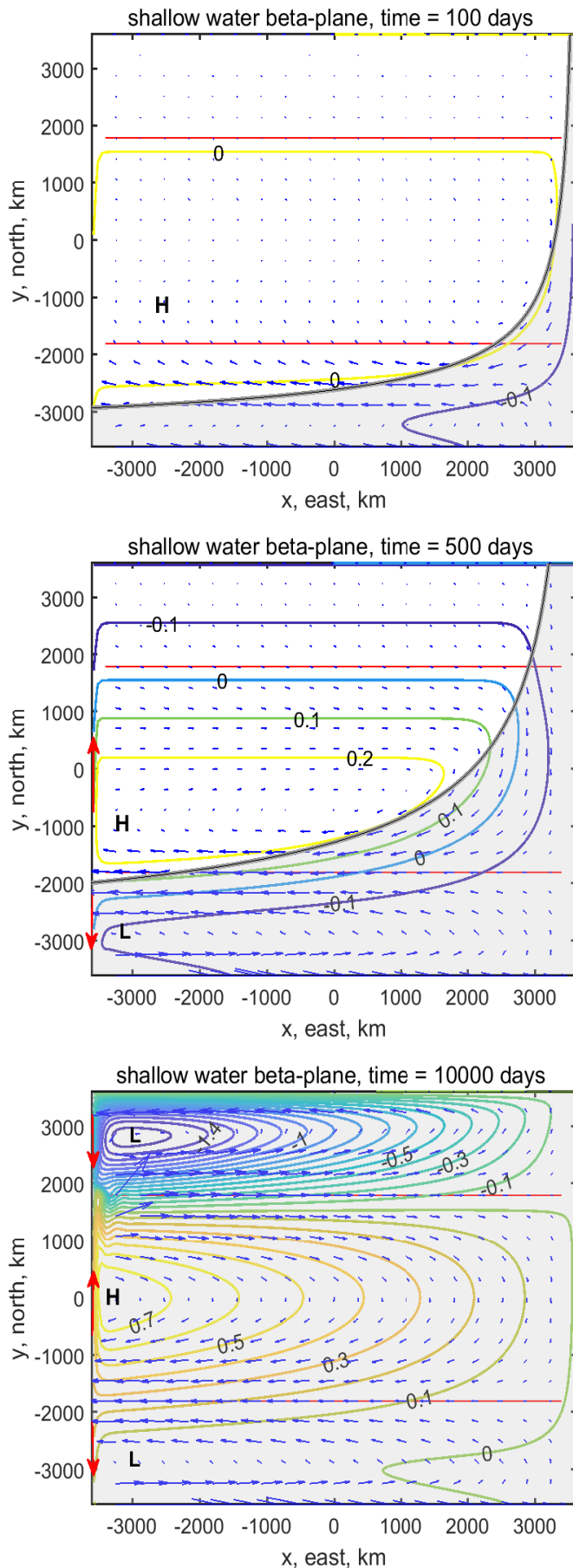


Figure 6: Three snapshots from a wind-driven experiment taken at, from top to bottom, 100, 500 and 10,000 days after the wind stress was switched on. The last time appears to be in a near-steady state throughout the interior of the basin. The thin red horizontal lines are the axis of the westerly and easterly wind stress (Fig. 5). The contours are SSH anomaly computed from thickness anomaly via the reduced gravity approximation; units are  $\Xi_{\tau}$ . The small blue arrows are the current, though with the comparatively very large currents within the wbc omitted (shown in Sec. 4.2). The sense of the wbc is indicated by the red arrows on the west edge of the model domain. The largest currents shown here are approx.  $0.3 \text{ m sec}^{-1}$ . The gray shading extends westward from the eastern boundary at the y-dependent speed of a long Rossby wave,  $\beta R_d^2$ , and was sketched on top of the solution. Notice that the onset of meridional flow is approximately coincident with the passage of this so-called eastern boundary Rossby wave. An animation of these data is at [www.whoi.edu/jpweb/threegyres.mp4](http://www.whoi.edu/jpweb/threegyres.mp4)

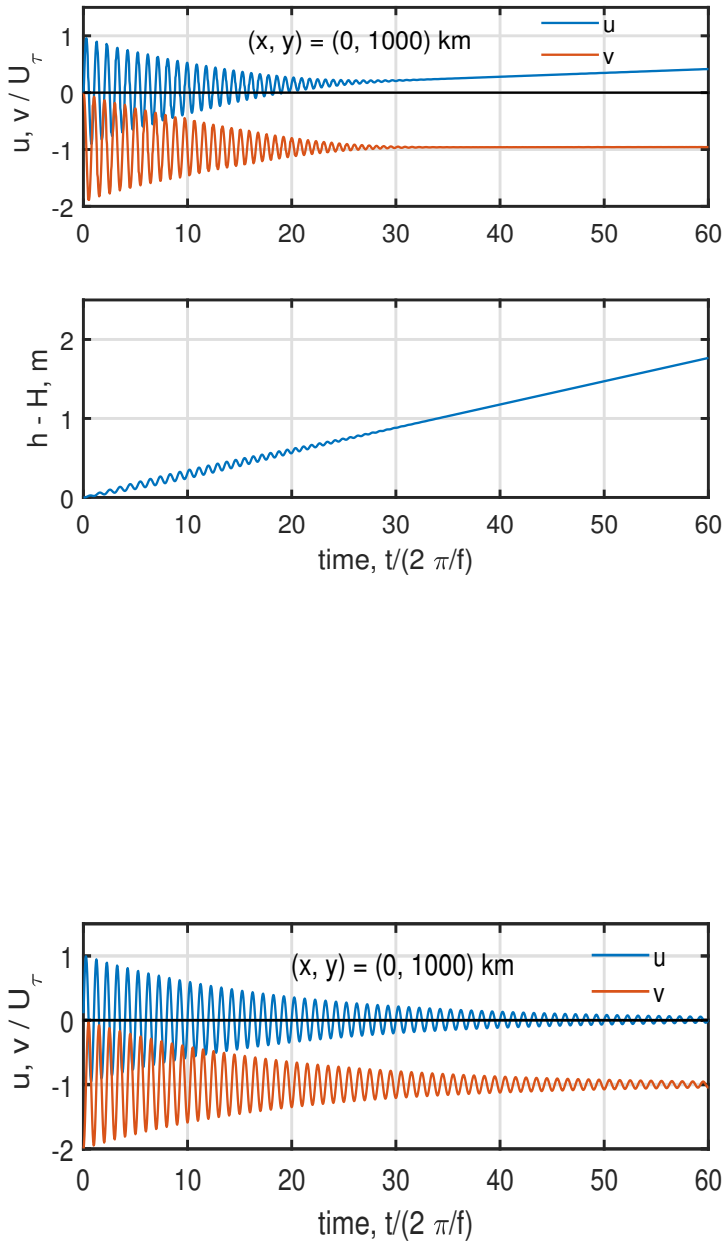


Figure 7: The short time evolution of currents. These data were sampled at 20 min. intervals on the northern side of the subtropical gyre,  $(x, y) = (0, 1000)$  km. This site was chosen since there is an appreciable wind stress,  $\tau^x = 0.08 \text{ N m}^{-2}$ , which is eastward, and also a significant divergence of the Ekman transport. **(upper)** A time series of east and north current components,  $u$  and  $v$ . These are shown in units of the wind-driven velocity scale,  $U_\tau$ . The high frequency oscillations are near-inertial motion; the time-mean (steady)  $v$  is southward Ekman flow which in these units has the value -1. **(lower)** Layer thickness anomaly,  $h - h_o$ , which shows a steady increase at about  $15 \text{ m year}^{-1}$ . This increase in layer thickness is caused by the convergence of Ekman transport, and the slow increase of the east current seen above is the associated zonal geostrophic flow (discussed in Sec 3.2). Notice the very small but dynamically significant oscillations of thickness in the first several weeks. These are evidence that the high frequency oscillations of the current are best described as near-inertial (very long wavelength) gravity wave motions.

Figure 8: The solution for local, damped wind-driven motion, Eqn. (39) that may be compared to the full model solution, Fig. (7). There is no layer thickness shown here since in this local model there is no velocity divergence, and hence  $h = h_o$  and constant.

Given an initial condition that is a state of rest,

$$u(t=0) = 0 \text{ and } v(t=0) = 0,$$

the solution for the so-called Stage 1 velocity is, in dimensional form,

$$\begin{pmatrix} u_{S1} \\ v_{S1} \end{pmatrix} = \frac{\tau^x}{\rho_o f h} \begin{pmatrix} 1 \\ 1 + (r/f)^2 \end{pmatrix} \begin{pmatrix} r/f + \exp(-rt)(\sin(ft) + (r/f)\cos(ft)) \\ -1 - \exp(-rt)(\cos(ft) - (r/f)\sin(ft)) \end{pmatrix}, \quad (38)$$

In non-dimensional form the same solution is

$$\begin{pmatrix} u_{S1} \\ v_{S1} \end{pmatrix} / U_\tau = \begin{pmatrix} 1 \\ 1 + E^2 \end{pmatrix} \begin{pmatrix} E + \exp(-E\gamma)(\sin(\gamma) + E\cos(\gamma)) \\ -1 - \exp(-E\gamma)(\cos(\gamma) - E\sin(\gamma)) \end{pmatrix}, \quad (39)$$

where

$$\gamma = tf$$

is time scaled by the rotation time,  $1/f$ ,

$$E = r/f \quad (40)$$

is the Ekman number, and finally

$$U_\tau = \frac{\tau^x}{\rho_o f h} \quad (41)$$

is the amplitude scale of the directly wind-driven velocity. Notice that the latter is just the direct, wind-stress induced acceleration Eqn. (28) times the rotation time scale,  $1/f$ .

The velocity of the local model (39) is the sum of a time-dependent inertial oscillation and a time-independent Ekman flow (Fig. 8).

### 3.1.1 Inertial oscillations\*

Inertial oscillations are a clockwise rotation of the velocity at a rate  $f$ ; at  $30^\circ$  N, the frequency is the Earth's rotation rate,  $\Omega = 7.292 \times 10^{-5} \text{ sec}^{-1}$ , and the period is just slightly less than one day (see problem 1). At the site sampled in Figs. (7) and (8)  $(x, y) = (0, 1000) \text{ km}$ , equivalent to about  $41^\circ$  N, the inertial period is about 17 hours and the wind stress is about  $\tau^x = 0.008 \text{ N m}^{-2}$ . The amplitude of the inertial oscillation at this site is thus  $U_\tau \approx 0.002 \text{ m sec}^{-1}$ , which is unrealistically small because of the excessively thick wind-driven layer,  $h = 500 \text{ m}$ . If the amplitude of inertial oscillations played an important part in the low frequency response (they do not), then this would be a serious shortcoming of a shallow water model. The inertial oscillation of (39) decay with time as  $\exp(-Eft)$ , e-folding in 15 days

631 due to Stokes drag. The time during which inertial oscillations are appreciable may be used to define the  
632 duration of

$$633 \text{ Stage 1: } 0 < t < \frac{1}{f}.$$

634 The inertial oscillations computed by the full shallow water model Fig. (7) differ from the solution  
635 of the local model (39) in that the frequency of rotation is a few percent greater than  $f$  (hard to see this in  
636 the present figure) and the amplitude decay is somewhat faster than is given by the frictional e-folding  
637 alone. These two features plus the very small but nevertheless significant oscillation of thickness (Fig. 7,  
638 lower) indicate that what appear to be inertial oscillations in the shallow water model solution are better  
639 described as very long wavelength, near-inertial gravity waves. The longer term (several weeks)  
640 evolution of the inertia-gravity waves is significantly influenced by the variable  $f$  of this shallow water  
641 model, which leads to propagation towards the equator.

### 642 3.1.2 Ekman currents and Ekman transport

643 Along with the (near) inertial oscillation, the wind-driven current has a time-mean value consistent with  
644 Ekman balance modified very slightly by friction,

$$645 \begin{pmatrix} U_{S1} \\ V_{S1} \end{pmatrix} / U_{\tau} \approx - \left( \frac{1}{1 + E^2} \right) \begin{pmatrix} E \\ -1 \end{pmatrix}. \quad (42)$$

646 Ignoring the small effects of friction, the amplitude of the Ekman flow is equal to the amplitude of the  
647 inertial oscillation, The amplitude of the Ekman current is  $\propto U_{\tau}$ , and is unrealistically small, as noted  
648 already. The direction is perpendicular and to the right of the wind stress, and so is southward at the site  
649 shown in Fig. (7) where the wind stress is eastward. The approximate solution for Ekman flow is  
650 indistinguishable from the solution computed by the shallow water model. The Ekman currents are  
651 present within hours of the start-up, and persist for the duration of the experiment since the wind stress is  
652 held steady.

653 The ideal ( $E = 0$ ) Ekman transport in this case is

$$654 M_{Ek}^y = hV_{S1} = - \frac{\tau^x}{\rho_o f} = - \frac{\xi}{\rho_o f} \sin(\pi y/L). \quad (43)$$

655 Ekman transport is independent of the layer thickness in general. This specific Ekman transport varies  
656 with  $y$  only. Ekman transport has the units  $l^2 t^{-1}$  for which we will reserve the symbol  $M$ . It is often

657 called 'volume transport per unit width', but we will call it just 'transport'. At the site shown in Fig. (7),  
 658 which is equivalent to about 41 °N, the Ekman transport is  $M_{Ek}^y \approx -1.3 \text{ m}^2 \text{ sec}^{-1}$ , which is a significant  
 659 magnitude. To find the consequent *volume* transport,  $l^3 t^{-1}$ , this  $M$  has to be integrated or multiplied over a  
 660 horizontal distance, say the width of the North Atlantic basin, to find a volume transport (symbol  $N$ ) at  
 661 this  $y$  (latitude) of about  $N_{Ek} = M_{Ek} * 2L = -10 \times 10^6 \text{ m}^3 \text{ sec}^{-1}$ , or 10 Sv southward. This is a  
 662 significant fraction of the total meridional transport at this latitude. Moreover, Ekman transport will be  
 663 made up from the shallowest and generally the warmest water in the water column, and so makes a very  
 664 important contribution to the heat flux carried by the ocean circulation.

665 It is notable that the amplitude of Ekman transport of (43) goes as  $1/f$ , and so for a given wind  
 666 stress, the Ekman transport is considerably larger in the tropics than in the subpolar region. The same  
 667 applies for a given pressure gradient and the amplitude of geostrophic currents, and is a part of the reason  
 668 that tropical SSH anomalies are comparatively small (Fig. 2).

669 While Ekman transport is significant in its own right, it has an even more important indirect role in  
 670 generating the changes in layer thickness that lead to geostrophic and Sverdrup transports, discussed in  
 671 Sec. 3.2 and forward.

### 672 3.1.3 Fast and slow time scales\*

673 It is implicit in the discussion above that currents and thickness vary on two quite different time scales,  
 674 the fast time scale of the (near) inertial motions, and a much slower variation that here looks like a linear  
 675 trend in the  $v$  velocity and in the thickness. When we see a much longer time series of these data, the  
 676 latter will emerge as a low frequency Rossby wave-like motion, and/or a part of the developing, steady  
 677 circulation. Given that our main interest here is the low frequency phenomenon, then it is reasonable to  
 678 ask whether it is desirable or necessary to also compute the high frequency phenomenon. The shallow  
 679 water system naturally includes both kinds of motions, but the high frequencies can be suppressed by  
 680 simply ramping the wind stress up gradually over a few weeks (vs. the nominal, impulsive start). The  
 681 resulting low frequency and steady circulation is the same either way the integration is started. This result  
 682 is consistent with the fundamental notion of the quasi-geostrophic system, that the most important winds  
 683 and currents are close to geostrophic balance to which the higher frequency near-inertial motions do not  
 684 contribute significantly. The resolution of the high frequency motions, as is required in a shallow water  
 685 model, is a computational burden that might thus be better avoided. It should be noted, however, that the  
 686 usual quasi-geostrophic system makes other approximations (constant layer thickness, and a constant,  
 687 background  $f$ , though with  $\beta$ ) that are not consistent with some aspects of the shallow water solutions

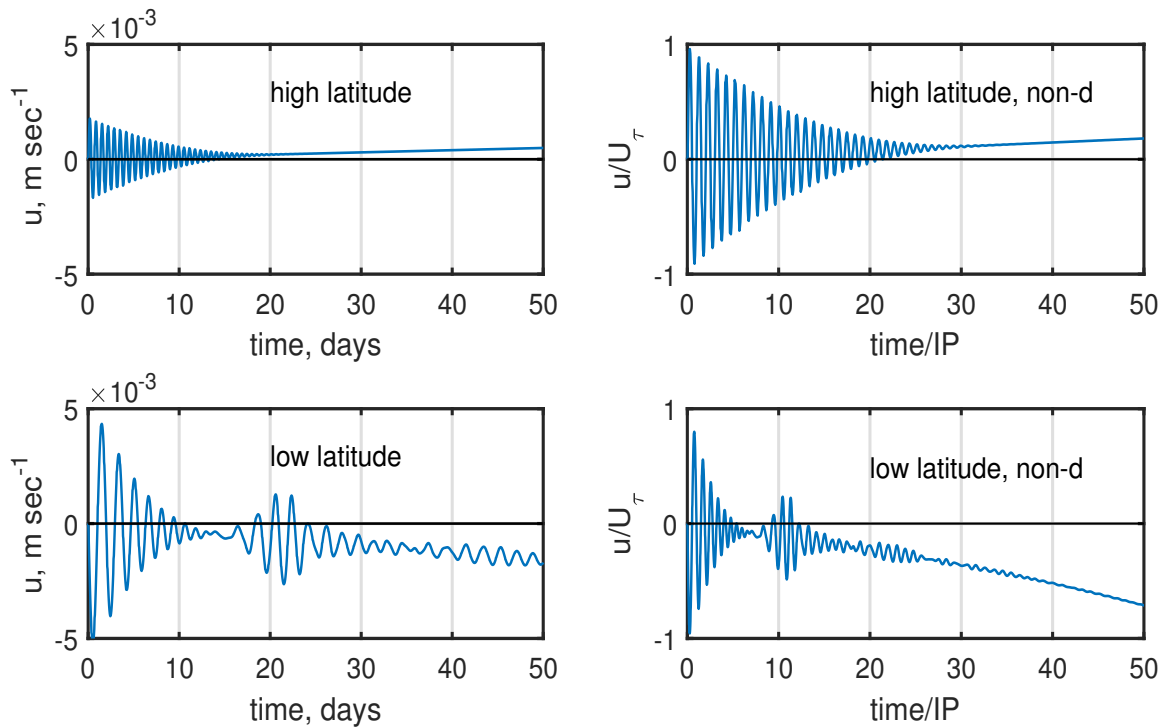


Figure 9: The zonal or  $u$  component of velocity sampled at two sites, (**upper row**) a comparatively high latitude site on the axis of the westerly winds, and (**lower row**) a low latitude site, the axis of the easterly winds. The data are plotted in dimensional format (**left column**) and in a non-dimensional format (**right column**). The former emphasizes the significant differences in the response due to the differing latitude, while the latter makes clear that the sites have two things in common; the amplitude of near-inertial motion goes as  $U_\tau$  and the period of the oscillation is approximately the local inertial period.

688 found here.<sup>13</sup>

### 689 3.1.4 Latitudinal dependence, scaling, and the equator\*

690 A subtheme of this essay is the latitudinal dependence of ocean circulation. With respect to the steady  
691 circulation, the natural demarcation of latitude is by gyre, i.e., supolar gyre, subtropical gyre. At this

<sup>13</sup>Most GFD texts (footnote 4) include a discussion of quasi-geostrophic theory, and a superb online source aimed mainly at meteorologists is <http://www.meteor.iastate.edu/classes/mt411/powerpoint/METR4424qgtheory.pdf>

692 stage there are no gyres, and so to investigate how the response varies with latitude we will just pick two  
 693 sites, the easterly and westerly wind maxima, roughly  $15^{\circ}\text{N}$  and  $45^{\circ}\text{N}$ , and consider the zonal,  $u$   
 694 velocity component only (Fig. 9). The data are shown in two formats; in dimensional form (Fig. 9, left  
 695 column) and in nondimensional form (right column) in which the speed is normalized with  
 696  $U_{\tau} = \tau/(\rho_0 f h)$  and time with the local inertial period,  $\text{IP} = 2\pi/f$ . The dimensional format doesn't  
 697 require any explanation (a good thing) but neither does it give anything more than a qualitative hint at  
 698 parameter dependence, i.e., it is clear that the amplitude of inertial motion and the period of the inertial  
 699 motion is greater at lower latitude.

700 Given the non-dimensional format, we can see that the amplitude is  $\approx 1$  at both sites, evidence that  
 701 the amplitude varies as  $U_{\tau}$ , and thus as  $1/f$ . Moreover, the period of the oscillation is very close to 1 IP at  
 702 both sites and thus the period of the high frequency oscillation is  $\propto 1/f$ . Neither of these results is the  
 703 least bit surprising given the solution Eqn. (39), but we could have made these inferences even without an  
 704 explicit solution given the appropriate nondimensional scaling. The latter may be found by dimensional  
 705 analysis and then verified with numerical experiments, a procedure that is generally far more accessible  
 706 than is an explicit solution. If the main goal of a modeling study is to explore and expose parameter  
 707 dependence rather than simulation of an observed case, then the non-dimensional format will generally  
 708 be preferred. That is certainly a part of our goal here, and so we will use nondimensional format (units)  
 709 when it adds value. Otherwise we will stay with more prosaic dimensional units.

710 The equator is noteworthy with respect to latitudinal dependence insofar as  $1/f$  is singular, and  
 711 hence geostrophy and the Ekman relation imply a blowup of the currents. However, rotation, and thus the  
 712 Coriolis force, is not a dominant process on or very near the equator, as the Ekman and geostrophic  
 713 relations presume, and such a blowup does not occur in the numerical solution. A somewhat trivial and  
 714 parochial reason is that the wind stress has been assumed to vanish on the equator. But even with a  
 715 significant equatorial stress included, which is more realistic of the real ocean, near-equatorial  
 716 wind-forced currents are effectively limited by a rapid baroclinic response manifested in (or by)  
 717 equatorial Kelvin wave propagation (Part 3, Sec. 4), which sets up a pressure gradient that opposes the  
 718 wind stress within a couple of weeks. In the experiments that we discuss here, the circulation very near  
 719 the equator is a consequence mainly of the larger scale circulation in the tropical gyre, and so  
 720 (unfortunately) we won't have much occasion to discuss distinctly equatorial phenomena. We will,  
 721 however, see this apparent equatorial singularity crop up again.

## 722 3.2 Stage 2: Long time, local response to wind stress curl

### 723 3.2.1 Divergent Ekman transport changes the stratification

724 An indirect effect of the wind becomes apparent over the next several hundred days as a wind-induced  
 725 change in the stratification (here just layer thickness) and thus the pressure field. The sense of the change  
 726 depends upon the overlying wind stress field: over the northern half of the subtropical gyre, westerly  
 727 winds produce a southward Ekman transport, while over the southern half of the gyre, easterly winds  
 728 produce a northward Ekman transport. The Ekman transport thus converges over the region between the  
 729 westerly and easterly wind maxima, roughly the middle half of the model domain (Fig. 5) and the region  
 730 of the developing subtropical gyre. The thickness tendency due to the converging Ekman transport may  
 731 be calculated from the continuity equation, Eqn. (31) and Eqn. (43),

$$732 \quad \frac{\partial h_{S2}}{\partial t} = -\nabla \cdot (h\mathbf{V}_{\text{Ek}}) = \frac{1}{\rho_o} \nabla \cdot \frac{\mathbf{k} \times \boldsymbol{\tau}}{f} = \frac{1}{\rho_o} \nabla \times \left( \frac{\boldsymbol{\tau}}{f} \right), \quad (44)$$

733 where the subscript *S2* indicates that this is the Stage 2 response only, and not the full thickness tendency  
 734 that will include divergence of the geostrophic transport as well. In the special case considered here that  
 735  $\boldsymbol{\tau}$  is  $\tau(y)$  only, then

$$736 \quad \frac{\partial h_{S2}}{\partial t} = \frac{1}{\rho_o} \frac{\partial}{\partial y} \left( \frac{\tau^x}{f} \right) = \frac{1}{\rho_o f} \left( \frac{\partial \tau^x}{\partial y} - \frac{\beta}{f} \tau^x \right), \quad (45)$$

737 and includes terms proportional to the wind stress curl and to  $\beta$  times the meridional component of the  
 738 Ekman transport. Both terms are important during the Stage 2 response and notice that the greatest  
 739 magnitude of thickness change within the (eventual) subtropical gyre occurs at about  $y = -1000$  km  
 740 during the initial several hundred days (Fig. 10, upper). As the flow continues to develop, the location of  
 741 the greatest thickness change migrates northward and eventually stabilizes on  $y = 0$ , which is the center  
 742 of the subtropical gyre and the maximum magnitude of the negative (clockwise) stress curl. There the  
 743 thickness tendency is  $35 \text{ m year}^{-1}$  and positive, indicating an increasing layer thickness. Since the  
 744 interface is pushed downwards by the converging Ekman transport, this sign of thickness tendency is  
 745 often called 'Ekman pumping'. When converted to SSH perturbation via the reduced gravity  
 746 approximation (33), this layer thickness change is equivalent to a SSH change of about  $+0.10$  m per 500  
 747 days, see Fig. (11). This raised SSH implies also a growing high pressure that characterizes the  
 748 subtropical gyre. Over the tropical and subpolar regions, the stress curl is positive and hence the interface  
 749 is raised ('Ekman suction'), the SSH is lowered and pressure is reduced. Notice in Eqn. (45) that for a  
 750 given wind stress curl, the thickness tendency and thus the rate of change of the pressure is  $\propto 1/f$  and so  
 751 for a given stress curl, is greater at lower latitudes.

752 Because the wind stress is constant once the wind stress is switched on, the Ekman pumping-induced

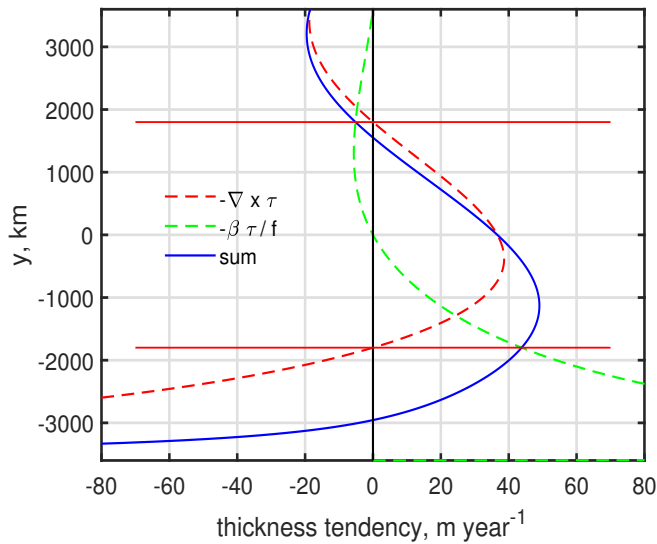


Figure 10: The divergence of the Ekman transport, Eqn. (45) (blue line), given the wind stress field Eqn. (27). This divergence causes thickness tendency, which is a very significant aspect of the wind forcing on the ocean. At higher latitudes the divergence is due mainly to the curl of the wind stress (dashed red line). The beta-induced divergence of the Ekman transport (dashed green line) is very appreciable at lower latitudes.

753 thickness tendency given by Eqn. (45), which starts almost immediately, is also constant in time (the first  
 754 50 days are shown in Fig. 7, lower panel). The actual thickness rate of change (inferred from Fig. 11) is  
 755 constant for a period of time that defines what is called here Stage 2 of the transient response. The  
 756 duration of Stage 2 depends very much upon location: at  $(x, y) = (0, 0)$  the thickness rate of change is  
 757 constant for about 1000 days, and then becomes very small as Stage 3 Sverdrup flow begins to develop at  
 758 that site (more on this in the next section). In this experiment — conducted in a closed basin and with a  
 759 wind stress field that is independent of  $x$  — it is very compelling that the duration of Stage 2 is greater  
 760 with greater distance from the eastern boundary. This need not be the case if the important zonal length  
 761 scale comes from the wind field rather than the basin geometry (Sec. 5.3).

### 762 3.2.2 Geostrophic currents accompany the changing stratification

763 The change in layer thickness causes an SSH anomaly,  $\eta$ , and thus a hydrostatic pressure anomaly,

$$764 \quad g\eta = g \frac{\delta\rho}{\rho_o} (h - h_o).$$

765 This pressure anomaly develops very slowly compared to  $1/f$ , and so is accompanied by zonal currents  
 766 that are very close to geostrophic balance,

$$767 \quad u_{geo} = -\frac{g'}{f} \frac{\partial\eta}{\partial y}. \quad (46)$$

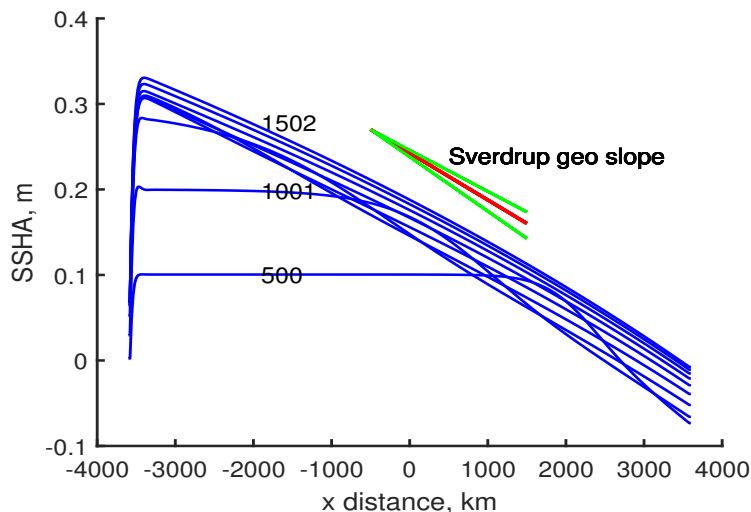


Figure 11: A sequence of sea surface height sections,  $\eta(x)$ , sampled at 500 day intervals up to 5000 days along  $y = 0$ , the center of the subtropical gyre (the colors here are random). These were computed from the layer thickness via the reduced gravity approximation,  $\eta = (\delta\rho/\rho_o)(h - h)$ . The Stage 2 response is a uniform rise of the sea surface, approx. 0.1 m per 500 days at this  $y$ . Stage 3 begins when the sea surface slopes down to the east and becomes quasi-steady; at  $x = 2000$  km (eastern side of the basin) this starts at about 500 days, and at  $x = -2000$  km (western side of the basin) the same thing starts much later, at about 1400 days. At this latitude  $\tau^x = 0$ , and the Ekman transport vanishes. Thus the steady or almost steady meridional transport over the interior region,  $x \geq -3400$  km, is geostrophic transport and may be characterized by sea surface slope. The geostrophic sea surface slope expected from the Sverdrup relation Eqn. (1) for this latitude and average layer thickness,  $h = 580$  m, is the black line that tilts down to the east. The flanking dashed lines are the sea surface slope for  $h = 500$  and  $h = 660$  m, which are found at the eastern and western ends of the section where the slope is slightly less and slightly greater than the average.

768 Substitution of (45) into (46) gives the time rate change of the geostrophic current due to Ekman  
769 pumping alone,

$$770 \quad \frac{\partial u_{S2}}{\partial t} = -\frac{g'}{\rho_o f} \frac{\partial^2}{\partial y^2} \left( \frac{\tau^x}{f} \right), \quad (47)$$

771 and again the subscript  $S2$  denotes that this is relevant to the transient Stage 2 only. Because the stress is  
772 constant once switched on,

$$773 \quad u_{S2}(y, t) = -\frac{g'}{\rho_o f} \frac{\partial^2}{\partial y^2} \left( \frac{\tau^x}{f} \right) t, \quad (48)$$

774 where  $t$  is the time elapsed since the start. In this experiment, the Stage 2 geostrophic current is purely  
775 zonal, since the Ekman pumping varies with  $y$  only, and it is independent of  $x$ , as is the wind stress. This  
776 is bound to fail near an impermeable meridional boundary. It fails also on or very near the equator, where  
777 the Ekman balance is not appropriate.

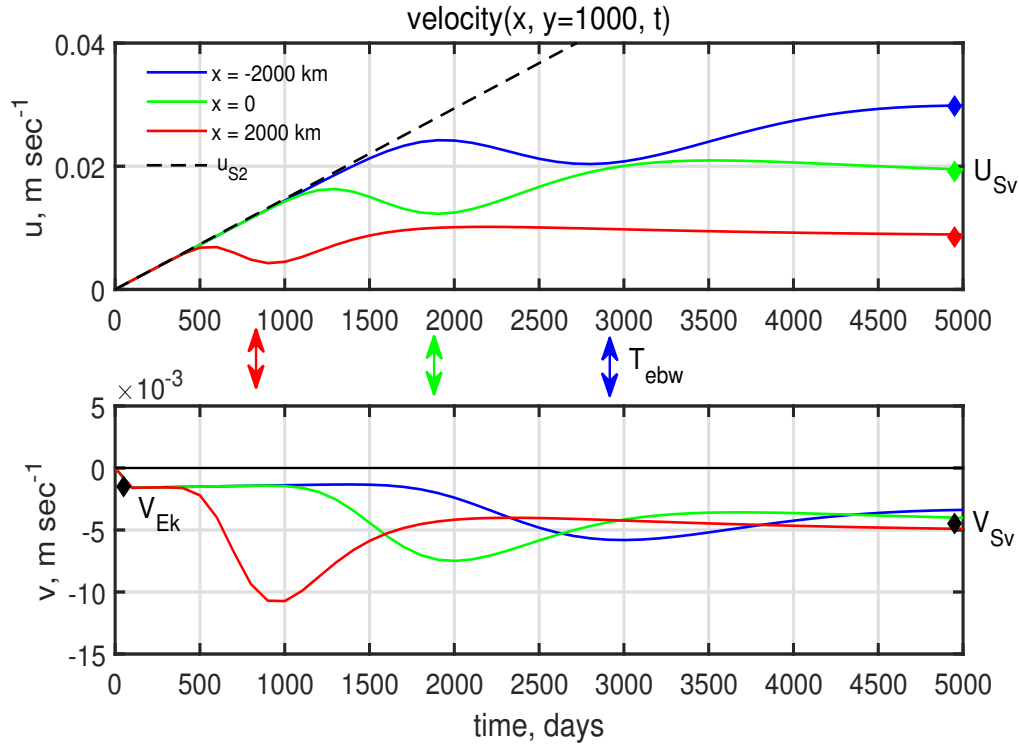


Figure 12: Current components sampled along the northern side of the subtropical gyre,  $y = 1000$  km, at three sites:  $x = 2000$  km (red line),  $x = 0$  (green line), and  $x = -2000$  (blue line), which are nearest to farthest from the eastern boundary. The sampling time interval in this figure, 100 days, misses the inertial motions generated at start up (Fig. 7). (This is, admittedly, a complex figure, but one that will repay patient study.) **(upper)** Zonal or east current component. The dashed black line is the estimate by Eqn. (48) of the zonal geostrophic current produced by Ekman pumping at this  $y$  and is the same at all  $x$ . The actual current follows this very closely for a few hundred or a few thousand days, depending upon distance from the eastern boundary, and then shows a low frequency oscillation as it settles into a quasi-steady state consistent with the expected Sverdrup flow, shown by the colored diamonds on the right margin. Notice that the steady state zonal current increases approximately linearly with distance from the eastern boundary. **(lower)** Meridional or north current component. For short times,  $t \leq 300$  days, this is Ekman flow, Eq. (42), which at this  $y$  is small. The expected Ekman current is noted by the black diamond at left margin. The red, green and blue double arrows denote the time,  $T_{ebw}$ , when a long Rossby wave starting on the eastern boundary at  $t = 0$  is expected to arrive at the corresponding  $x$ . Notice that this coincides approximately with the transition from Ekman flow to Sverdrup flow in the meridional component (lower panel) and to the end of the constant acceleration of the zonal flow (upper panel). The expected Sverdrup flow at this  $y$  and for a nominal  $h$  is noted by the black diamond at right.

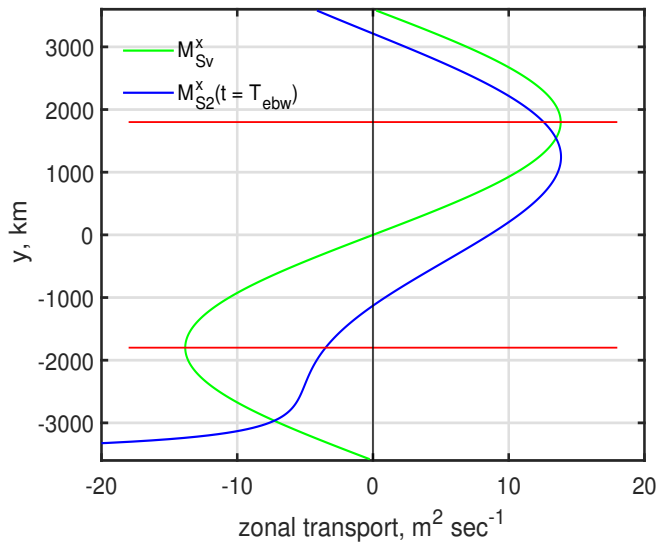


Figure 13: The zonal transport (per unit width) that accompanies the Sverdrup relation (green line) and the Stage 2 zonal current evaluated at  $t = T_{ebw}$  (blue line) argued in Sec. 3.1.3. At higher latitudes these currents are somewhat similar, but they are quite different at lower latitudes. The initial zonal currents in the interior closely match the Stage 2 profile, while the steady state zonal currents follow the Sverdrup profile.

778 The Stage 2 geostrophic current (48) evaluated at  $y = 1000$  km is sketched onto Fig. (12) as a  
 779 dashed black line. It gives a very good account of the actual zonal currents in the interior of the basin for  
 780 a period of time — within the central subtropical gyre, (Fig. 12, the green line was sampled at  $x = 0$ ) Eqn.  
 781 (48) is valid for about 1000 days, just as noted before in the discussion of the Stage 2 layer thickness. The  
 782 duration of Stage 2 depends upon both the latitude, being longer at higher latitudes, and longer also with  
 783 increasing distance from the eastern boundary (the red, green and blue lines of Fig. (12) are at the same  $y$ ,  
 784 but increasing distance from the eastern boundary). An explicit estimate of the duration of Stage 2 will  
 785 become apparent when we consider the onset of Stage 3 in the next section.

786 The Stage 2 geostrophic current given by (48) is proportional to  $1/f^2$ , and, all else equal, is much  
 787 larger at lower latitudes than at higher latitudes (Fig. 13). Most of this essay emphasizes Sverdrup flow  
 788 and western boundary currents, since these transport sea water properties equatorward and poleward  
 789 (subtropical gyre) and so are generally of greater significance for Earth's climate. However, this locally  
 790 wind-forced, zonal current is a robust signal of the time-dependent circulation, and for example the  
 791 response of the tropical ocean to an annually-varying wind (Sec. 1.1.2) appears to be at least in part of  
 792 this kind (more on this in Sec. 5.1).

### 793 **3.3 Stage 3: Blocking by the meridional boundaries and the onset of meridional** 794 **flow**

795 Imagine that the meridional boundaries are removed, and that the no-flow boundary condition on those  
796 boundaries is replaced by a symmetric or reentrant condition that  $u(x = -L) = u(x = L)$ , and the same  
797 for other variables. The domain would then be an east-west oriented channel, as more or less actually  
798 occurs in the Antarctic Circumpolar region. In a channel domain, the zonally-oriented thickness  
799 anomalies and geostrophic currents of the Stage 2 response would grow until the currents either became  
800 unstable and began to spread vertically and horizontally, or, drag on the current reached an equilibrium  
801 with the wind stress. Because the present experiment is set within an enclosed, finite basin having  
802 impermeable meridional boundaries, something quite different happens first: the zonal flow that  
803 approaches a meridional boundary is blocked, and must turn either north or south. The meridional  
804 boundaries thus have the effect of breaking the zonal symmetry that characterizes the Stage 2 response.  
805 As this 'blocking effect' of meridional boundaries becomes important, the overall pattern of the layer  
806 thickness anomaly and geostrophic currents begins to resemble a closed, gyre-like circulation, e.g.,  
807 within the eastern part of the subtropical gyre,  $x > 2000$  km, this is evident by about 500 days (Fig. 6).

808 The meridional flows can be described in two distinctly different regions: by far the greatest part of  
809 the basin develops a very slow Sverdrup flow, and there is a comparatively narrow western boundary  
810 region having a width of about 100 km.

#### 811 **3.3.1 Sverdrup flow in the basin interior**

812 The blocking effect of the eastern meridional boundary — a zonal tilt of SSH and thus a change from  
813 purely zonal to at least partly meridional flow — propagates westwards into the interior of the basin. At  
814  $y = 0$ , equivalent to  $30^\circ$  N, the propagation occurs at the slow but steady rate of about 3 km per day (Fig.  
815 6), which is roughly the westward propagation speed of mesoscale eddies at that latitude (Part 3, and  
816 reviewed briefly in Sec. 1.1).

817 There are two fairly compelling reasons to conclude that this westward propagation of eastern  
818 boundary blocking is the same thing as the westward propagation of a long, divergent Rossby wave  
819 reviewed in Sec 1.1 (and more detail in Part 3, Sec. 2.5). First, the balance of potential vorticity is  
820 consistent with long Rossby wave motions. A  $\beta$ -effect (Part 3) begins immediately with the meridional  
821 component of the current. Because the horizontal scale of the currents is the scale of the wind stress and

822 very much larger than the radius of deformation, the  $\beta$ -effect produces mainly a change in layer thickness  
 823 rather than a change of relative vorticity (Part 3, Section 2.4), which remains very, very small, i.e.,  
 824  $\nabla \times \mathbf{u} \ll f$  (this is not true near the western boundary, however). Thus the potential vorticity balance in  
 825 the vicinity of the spreading eastern boundary blocking is linear and divergent, Eqn. (2), in common with  
 826 long Rossby waves. The motion is also very nearly geostrophic, and so the first order wave equation (13)  
 827 is expected to be valid and predicts this westward propagation. Second, judging from Fig. (6), the  
 828 westward propagation of eastern boundary blocking is markedly faster at lower latitudes. This invites a  
 829 direct comparison to the long Rossby wave speed (Eqn. 12), which has been used to define a gray-shaded  
 830 mask that extends westward from the eastern boundary by

$$831 \quad X = C_{longRo} t = -\beta \frac{C^2}{f^2} t, \quad (49)$$

832 Fig. (6).<sup>14</sup> The long Rossby wave speed varies strongly with latitude; the gravity wave speed  $C$  is  
 833 somewhat reduced at higher latitudes due to reduced stratification, but much more important at this early  
 834 stage is the  $1/f^2$  dependence, which implies much larger  $C_{longRo}$  at lower latitudes. Notice that the  
 835 disruption of the Stage 2, zonal geostrophic flow is indeed closely coincident with the expectations of  
 836 (49) at all latitudes (equator aside, Fig. 6). Given this line of evidence, the westward propagation of the  
 837 boundary blocking effect will be referred to as an 'eastern boundary Rossby wave', or 'ebw', despite that  
 838 the profile  $h(x,t)$  looks nothing like an elementary wave (Fig. 11).

839 The end of the Stage 2 local response to Ekman pumping and the start of the Stage 3 non-local or  
 840 basin scale response may then be estimated by

$$841 \quad \text{Stage 2} \rightarrow \text{Stage 3}: \quad t = T_{ebw}, \quad (50)$$

842 where

$$843 \quad T_{ebw} = -\frac{(L-x)}{C_{longRo}} \quad (51)$$

844 with  $(L-x)$  the distance from the eastern boundary. Thus  $T_{ebw}$  is  $T_{ebw}(x,y)$  since  $C_{longRo}$  varies with  $y$ .  
 845 Subsequent to  $T_{ebw}$ , the volume transport has a significant meridional component that approximates  
 846 Sverdrup balance, Eqn. (1), Figs. (11) and (12), lower.

847 Judging from Fig. (12), the flow does not switch instantaneously from zonal to purely Sverdrup at  
 848  $t = T_{ebw}$ . The eastern boundary wave has a very gradual leading edge, Fig. (11), and a close Sverdrup  
 849 balance requires as much as  $2^*T_{ebw}$ , which can be another few hundred or even a thousand days,

---

<sup>14</sup>The equatorial limit  $f \rightarrow 0$  is handled by assuming that the westward wave speed can be no faster than the fastest, westward propagating equatorial Rossby wave,  $-2C/3 \approx -2 \text{ m sec}^{-1}$ . See Part 3, Sec. 3 for a little more on equatorial wave dynamics.

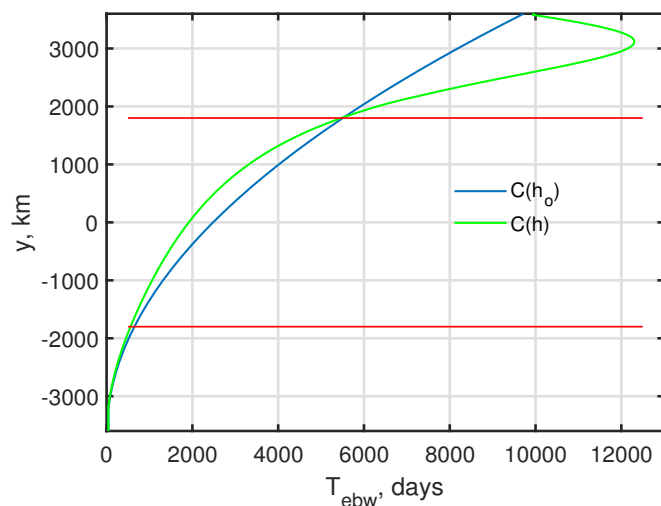


Figure 14: Transit time from the eastern boundary to the western boundary at the long Rossby wave speed. The blue line assumes the nominal layer thickness  $h_o = 500$  m for evaluating the baroclinic gravity wave speed, while the green line uses the actual, steady, zonal average thickness, which is somewhat different, especially in the western part of the sub-polar gyre where  $h \approx 100$  m. The expected transit times for the gyre centers are: tropical gyre, 350 days; sub-tropical gyre, 2500 (2000) days; sub-polar gyre, 7500 (12000) days.

850 depending upon latitude and distance from the eastern boundary. The key point is that the time required  
 851 for the eastern boundary (blocking) effect to reach a given point in the interior is proportional to  $T_{eww}$ , and  
 852 thus is strongly dependent upon latitude and distance from the eastern boundary. In this important  
 853 respect, low latitude oceans exhibit a comparatively fast response to changing wind stress. The  
 854 latitudinal-dependence of the long Rossby wave speed Eqn. (12) is thus a very prominent, qualitative  
 855 feature of the developing gyre circulation in this experiment, and often in the real ocean (Part 3, Sec. 2.6).  
 856 (see Sec. 7.2, 5)

### 857 3.3.2 Western boundary currents

858 At the same time that the interior is developing very slow and broadly distributed currents, something  
 859 quite different is happening near the western boundary. The Stage 2 response includes zonal currents that  
 860 impinge on the western boundary just as much as occurs on the eastern boundary. The result is  
 861 necessarily meridional currents along the western boundary that are subject to a beta effect. Propagation  
 862 of this western boundary blocking into the interior by wave propagation requires an *eastward* group  
 863 velocity. You may recall from Part 3, Sec. 2.3, that while short Rossby waves do have an eastward group  
 864 velocity, the maximum eastward group velocity of baroclinic Rossby waves is very, very slow, only a few  
 865 hundred meters per day, which is just a few percent of the western group velocity of long waves,  $C_{longRo}$ .  
 866 Moreover, eastward group velocity obtains only for short waves,  $kR_d \leq -1$  and  $k \leq 0$ . Such short waves  
 867 are just barely resolved in the present numerical solution, and so it is not too surprising there is very little  
 868 evidence of eastward propagation, and the meridional currents along the western boundary are effectively

869 trapped to the boundary on a width of 50 - 100 km (Fig. 15). As we will see below, the e-folding width of  
 870 the wbc is roughly the local radius of deformation. The resulting western boundary current is  
 871 comparatively very fast, up to  $1 \text{ m sec}^{-1}$ . Within the subtropical gyre, the flow near the western boundary  
 872 is northward, opposite the Sverdrup flow in the interior. It begins to appear within a few hundred days  
 873 after the start of the wind stress, and reaches its full, steady state amplitude in about 1500 days. This is  
 874 about the same time scale on which the subtropical gyre reaches steady state Sverdrup flow.

875 The water that makes up the western boundary current of the subtropical gyre flows into the  
 876 boundary current from the eastern side. This inflow begins with the start of the Stage 2 zonal current, and  
 877 continues into the steady state. Assuming that the inflowing water conserves its potential vorticity and  
 878 that the across stream momentum balance is geostrophic, we can make an estimate of the boundary  
 879 current profile and width. (See Stommel (1966)<sup>4</sup>, Ch. 8, who has an interesting discussion of this applied  
 880 to the actual Gulf Stream.) The relative vorticity is approximated well by the  $x$  variation of the north  
 881 component of the current, and hence the potential vorticity inside and just outside of the western  
 882 boundary current are

$$883 \quad \frac{f + \frac{\partial v}{\partial x}}{h} = \frac{f}{h_0}, \quad (52)$$

884 where  $h_0$  is the thickness just outside the boundary current. If we evaluate this at  $y = 0$ ,  $h_0 \approx 600 \text{ m}$ . The  
 885 momentum balance is very nearly geostrophic,

$$886 \quad fv = g' \frac{\partial h}{\partial x},$$

887 which may be combined with (52) to form a single equation for the boundary current velocity,

$$888 \quad \frac{\partial^2 v}{\partial x^2} = \frac{f^2}{g'h_0} v. \quad (53)$$

889 This has exponential solutions

$$890 \quad v(x) = V_0 \exp(\pm((x+L)/R_d)), \quad (54)$$

891 where  $R_d = \sqrt{g'h}/f$  is the familiar radius of deformation. Suitable boundary conditions are that  $v \rightarrow 0$   
 892 as  $x+L$  becomes large, which selects the minus sign in the exponential, and then we are free to choose  
 893 the amplitude,  $V_0$ . For the central latitude of the subtropical gyre,  $y = 0$  of Fig. (17),  $V_0 = 1.0 \text{ m sec}^{-1}$ .  
 894 The solution for  $v(x)$  is then complete, and the corresponding geostrophic thickness, represented here by  
 895 the SSH anomaly  $\eta$ , may then be easily computed as well (Fig. 17, red lines). These make quite good  
 896 representations of the actual velocity and thickness (or  $\eta$ ), and hence we can conclude that the width of  
 897 the western boundary current is approximated well by the radius of deformation, the natural length scale  
 898 of the shallow water model. That is a neat and satisfying result that we will cite repeatedly in the  
 899 description of the circulation. However, closer inspection and thought suggests that there may be more to

900 this than the simple, local inflow model takes account of. First, this simple model doesn't work so well  
 901 along the northern side of the subtropical gyre,  $y = 1000$  km (upper panel of Fig. 15) where the boundary  
 902 layer current appears to have a reversal offshore that is not captured by the monotonic profile (54). In one  
 903 respect that is not all bad, since that region is characterized by *outflow* from the wbc into the interior, not  
 904 an inflow. So, there is evidently more to the wbc dynamics than just (53). Second, the water that makes  
 905 up the wbc at  $y = 0$ , say, came mostly from lower latitudes, not from a local inflow. If the wbc current  
 906 was  $q$  conserving along stream, then the  $q$  at that latitude should be lower than the local  $q$ . Later we will  
 907 see that frictional effects are expected to be significant in the western boundary current, and friction acts  
 908 to increase  $q$  along the path of the current. Friction implies a length scale that, for the  $r$  used here, is the  
 909 same order as  $R_d$  (Sec. 4.2.2). It appears that while Eqn. (53) works very well in a numerical sense, local  
 910 inflow and  $q$  conservation are not a complete explanation.

911 A very important bulk property of a western boundary current (or any current) is volume transport,

$$912 \quad N_{wb} = \int_{-L}^{-L+L_{wb}} v h dx,$$

913 where  $L_{wb} = 150$  km, by inspection (or several times  $R_d$ ). The speed and the volume transport of the  
 914 western boundary currents (Fig. 16) increase roughly linearly with time until reaching full amplitude and  
 915 steady state several hundreds of days after arrival of the eastern boundary Rossby wave on the western  
 916 boundary; at  $y = 0$ , equivalent to  $30^\circ$  N, this occurs at about 1500 days. As discussed above, the arrival of  
 917 an eastern boundary Rossby wave is not the dramatic event that the words seem to promise. And too, the  
 918 coincidence in time does not imply that the eastern boundary Rossby wave is the cause of the western  
 919 boundary current except in a very indirect way: the arrival of the eastern boundary wave implies that the  
 920 interior region to the east and equatorward (subtropical gyre) is close to being in steady state with regards  
 921 to meridional transport and the Sverdrup relation.

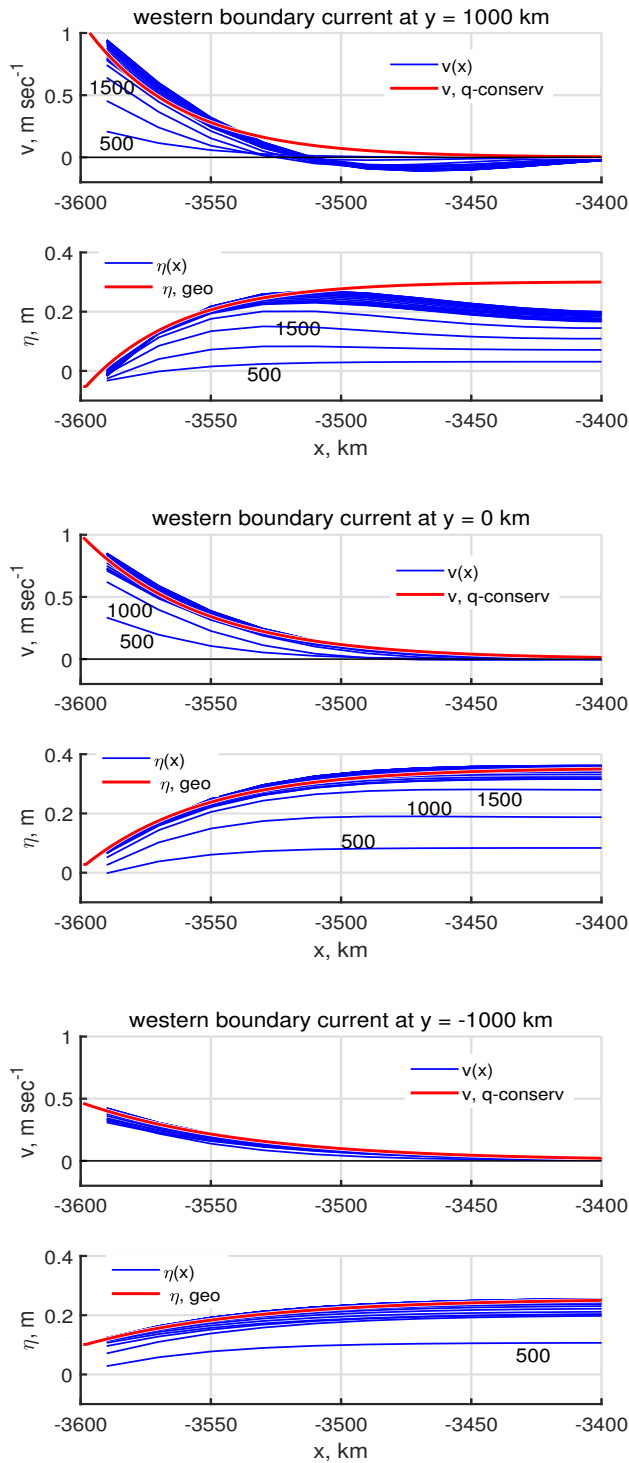


Figure 15: Zonal profiles of the north velocity and the SSH anomaly within 200 km of the western boundary at three sites within the developing subtropical gyre: **(upper)**  $y = 1000$  km, on the north side of the subtropical gyre, **(middle)**,  $y = 0$ , the center of the subtropical gyre, and **(lower)**  $y = -1000$  km, the south side of the subtropical gyre. Profiles are shown as the blue lines at 500 day intervals. The north velocity expected for a q-conserving inflow is shown as the red line, an exponential with the  $x$  scale being the radius of deformation, at  $y = 1000$  km,  $R_d = 36$  km; at  $y = 0$ ,  $R_d = 45$  km, and at  $y = -1000$  km,  $R_d = 64$  km (discussed in Sec. 3.2). The corresponding SSH anomaly profiles are computed from the respective q-conserving velocity using geostrophy (also plotted as a red line). Notice that currents and stratification at the more southerly site (lower panels) reach steady state in about 500 days, while the higher latitude site (upper panels) requires about 2000 days.

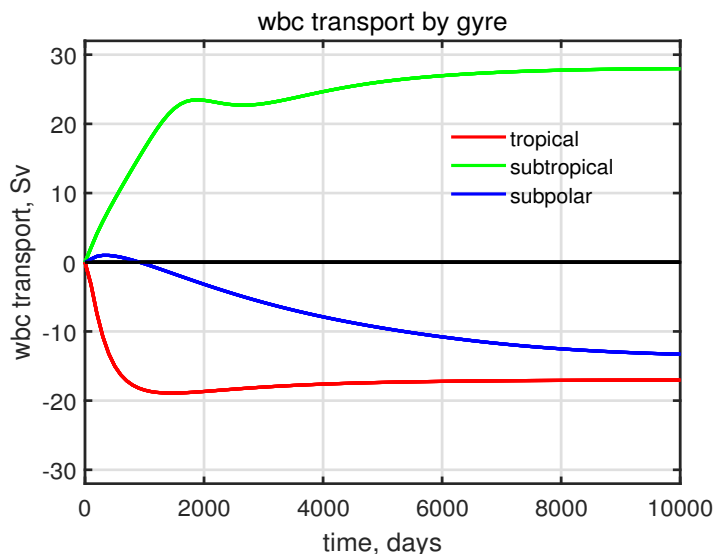


Figure 16: Meridional volume transport  $N_{wb}$  within the western boundary currents of the three gyres. These were sampled at the north-south center of the gyres. Notice that the wbc of the tropical gyre reaches a steady state within about 700 days after the start of the experiment, while the wbc of the subpolar gyre requires much longer, roughly 12,000 days.

922 The immediate cause of a western boundary current is zonal inflow: in the subtropical gyre, there is  
 923 an inflow to the wbc at latitudes  $0 > y > -L/4$ , and an outflow at latitudes  $L/4 > y > 0$ . During the  
 924 first one thousand days of the experiment, the zonal current near the wbc is mainly the Stage 2  
 925 geostrophic flow discussed in the previous subsection. As time runs, the inflow is better described as the  
 926 Sverdrup zonal flow. From this we can infer that the time scale for development of the wbc is  
 927 proportional to  $U_{S2}$  and thus proportional to  $1/f^2$ , i.e., much faster at lower latitudes (Fig. 15, cf upper  
 928 and lower panels). The same attends the volume transports of the wbc in the three gyres: — wbc steady  
 929 state requires about 1000 days in the tropical gyre, and about 10,000 - 12,000 days in the subpolar gyre  
 930 (Fig. 16), a factor of roughly ten.

### 931 3.3.3 Changing stratification\*

932 The western boundary currents of the tropical and subpolar gyres are southward, and opposite the  
 933 Sverdrup flow in those regions. This suggests that perhaps the wbc just mirrors (compensates) the  
 934 Sverdrup flow of the interior. To test this, we can evaluate the volume fluxes over a control volume that  
 935 we are free to choose: for this case, the entire southern half of the basin (the light green shading of Fig.  
 936 17). The areally integrated continuity equation appropriate to a control volume having an area  $A$  is

$$937 \quad A \frac{dh_{avg}}{dt} = \oint h \mathbf{V} \cdot \mathbf{n} ds$$

938 since our shallow water model has no source term, i.e., no mechanism to convert upper layer water to  
 939 abyssal water, for example. Thus the areal-average thickness of the layer within the control volume can

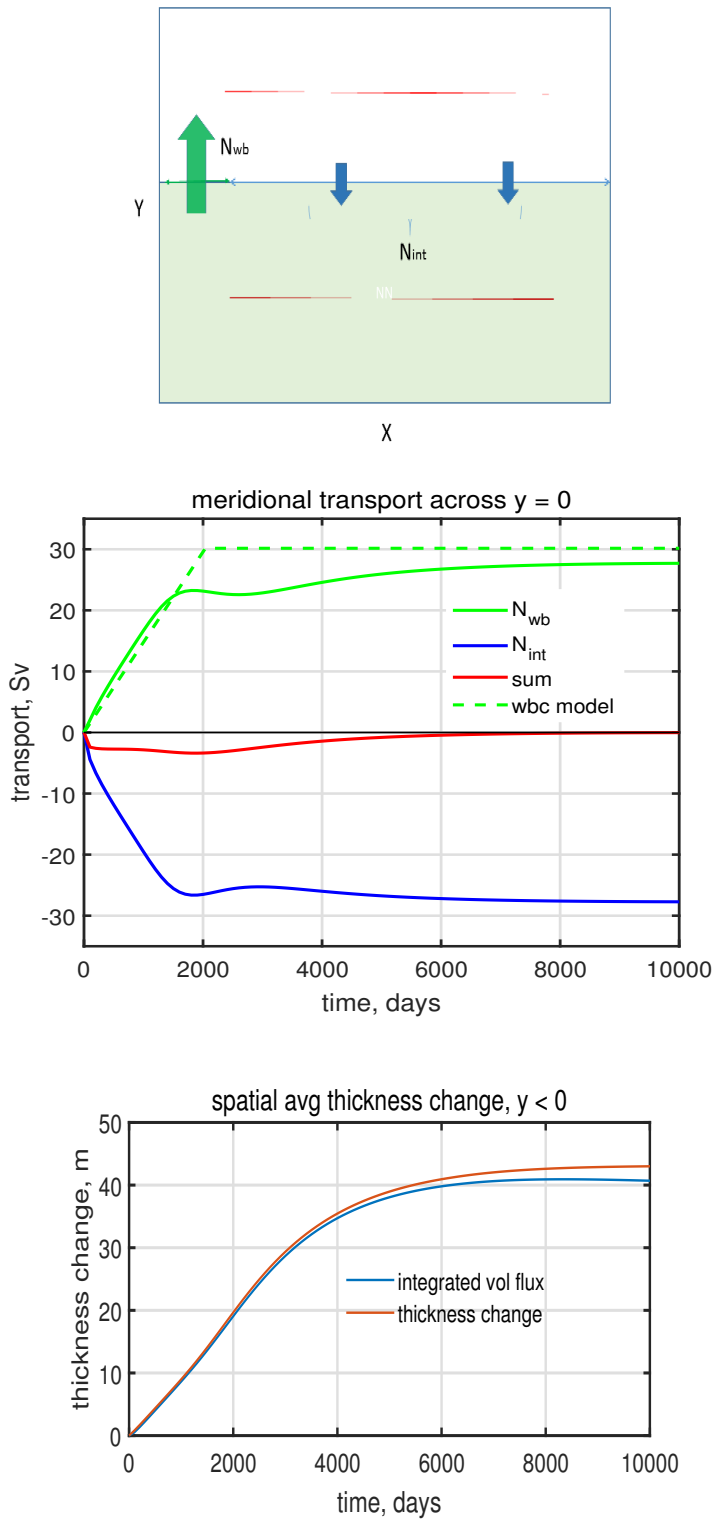


Figure 17: **(upper)** A control volume (light green area A) defined over the southern half of the basin. The volume transport through  $y = 0$  is evaluated over a western boundary,  $N_{wb}$ , and an interior,  $N_{int}$ . **(middle)** The volume transports through  $y = 0$  (green and blue lines) and their sum (red line). The dashed green line is a model of wbc transport, Eqns. (55) and (56). **(lower)** The time-integrated net volume flux into the control volume (blue line) and the observed thickness change over the control volume (red line), about 40 m. Given the adiabatic continuity equation (31), these should be exactly equal.

940 change only if there is a net volume flux across the horizontal sides of the control volume. In practice we  
 941 can break up the line integral into pieces that represent the flow across specific sides of the control  
 942 volume, e.g., in this case

$$943 \quad N_{int} = \int_{-L+L_{wb}}^L v h dx,$$

944 is the volume transport across  $y = 0$  in the interior of the basin (no need to identify this as Sverdrup flow),  
 945 and the volume flux of the comparatively very narrow and intense northward flowing western boundary  
 946 current (Fig. 15) is  $N_{wb}$ , already noted. The integrated mass balance (continuity equation) then reads

$$947 \quad A \frac{dh_{avg}}{dt} = N_{int} + N_{wb}.$$

948 Either of the volume flux terms are considerably larger than the storage term, but they do not sum to zero:  
 949 during the first several thousand days of the experiment there is a small but significant net meridional  
 950 transport across  $y = 0$ ,  $N_{Sv} + N_{wb}$ , (the red line of Fig. 17, middle). The subtropical gyre is a region of  
 951 increased layer thickness, and thus elevated SSH and higher pressure. Indeed, the subtropical gyre is  
 952 characterized mainly by this high pressure (although we discuss mainly the associated currents). The  
 953 volume of fluid required to thicken the layer in the region south of  $y = 0$  is provided by (must be provided  
 954 by) the net (basin-wide) meridional volume flux across  $y = 0$  (Fig. 17, lower). As the region to the south  
 955 of  $y = 0$  reaches a steady state and  $\partial h / \partial t = 0$ , which requires a little more than 5000 days, the net  
 956 volume flux across  $y = 0$  also vanishes. Note that this is a considerably longer than the time required to  
 957 reach a steady state within the subtropical gyre alone.

### 958 3.3.4 A simple model of transport in a time-dependent wbc\*

959 We can construct a very simple estimate of the time-dependent western boundary transport on the  
 960 assumption that the transport will be opposite and equal to the meridional Sverdrup transport to the east  
 961 of the eastern boundary Rossby wave, i.e., as if

$$962 \quad N_{int} + N_{wb} = 0.$$

963 and now  $N_{int} = N_{Sv}$ . While the eastern boundary wave is in transit across the basin,

$$964 \quad 0 < t < T_{ebw}(x = -L, y); \quad N_{wb} = -\frac{\nabla \times \tau}{\rho_o \beta} C_{longRo} t = -N_{Sv} \quad (55)$$

965 The wind stress curl and the long Rossby wave speed are evaluated at the  $y$  of the wbc observation, in Fig.  
 966 (16), the center of the subtropical gyre,  $y = 0$ . After the wave arrives on the western boundary, the

967 western boundary transport is assumed to exactly compensate the steady state Sverdrup transport across  
 968 the basin interior and so for longer times,

$$969 \quad t > T_{ebw}; \quad N_{wb} = constant = -\frac{\nabla \times \tau}{\rho_o \beta} 2L. \quad (56)$$

970 This estimate (55) and (56) is shown as the green dotted line of Fig. (17) middle, and is a plausible first  
 971 description of the actual (numerical) boundary current transport, though far from perfect. There are two  
 972 ways we know that this model and this estimate are inconsistent in detail with the numerical solution: the  
 973 transition from Stage 2 purely zonal, local flow to Stage 3 Sverdrup flow is not instantaneous as Eqn. (55)  
 974 assumes, and, the northward wbc transport does not return all of the southward Sverdrup transport during  
 975 the first several thousand days of the experiment when some fluid is stored at the rate of several Sv within  
 976 the thickening layer south of  $y = 0$ . Those fairly significant details aside, what is most striking and very  
 977 robust is that a wbc develops much faster in the tropical gyre, within very roughly 1000 days, than in the  
 978 subpolar gyre, where the time scale is closer to 10,000 days (Fig. 16). This very large difference in the  
 979 rise time of the wbc in these gyres is a consequence of the  $1/f^2$  dependence of the Stage 2, locally  
 980 wind-forced geostrophic current, Eqn. (48), and of the long Rossby wave transit time, Eqn. (51).

### 981 3.4 Stage 4: Intra- and inter-gyre exchange, and basin-wide steady state

982 The three gyres come into steady state at quite different times, as described above, and clearly the laggard  
 983 is the subpolar gyre. Most of the subpolar region is still in Stage 2 even after 2000 days, and continuing  
 984 to lose volume since  $\nabla \times \tau > 0$  (Ekman suction). The decrease of layer thickness within the subpolar gyre  
 985 is quite pronounced, with  $h$  eventually reaching a minimum of about 100 m just offshore of the western  
 986 boundary current (Fig. 6, bottom). The basin-wide volume of the layer is conserved and so the fluid that  
 987 is expelled from the subpolar gyre is absorbed into the subtropics and tropics where the layers continue to  
 988 slowly thicken more or less uniformly for some time after the thickness slope and the currents have  
 989 become essentially steady. A literal steady state of the subtropics, i.e., constant  $h$  and constant  $\mathbf{v}$ , here  
 990 dubbed Stage 4, requires that the entire basin, subpolar region included, must be swept by an eastern  
 991 boundary Rossby wave. Thus a basin-wide steady state requires an elapsed time

$$992 \quad \text{Stage 4: } t = \max(T_{ebw}) = \frac{2L(f_o + \beta L)^2}{\beta C^2},$$

993 where  $\max$  is evaluated over the basin as a whole. If we use a nominal value of the gravity wave speed,  
 994  $C = 3 \text{ m sec}^{-1}$ , then we find  $\max(T_{ebw}) \approx 9200$  days. In fact, the numerical solution indicates a  
 995 somewhat longer time, closer to 10,000 -12,000 days, mainly because the gravity wave speed is  
 996 significantly reduced within the subpolar gyre (Fig. 14) due to the greatly reduced layer thickness in  
 997 especially the western part of the gyre (Fig. 6, lower panel). (see Sec. 7.2, 4)

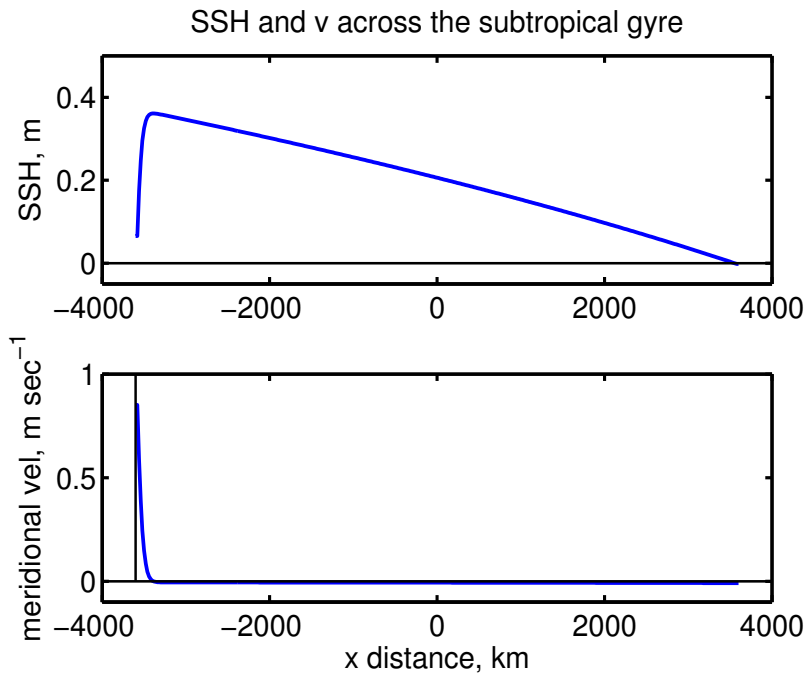


Figure 18: **(upper)** A zonal section of SSH across the center of the subtropical gyre,  $y = 0$ , computed from layer thickness anomaly via the reduced gravity approximation. The basin-scale variation of SSH is much like that seen in the North Atlantic (Fig. 1); a very narrow western boundary current and a broad interior with almost uniform slope down to the east. Notice, though, that the amplitude of the SSH high in this model solution is considerably less than is observed in the real North Atlantic subtropical gyre (about which more in Sec. 7). **(lower)** The meridional velocity along the section above. The velocity is very nearly geostrophic and is northward and very fast in a thin western boundary current, up to about  $1 \text{ m sec}^{-1}$ . The interior, meridional velocity is southward and very slow, a little less than  $0.01 \text{ m sec}^{-1}$ .

## 998 4 The (almost) steady circulation

999 The currents and stratification in the interior of the basin eventually reach an instantaneous steady state,  
 1000  $\partial(\cdot)/\partial t = 0$ . However, there is one region where the flow never becomes even approximately steady, the  
 1001 confluence of the western boundary currents of the subtropical and subpolar gyres at around  $y = 1800 \text{ km}$ .  
 1002 There the colliding western boundary currents meander and produce intense, mesoscale eddies of both  
 1003 signs. The eddies remain close to the western boundary, and do not appear to affect the interior region.  
 1004 The confluence region does become steady in the statistical sense that the eddy amplitude, size and  
 1005 frequency are no longer changing after about 10,000 days. So, whenever we say 'steady' in reference to  
 1006 the basin-wide circulation, read that as a shorthand for steady excepting the wbc confluence region.

1007 One straightforward way to characterize the basin-wide, steady circulation is to simply make a cut of  
 1008 SSH anomaly and northward velocity through the center of the subtropical gyre Fig. (18), which may be  
 1009 compared to Fig. (1). There is a comparatively very narrow western boundary region, e-folding on the  
 1010 radius of deformation and so the full width is  $O(100 \text{ km})$ , within which SSH slopes up to the east and the

1011 current is northward and fast, up to  $1 \text{ m sec}^{-1}$ . Over the much broader interior region — the rest of the  
 1012 basin — there is a quasi-linear decrease of SSH all the way to the eastern boundary (Fig. 18). Given the  
 1013 zonally uniform wind stress curl of the model winds, this nearly constant slope of SSH would be  
 1014 expected for a linear Sverdrup interior for which  $\delta h \ll H_o$ . This is the shallow water model-equivalent of  
 1015 the east-west asymmetry of the observed wind-driven ocean circulation noted as O1 in Sec. 1.1.

#### 1016 4.1 A streamfunction depiction of the circulation

1017 A second useful way to characterize the basin-wide steady circulation is to construct a map of the  
 1018 streamfunction. When the solution is in steady state,  $\partial h / \partial t = 0$ , the volume transport,  $\mathbf{M} = H\mathbf{V}$ , is  
 1019 nondivergent,  $\nabla \cdot \mathbf{M} = 0$ . In that case the vector field  $\mathbf{M}(x, y)$  may be represented by a scalar field, the  
 1020 streamfunction,  $\Psi(x, y)$ , without loss of information. The streamfunction is related to the east and north  
 1021 components of  $\mathbf{M}$  by

$$1022 \quad \frac{\partial \Psi}{\partial y} = HU \quad \text{and} \quad \frac{\partial \Psi}{\partial x} = -HV, \quad (57)$$

or in a vector form,

$$\mathbf{M} = -\mathbf{k} \times \nabla \Psi$$

1023 where the upper case  $H$  and  $U, V$  are the steady state thickness and velocity components. The sign  
 1024 convention of (57) is arbitrary, and may be reversed in some applications. The streamfunction may be  
 1025 computed from the vector field by integrating either of (57). Here we integrate the  $HV$  term westward,  
 1026 starting from the eastern boundary,

$$1027 \quad \Psi(x, y) = \Psi(L, y) - \int_L^x H(x, y)V(x, y)dx. \quad (58)$$

1028 The dimensions (units) of this streamfunction is volume transport,  $\text{m}^3 \text{ sec}^{-1}$ . The volume transport of  
 1029 major ocean currents is in the range  $1 - 150 \times 10^6 \text{ m}^3 \text{ sec}^{-1}$  and often reported in a non-SI but widely  
 1030 used and accepted unit, 'Sverdrups', with  $1 \text{ Sv} = 10^6 \text{ m}^3 \text{ sec}^{-1}$ . The normal component of the velocity  
 1031 vanishes on all of the side walls, and hence  $\Psi(L, y) = \text{constant}$ , that may as well be taken to be zero. It  
 1032 would be equally valid to perform an integration of  $HU$  in the  $y$  direction. The resulting streamfunction  
 1033 lines (Fig. 19, left) are everywhere parallel to  $\mathbf{M}$ , and hence the streamfunction makes a very clear  
 1034 presentation of the direction of the underlying vector field. With this choice of sign, lower values of  $\Psi$   
 1035 are to the right of the vectors (which is opposite the geostrophic relationship for SSH). The density of  
 1036 streamfunction lines is proportional to the magnitude of  $\mathbf{M}$  and notice that  $\partial \Psi / \partial x$  is very large in thin  
 1037 western boundary regions where the wbc current is correspondingly very large compared to the currents  
 1038 in the interior of the basin.

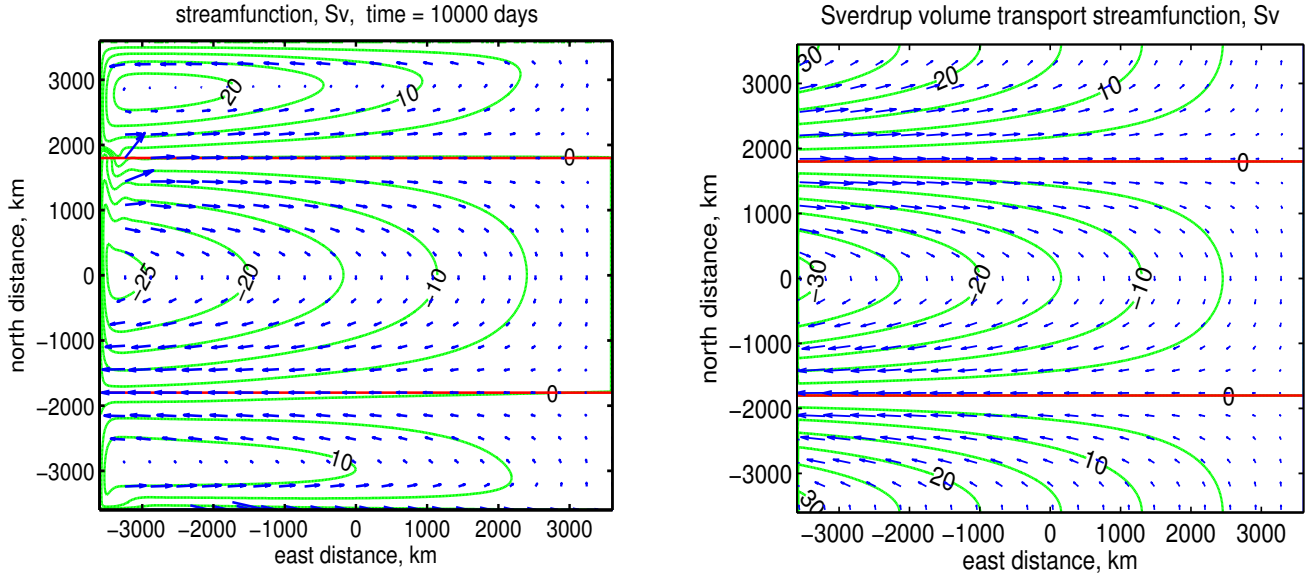


Figure 19: **(left)** The volume transport streamfunction (green lines) computed from the steady state numerical solution by integrating Eqn. (58) starting from the eastern boundary. Labeled in Sverdrups,  $10^6 \text{ m}^3 \text{ sec}^{-1}$ . The blue vectors are the volume transport per unit width,  $\mathbf{M}$ , and are parallel to lines of constant streamfunction. The very large  $\mathbf{M}$  vectors in the western boundary regions are omitted here but shown in a later Fig. 14. The red horizontal lines are the axes of the westerly and easterly winds, and also approximate gyre boundaries. **(right)** The Sverdrup volume transport streamfunction (green lines) computed from the wind stress of the numerical experiment (Fig. 5) and Eqn. (59) and starting from the eastern boundary. In the numerical model-computed streamfunction field at left,  $\Psi = 0$  is found on all of the boundaries, indicating no normal flow through the boundaries, as should hold exactly. The Sverdrup streamfunction at right can not satisfy a zero normal flow condition on more than one boundary, here chosen to be the eastern boundary.

1039 Sverdrup transport may also be represented by a streamfunction (Fig. 19, right), here computed  
 1040 from Eqns. (1) and (58) and integrating westward from the eastern boundary,

$$1041 \quad \Psi_{Sv}(x, y) = \Psi_{Sv}(L, y) + \frac{1}{\rho_o \beta} \int_L^x \nabla \times \tau(x, y) dx. \quad (59)$$

1042 The starting value is taken to be  $\Psi_{Sv}(L, y) = 0$  for all  $y$ , which ensures that there is no normal flow  
 1043 through the eastern boundary. Since only one integration is needed to compute  $\Psi_{Sv}$ , no other boundary  
 1044 data may be applied and so the Sverdrup streamfunction can not satisfy a no normal flow condition  
 1045 through any of the other boundaries. In this case the stress curl  $\nabla \times \tau(x, y) = -\partial \tau^x / \partial y$  and independent  
 1046 of  $x$  and hence the streamfunction is

$$1047 \quad \Psi_{Sv}(x, y) = -\frac{(L-x)}{\rho_o \beta} \frac{\partial \tau^x}{\partial y}. \quad (60)$$

1048 The zonal component of mass transport is then

$$1049 \quad HU = \frac{\partial}{\partial y} \Psi_{Sv}(x, y) = - \frac{(L-x)}{\rho_o \beta} \frac{\partial^2 \tau^x}{\partial y^2}, \quad (61)$$

1050 and the meridional component is Sverdrup transport,

$$1051 \quad HV = - \frac{\partial}{\partial x} \Psi_{Sv}(x, y) = - \frac{1}{\rho_o \beta} \frac{\partial \tau^x}{\partial y}, \quad (62)$$

1052 as expected.

1053 A comparison of the two streamfunction fields (Fig. 19) is one way to see where Sverdrup balance is  
 1054 valid in the numerical solution. The steady circulation in this experiment consist of three gyres within  
 1055 which the meridional flow has the sign of the wind stress curl, e.g., equatorward in the subtropical gyre  
 1056 where  $\nabla \times \tau < 0$ , and so qualitatively consistent with the Sverdrup relation Eqn. (1). Each of these gyres  
 1057 is very strongly compressed onto the western side of the basin in the sense that the largest SSH and thus  
 1058 the largest pressure anomaly is found about a hundred kilometers offshore of the western boundary. (see  
 1059 Sec. 7.2, 6)

1060 Another and more quantitative way is to evaluate the interior meridional transport for all  $y$ , Fig (20).  
 1061 The Sverdrup relation gives a fairly accurate account of the meridional transport over the interior of most  
 1062 of the subtropical gyre, and to a much lesser degree, the subpolar and tropical gyres. The Sverdrup  
 1063 relation is clearly not valid within about 100 km of a western boundary as discussed in Sec. 3.3, nor is it  
 1064 valid within roughly 500 - 1000 km of the northern and southern zonal boundary regions. In the zonal  
 1065 boundary regions the Sverdrup relation indicates significant meridional flow which does not happen in  
 1066 the numerical model solution. What is perhaps surprising is how broad the affected zonal boundary  
 1067 regions are (more on this in Sec. 4.3). One consequence of such broad zonal boundary regions is that the  
 1068 transport of the western boundary currents of the tropical and the subpolar gyres is somewhat less than is  
 1069 the transport of the subtropical gyre, which is not similarly affected by a zonal boundary (Fig. 16).

## 1070 4.2 Dynamics of the steady circulation: the balance of potential vorticity

1071 The dynamics of the circulation may be described most fruitfully in terms of the balance of potential  
 1072 vorticity, Eqn. (35), here expanded and multiplied by  $H$ ,

$$1073 \quad \beta VH = \frac{1}{\rho_o} \nabla \times \tau - rh_o \nabla \times \mathbf{V} + HOT, \quad (63)$$

$$1074 \quad \textit{beta} = \textit{curl tau} + \textit{curl drag} + \textit{higher order terms}.$$

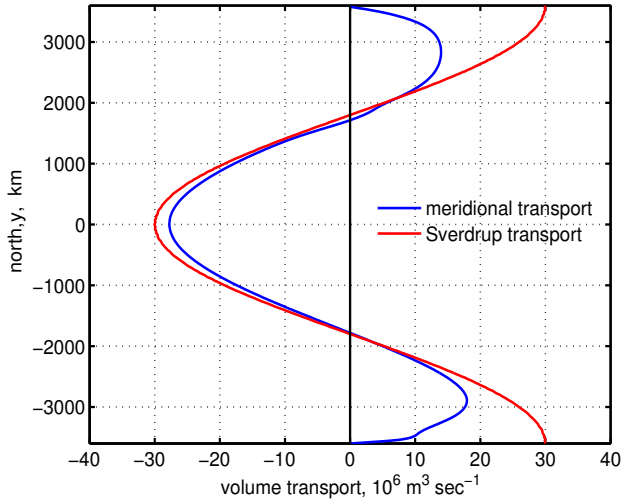


Figure 20: The north-south variation of the zonally-integrated meridional transport computed from the steady model solution (blue line) and computed via the ideal Sverdrup transport relation, Eqn. (1) (red line). The integration extends from the eastern boundary to just outside of the western boundary current. Notice that the actual (numerical) meridional transport vanishes on the zonal boundaries at  $y = \pm 3600$  km due to a no normal flow boundary condition. This is something that the Sverdrup relation (red line) can take no account of. The north-south extent of the affected zonal boundary region is 500 - 1000 km, which is a significant part of the tropical and subpolar gyres.

1075 The higher order terms are the collected nonlinear terms involving the advection of potential vorticity and  
 1076 the gradient of layer thickness;

$$1077 \quad HOT = -H\mathbf{V} \cdot \nabla \xi + h_o H Q \mathbf{V} \cdot \nabla H - \frac{1}{\rho_o h} \boldsymbol{\tau} \times \nabla H + \frac{r h_o}{H} \mathbf{V} \times \nabla H.$$

1078 In general, the steady potential vorticity balance includes a contribution from all of these terms, including  
 1079 the  $HOT$ . However, in this solution the nonlinear  $HOT$  terms are important only in special places  
 1080 (marked with red dots in Fig. 21) where large currents are combined with large horizontal gradients, e.g.,  
 1081 the confluence of the subtropical and subpolar western boundary currents near  
 1082  $(x, y) = (-L, L/2) = (-3600, 1800)$  km.

#### 1083 4.2.1 Sverdrup interior

1084 Aside from these important but spatially limited regions, the steady potential vorticity balance can be  
 1085 characterized by the regional distribution of two term balances or modes among the linear terms of Eqn.  
 1086 (63), Fig. (21). One of these, the Sverdrup mode,

$$1087 \quad \beta V H = \frac{\nabla \times \boldsymbol{\tau}}{\rho_o}, \quad (64)$$

$$1088 \quad \text{beta} = \text{curltau},$$

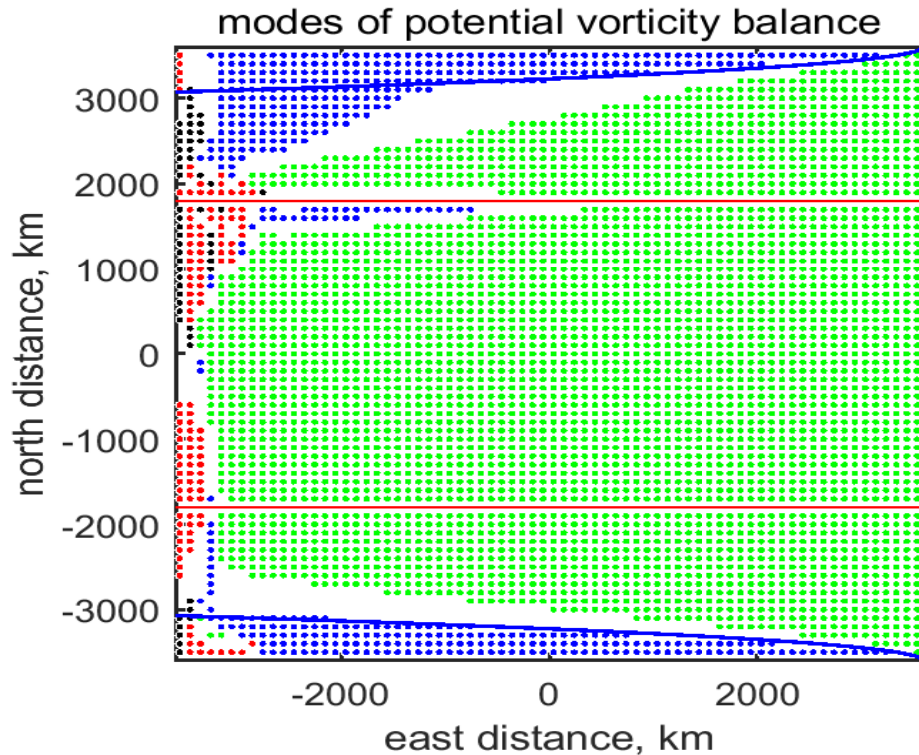


Figure 21: The steady potential vorticity balance characterized by the distribution of the modes (approximate two term balances) of Eqn. (63). Horizontal red lines are the gyre (wind stress curl) boundaries as before. A **green dot** indicates that the Sverdrup mode,  $\beta = \text{curl}\tau$ , accounts for more than 90% of the variance of the steady potential vorticity balance at that point. This (approximate) Sverdrup balance holds over about 75% of the basin. A **black dot**, shows where  $\beta = \text{drag}$  is the dominant mode, mainly near the western boundary. A **blue dot** indicates the mode  $0 = \text{curl}\tau + \text{drag}$  found near the northern and southern zonal boundaries. A **red dot** indicates that the *HOT*, the collection of nonlinear terms, was larger than two of the linear terms. If there is **no colored dot**, then there is no dominant mode, and the balance of potential vorticity is shared among at least three of the terms of Eqn. (63). The blue lines near the northern and southern zonal boundaries are a simple, linear estimate of zonal boundary region width that is discussed in Sec. 4.2.3.

1089 accounts for at least 90% of the variance of the potential vorticity balance over most of the interior region  
 1090 of the basin (the green dots of Fig. 21), especially within the subtropical gyre, and which is often and  
 1091 appropriately called the Sverdrup interior.

1092 Eqn. (35) describes the potential vorticity balance at a fixed point. Consider a site in the subtropical  
 1093 gyre interior where the wind stress curl is negative, which by itself would cause  $Q$  to decrease with time.  
 1094 A steady state will occur if the meridional flow advects higher  $Q$  water from the north at the same rate  
 1095 (opposite sign) of the stress curl. Since the potential vorticity in the interior is approximated well by the

1096 planetary vorticity,  $Q \approx f/h_o$  (with  $h_o$  a constant), then this occurs by the advection of planetary vorticity,  
 1097  $V\partial f/\partial y$ , as if  $f$  was a fluid property. For this steady, Sverdrup balance to exist throughout the interior of  
 1098 the basin, there must be some mechanism that serves to recharge the higher latitudes (within the  
 1099 subtropical gyre) with high  $Q$  water, or specifically, with water having  $Q \approx f/h_o$ . What is the source of  
 1100 this high  $Q$  water? The western boundary current, described next. (see Sec. 7.2, 7)

#### 1101 4.2.2 Western boundary currents

1102 The Sverdrup balance certainly does not hold within the western boundary currents (Figs. 18 and 19),  
 1103 where the meridional current is counter to the Sverdrup flow. The beta effect on a fast-flowing wbc  
 1104 current is in any case far larger than can be balanced by the curl of the wind stress (as occurs in the  
 1105 Sverdrup interior), and so in this model the steady vorticity balance within a wbc is mainly between the  
 1106 beta effect and the curl of the friction, 'drag',

$$1107 \quad \beta VH \quad \approx \quad - \quad rh_o \nabla \times \mathbf{V}, \quad (65)$$

$$1108 \quad \textit{beta} \quad \quad \quad \textit{drag}.$$

1109 For example, the western boundary current of the subtropical gyre has very large negative relative  
 1110 vorticity (Fig. 15) , and a correspondingly large, positive, curl of the friction, or 'drag'. This drag largely  
 1111 balances the negative vorticity tendency of the beta effect, allowing a steady state within the subtropical  
 1112 wbc. Regions where this frictional balance holds in the sense described above are denoted by the black  
 1113 dots in Fig. (21), and are very near the western boundary in all three gyres.

1114 To characterize this balance we can define an Ekman number equivalent for the vorticity balance,

$$1115 \quad E_Q = \frac{\textit{drag}}{\textit{beta}} = \frac{r \nabla \times \mathbf{V}}{\beta V}, \quad (66)$$

1116 ignoring signs and taking  $H = h_o$ . The usual Ekman number is the ratio of frictional force to Coriolis  
 1117 force, but in this case we have curl of the friction divided by (compared to) the beta effect (see Problem  
 1118 11, Sec. 7.2). To evaluate  $E_Q$  it is helpful to use a streamfunction representation of the velocity and its  
 1119 curl. Thus

$$1120 \quad V \approx \frac{\Psi}{L_{wb}},$$

1121 where  $L_{wb}$  is the east-west width of the wbc, which for now we will treat as an unknown. Within the  
 1122 narrow western boundary current, the horizontal scale in the x direction (normal to the boundary) is much

1123 less than the scale in the  $y$  direction and hence the curl of the velocity (the Laplacian of the  
1124 streamfunction) is approximately

$$1125 \quad \nabla \times \mathbf{V} = \nabla^2 \Psi \approx \frac{\partial^2 \Psi}{\partial x^2} \approx \frac{\Psi}{L_{wb}^2}.$$

1126 Using these estimates in (66) gives

$$1127 \quad E_Q = \frac{r}{\beta L_{wb}}. \quad (67)$$

1128 If the balance is indeed Eqn. (65), then we can assert  $E_Q \approx 1$  and readily solve for the purely  
1129 frictional wbc width,  $L_{wb} = L_{fric}$  and find

$$1130 \quad L_{fric} = \frac{r}{\beta}. \quad (68)$$

1131 For the present values of  $r$  and  $\beta$ ,  $L_{fric} \approx 50$  km, which is numerically about the same as the (subtropical)  
1132 radius of deformation (Sec. 3.3.2). Said a little differently, for the present  $r$ , the  $Q$  balance of a wbc  
1133 having a width equal to the radius of deformation is significantly frictional. Recall (Sec. 2.3) that in this  
1134 experiment, the value  $r = 1/15$  days, was chosen in an *ad hoc* manner, the minimum  $r$  (least viscous)  
1135 that permitted a near steady state solution. This is a partial rationalization of this choice. However, there  
1136 is no independent means for identifying an appropriate value of  $r$  (that I know of), and so we have to be  
1137 cautious about interpreting the present model solution as if it were a fully realistic model of a real wbc.

1138 To understand the shallow water model solution, at a minimum we need to know what happens  
1139 when  $r$  is changed; say that  $r$  is doubled to  $1/7.5$  days, which makes the solution more viscous. The  
1140 pattern of the Sverdrup interior is unaffected, but the amplitude of the Sverdrup transport is reduced  
1141 slightly, a few percent. The Sverdrup interior is thus not much affected by the choice of  $r$ . The wbc  
1142 becomes somewhat thicker, as (68) indicates it should. Since the wbc transport is reduced and the wbc  
1143 width increased, the wbc speed is reduced considerably, by about 30%. In that event the flow is steady  
1144 throughout the model domain. More interesting is that  $r$  is reduced to half the present value, to  $r = 1/30$   
1145 days. The volume transport in the interior is then a few percent greater and so is a better match to the  
1146 ideal Sverdrup transport. But again the overall pattern of the interior circulation is indistinguishable from  
1147 the nominal experiment. The width of the subtropical wbc is slightly narrower, though not nearly as  
1148 much as the purely frictional boundary layer width (68) suggests, and so it appears that  $L_{wb} = R_d$  is a  
1149 lower limit that obtains for smallish friction. The wbc current speed is slightly greater, by about 10%, and  
1150 so the inertia of the wbc is also greater. The nonlinear terms of the  $q$  balance are enhanced, and the  
1151 colliding western boundary currents at the subpolar/subtropical gyre confluence (on the western  
1152 boundary at about  $y = 1800$  km; the largest red dot region of Fig. 21) are considerably more vigorous  
1153 than in the nominal experiment (Fig. 6, lower). This kind of unstable, eddying flow is an important and

1154 interesting characteristic of nearly all strong ocean currents that are not constrained by topography.  
 1155 However, this aspect of boundary current dynamics is sensitively dependent upon details of the ocean  
 1156 bottom topography and the vertical structure of currents, among others, and so is outside the scope of a  
 1157 shallow water model and of this essay. (see Sec. 7.2, 9, 11)

### 1158 4.2.3 Zonal boundary regions

1159 There are extensive regions adjacent to the zonal boundaries (northern and southern boundaries) where  
 1160 the ideal Sverdrup balance does not hold, as evident in the qualitative mismatch of Sverdrup transport  
 1161 with the actual transport within about 500 to 1000 km of the zonal boundaries (Figs. 19 and 20). As  
 1162 noted at the outset, the Sverdrup balance *per se* is unable to satisfy the boundary condition that the  
 1163 meridional current must vanish on the zonal boundaries, and so if there is wind stress curl on these  
 1164 boundaries (as there is here, Fig. 5) then the Sverdrup balance will necessarily fail; something else must  
 1165 happen. Very near the zonal boundaries there is no meridional velocity and thus no  $\beta$  effect. The steady,  
 1166 linear potential vorticity balance in this model must reduce to the steady, linear, forced, damped mode,

$$\begin{aligned}
 1167 \quad 0 &= \frac{1}{\rho_o} \nabla \times \tau - r h_o \nabla \times \mathbf{V} & (69) \\
 1168 \quad &= \text{curltau} + \text{drag},
 \end{aligned}$$

1169 indicated by blue dots in Fig. (21).

1170 Like the wbc, this boundary region is also anisotropic, but in this case the meridional, north-south  
 1171 scale is much less than the zonal, east-west scale and hence  $\nabla^2 \Psi \approx \frac{\partial^2 \Psi}{\partial y^2}$ . The balance (69) may then be  
 1172 written via the streamfunction as

$$1173 \quad 0 \approx \frac{1}{\rho_o} \nabla \times \tau + r \frac{\partial^2 \Psi}{\partial y^2}.$$

1174 The curl of the drag has to be large enough to balance the wind stress curl in the zonal boundary region,  
 1175 and the question is what zonal boundary layer width,  $L_{zb}$ , is required to achieve this? Estimating  
 1176  $\partial(\ )/\partial y \approx 1/L_{zb}$  and  $\partial^2(\ )/\partial y^2 \approx 1/L_{zb}^2$ , then

$$1177 \quad 0 = \frac{1}{\rho_o} \nabla \times \tau - \frac{r \Psi}{L_{zb}^2}.$$

1178 It is not obvious what  $\Psi$  should be, but as a first guess, let's try the Sverdrup streamfunction, Eqn. (59),  
 1179 even though we know for sure that the Sverdrup  $\Psi$  can not be correct right on the boundary. We can be a  
 1180 little bit bold with this, since we can check the result against the numerical solution. Given a tentative

1181 estimate  $\Psi = (L - x)\nabla \times \tau / \rho_o \beta$ , where  $L - x$  is the distance from the eastern boundary (positive), the  
 1182 boundary layer width is easily found to be

$$1183 \quad L_{zb} = \sqrt{\frac{r(L-x)}{\beta}}. \quad (70)$$

1184 This is sketched onto Fig. (21 as blue lines near the southern and northern zonal boundaries. At the  
 1185 midpoint of a zonal boundary,  $x = 0$ ,  $L_{zb} \approx 400$  km, which is a reasonable estimate of the half-width of  
 1186 the zonal boundary region evident in Figs. (21) and (20). Notice that the region significantly affected by  
 1187 the zonal boundary dynamics (the no dot transition region between the blue and green dot regions) is  
 1188 about twice this width.

1189 The width of this boundary layer estimate decreases toward the east, which is qualitatively consistent  
 1190 with the distribution of modal balances, i.e., a narrower blue region toward the east. An eastward  
 1191 decrease of  $L_{zb}$  arises because, while the vorticity needed to achieve the balance  $0 = \text{curl}\tau + \text{drag}$  on  
 1192 the zonal boundary is uniform along the boundary (recall that  $\text{curl}\tau$  is here taken to be uniform in  $x$ ,  
 1193 which is generally not true over the real oceans, Fig. 4) and hence the zonal current, which is qualitatively  
 1194 the zonal component implicit in the Sverdrup relation, decreases eastward. As a consequence, the  
 1195 north-south horizontal scale over which the current varies must also decrease eastward in order to have  
 1196 the necessary relative vorticity and thus curl of the friction sufficient to balance the curl of the wind stress.

1197 Like the western boundary layer, the width of the zonal boundary regions is expected to be  
 1198 independent of  $f$  and thus should be the same along the southern and northern zonal boundaries since the  
 1199 imposed wind stress is the same on those boundaries (Sec. 4.2). However, judging from the east-west  
 1200 distribution of  $q$ -balance modes found in the numerical model solution (Fig. 21), the zonal boundary  
 1201 layer is in fact markedly wider in the western-most third of the sub-polar zonal boundary region. The  
 1202 reason for this discrepancy is mainly that the subpolar gyre of this numerical experiment has a  
 1203 significantly reduced layer thickness compared to the initial thickness,  $h$  is as little as 100 m in the  
 1204 western subpolar gyre, and hence there is considerably greater drag than is accounted for by the linear  
 1205 equation (69) that presumed  $H = h_o = 500$  m. A straightforward experimental test of this hypothesis  
 1206 follows from setting the imposed wind stress small enough —  $\tau_o = 0.01 \text{ N m}^{-2}$  suffices — that the  
 1207 dynamics are linear in the respect that  $H \approx h_o$  throughout the model domain. In that case the comparison  
 1208 between the numerical and the estimated boundary layer width (70) is quite good throughout. Thus the  
 1209 linear estimate of zonal boundary layer width (70) is valid for a linear problem, and it is straightforward  
 1210 to understand the sense and the approximate magnitude of the finite amplitude effects that occur when  
 1211 there are large spatial variations in layer thickness, as do occur in this numerical solution.

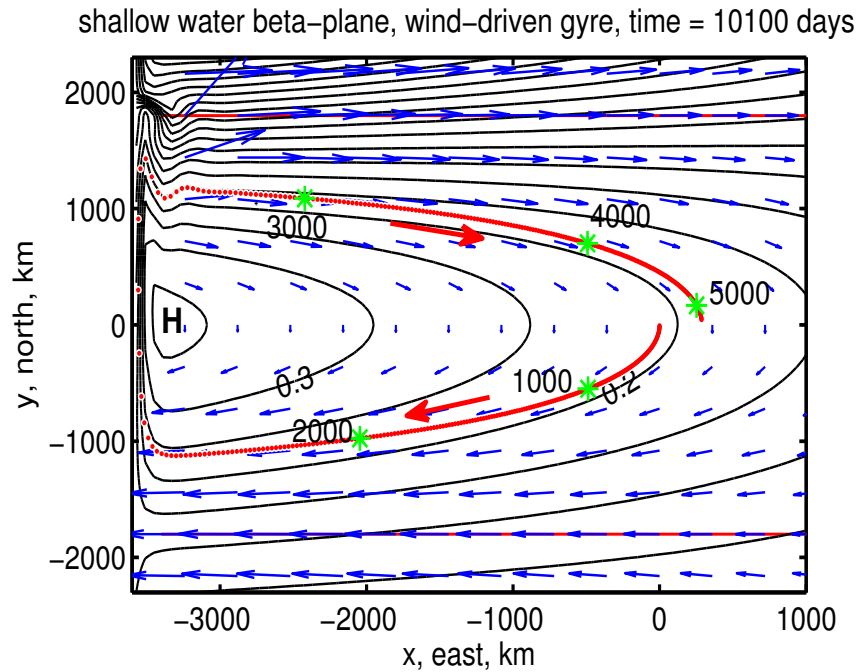


Figure 22: The (almost) steady subtropical gyre, shown by contours of SSH anomaly and a field of velocity vectors. A parcel trajectory that was started at  $(x, y) = (0, 0)$  and followed for 5,500 days is the red line. The green asterisks along the trajectory are at 1000 day intervals. The parcel entered the western boundary current at about 2,600 days after starting, and it exited the western boundary current about 200 days later. The parcel returned close to its starting position. Notice that the trajectory is almost parallel to isolines of SSH, but not exactly so.

### 1212 4.3 A trip around the subtropical gyre

1213 In the previous section, our analysis considered the currents, vorticity, etc., as observed at fixed locations,  
 1214 a point of view often dubbed 'Eulerian'. This is the natural starting point, since the shallow water  
 1215 equations and their numerical implementation are Eulerian. However, our intuition for classical  
 1216 mechanics has roots in a parcel-following, or 'Lagrangian' description, since the  $m$  and the  $a$  of  $F = ma$   
 1217 are the mass and acceleration of a specific chunk of material, and not the fluid properties observed at a  
 1218 point in space (the Eulerian view). In this section we will take this kind of parcel-following view on a  
 1219 complete trip around the gyre. Besides connecting a little better with our intuition for mechanics, this  
 1220 also gives a holistic view of the circulation in that it shows how the western boundary current is an  
 1221 essential component of a steady circulation.

1222 To construct a Lagrangian description we have to solve for parcel trajectories,

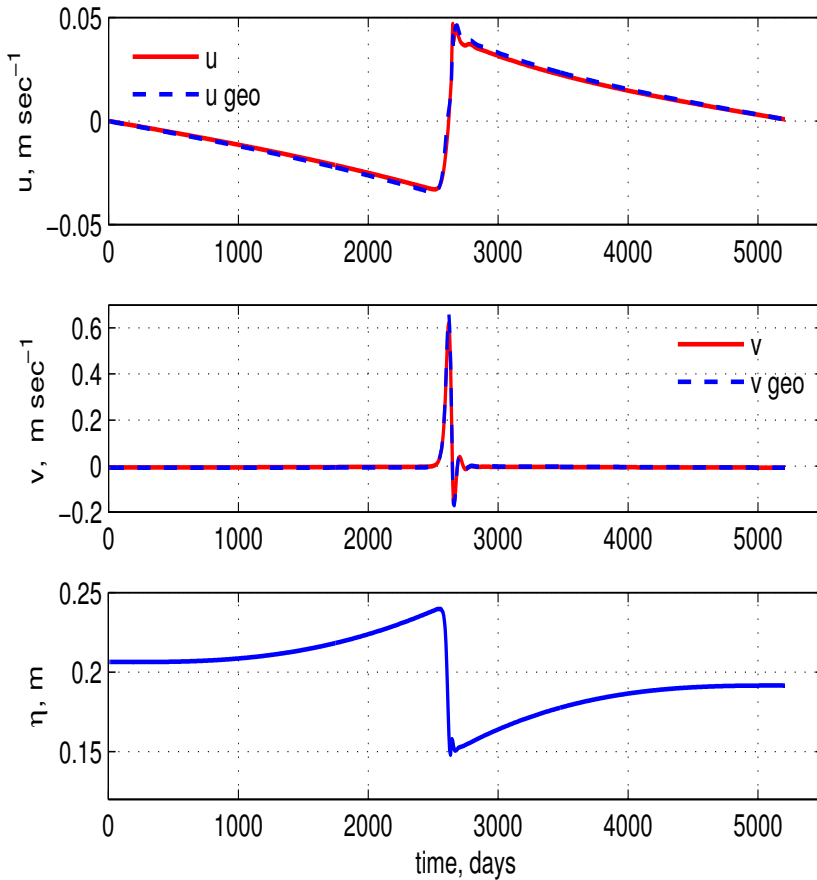


Figure 23: Velocity components along the trajectory of Fig. (22). **(upper)** East velocity (red line) and the geostrophic velocity estimated from the layer thickness (dashed blue line). **(middle)** North component of velocity. Note the very large change in the scale compared to the east component above. The actual velocity and the geostrophic velocity are close enough that the lines are difficult to distinguish. **(lower)** The SSH anomaly along the trajectory. While within the interior region, the parcel slowly climbs the SSH high of the subtropical gyre. While in the wbc, it descends comparatively very rapidly.

1223  $X(t; (X_o, Y_o)), Y(t; (X_o, Y_o))$  by integrating the velocity along the path of a specific parcel,

$$1224 \quad X(t) = \int_0^t U(x, y) dt + X_o, \quad \text{and}, \quad Y(t) = \int_0^t V(x, y) dt + Y_o, \quad (71)$$

1225 where  $(X_o, Y_o)$  is the initial position and the  $t = 0$  here is the time this integration starts (not the starting  
 1226 time of the numerical integration as in Sec. 3). The key thing is that the  $(x, y)$  dependence of the velocity  
 1227 field is continually updated as the integration proceeds, i.e., the  $(x, y)$  in the integrand is set  $= (X, Y)$   
 1228 at each time step. Since the velocity field is available only at the 20 km resolution of the numerical model,  
 1229 the evaluation of velocity at an arbitrary parcel position requires an interpolation of the discrete model  
 1230 data, which is bound to incur some error, much like the finite difference evaluation of a derivative.

1231 The initial position may be chosen anywhere in the model domain; the trajectory shown in red in Fig.  
 1232 (22) was started in the center,  $(X_o, Y_o) = (0, 0)$ . The initial position is, in effect, the tag on the parcel  
 1233 that happened to be there at the time  $t_o$ . Not surprisingly, different initial positions result in different

1234 trajectories. In this circulation, small initial position differences yield only rather small trajectory  
 1235 differences (some examples to follow). A flow having this property may be described as 'laminar'.<sup>15</sup>

1236 A complete trip around the subtropical gyre from this starting position  $(X_o, Y_o) = (0, 0)$  requires a  
 1237 little more than 5000 days and extends over about 11,000 km. If the circulation was exactly steady (it  
 1238 isn't quite), and if the integration method used to construct the trajectory was without error (it can not be),  
 1239 then the parcel would return to it's starting point. Notice that this parcel didn't quite make it (Fig. 22).  
 1240 However, the interesting changes in parcel properties along the track are considerably larger than the  
 1241 starting point/ending point mismatch, and so the semi-quantitative inferences that we can make from this  
 1242 trajectory are reliable.

1243 Assuming that the fluid is not at rest, then there is no Lagrangian steady state comparable to the  
 1244 steady state of an Eulerian frame. Rather, fluid parcels continuously change position and generally all  
 1245 other properties with time. To find say the potential vorticity of the parcel, we can either evaluate the  
 1246 (presumably known)  $q(x, y)$  field at the parcel position, or, integrate the  $q$  conservation equation along the  
 1247 trajectory.

#### 1248 4.3.1 Momentum balance and energy exchanges

1249 The relationship of parcel motion to the local slope of the SSH anomaly (the pressure or geopotential  
 1250 anomaly) is closely analogous to the motion of a dense parcel on a slope studied in Part 1. Differences in  
 1251 detail include that the slope changes quite a lot along the trajectory, especially near the western boundary,  
 1252 and, there is an additional external force, the wind stress, which is essential for compensating the slow  
 1253 but inexorable effects of friction.

1254 During the first several hundred days, the parcel moved very slowly toward the south, which is  
 1255 consistent with the meridional Sverdrup flow at the starting latitude. Eventually, the parcel turned toward  
 1256 the southwest (Fig. 23) and began to pick up some speed. The trajectory was roughly parallel to the SSH  
 1257 lines with higher SSH to the right. Thus the parcel motion was, to a first approximation, geostrophic.

1258 An important departure from strict geostrophy is that the parcel had a rather small but systematic  
 1259 component of motion across the SSH lines. While the parcel was in the interior, it slowly climbed up the

---

<sup>15</sup>If instead the sensitivity to initial position was large, then the flow would be characterized as chaotic or turbulent. Most large scale fluid flows, and including the real ocean circulation, are turbulent in this sense.

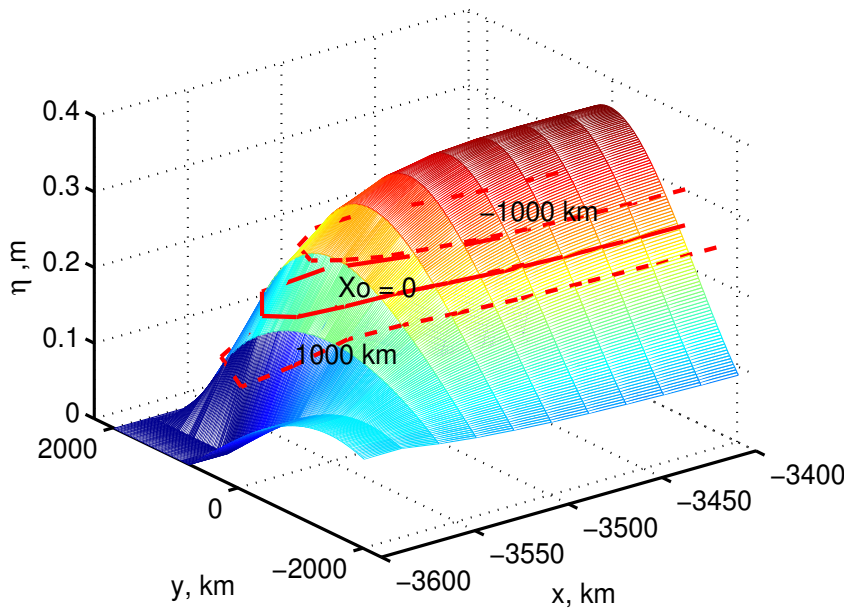


Figure 24: Three trajectories superimposed on the SSH anomaly,  $\eta$ , of the western side of the subtropical gyre. The trajectories differ in their starting points,  $X_o$ , that is noted. The solid red trajectory has  $X_o = 0$  and is shown also in Fig. (22). Notice that the  $x$  scale is greatly expanded compared to the  $y$  scale so that the very large zonal slope of SSH within the wbc and its relationship to these trajectories is apparent.

1260 SSH high of the subtropical gyre. The damping effect of friction causes the parcel to descend the local  
 1261 SSH slope, though at a very small angle consistent with the small Ekman number,  $E$  is  $O(0.01)$ . We can  
 1262 therefore infer that the small component of motion toward higher SSH is a consequence of the wind  
 1263 stress. From an energy perspective, the positive wind work that occurred while the parcel was in the  
 1264 interior was stored as potential energy.

1265 After several thousand days, the parcel began to approach the western boundary, where the SSH  
 1266 topography was by comparison, very steep, about two orders of magnitude greater than in the interior. As  
 1267 the parcel neared the western boundary it accelerated to the north, reaching speeds of  $O(1 \text{ m sec}^{-1})$ , or  
 1268 about two orders of magnitude greater than the speeds that characterize the slow, Sverdrup flow of the  
 1269 interior. The parcel motion never showed any significant inertial motion, and the momentum balance  
 1270 remained almost geostrophic (Fig. 23, middle). This implies that the acceleration associated with the  
 1271 steep wbc topography was slowly-varying compared to the rotation time,  $1/f$ . The kinetic energy  
 1272 associated with the rapid northward flow came from the potential energy that was released as the parcel  
 1273 descended about 0.1 m while within the western boundary current (Fig. 23, lower). There was also some  
 1274 energy loss to friction. After about 200 days, the parcel left the western boundary current and entered the  
 1275 slow eastward flow along the north side of the subtropical gyre. While moving eastward, it slowly  
 1276 climbed back up the high SSH of the subtropical gyre and returned close to its starting value of SSH  
 1277 anomaly.

1278 **4.3.2 Potential vorticity balance**

1279 Potential vorticity conservation provides another way to think of the Sverdrup relation. Given that the  
 1280 field of  $q$  is presumed to be steady at fixed locations,  $\partial q/\partial t = 0$ , then the  $q$  of the moving parcel is just  
 1281 the  $q$  at it's present position (this sounds both profound and trivial at the same, but be sure to understand  
 1282 this before going on) . Moreover, the spatial variation of  $Q$  is due mainly to the spatial variation of  $f$ , at  
 1283 least in the subtropical gyre interior, where the circulation is very slow. The parcel was subject to the  
 1284 overlying wind stress, whose curl was negative, and thus would tend to reduce the  $q$  of the parcel (Fig.  
 1285 25, upper). Since the  $q$  of the parcel had to be consistent with the  $q$  of the presumed steady field, the  
 1286 parcel must move southward toward lower  $q$ , assuming that the  $q$  field is dominated by the meridional  
 1287 variation of  $f$ . Said a little differently, the southward motion of the parcel must be just sufficient to keep  
 1288 the  $q$  of the parcel consistent with the steady field of potential vorticity,  $(\nabla \times v + f)/h$ . In the subtropical  
 1289 gyre, the spatial variation of  $q$  is due mainly to the latitudinal variation of  $f$ , and hence we are led to the  
 1290 Sverdrup relation. This is a rigorous argument for the Sverdrup relation, given the assumptions of a  
 1291 steady, linear  $q$  balance. However, it feels awfully thin as an explanation for existence of the circulation  
 1292 in the first place. And of course, so does the usual (Eulerian) Sverdrup relation.

1293 It is a fair surmise that a parcel can not be subject solely to a negative wind stress curl, or else the  
 1294 basin-wide average of  $q$  would surely decrease with time, which is not consistent with the steady state of  
 1295 the Eulerian circulation. It must be the case that parcels occasionally experience a process that increases  
 1296  $q$  — a (relatively) quick pass through the western boundary current where there is a very strong, positive  
 1297 curl of the drag. This positive drag curl resets the parcel's  $q$  to a value that is consistent with the interior  $q$   
 1298 (Fig. 25) where it reenters the Sverdrup interior. Thus the western boundary current is a crucial part of  
 1299 the gyre-scale circulation with respect to potential vorticity.

1300 **4.3.3 Depth dependence\***

1301 The shallow water form of the Sverdrup relation implies that the wind stress acts upon the entire layer of  
 1302 thickness  $h$  that participates in the Sverdrup transport. That is indeed exactly what happens in a shallow  
 1303 water model, but not within the real ocean. Instead, the Sverdrup transport occurs within an Ekman layer  
 1304 of thickness  $d_{Ek}$  that is typically  $O(100\text{ m})$  that absorbs all of the direct wind stress, i.e.,  $\tau(z < -d_{Ek}) = 0$ ,  
 1305 and a geostrophic layer that is much thicker,  $O(1000\text{ m})$ . If the wind stress penetrates no deeper than 100  
 1306 m, say, then how is the much thicker geostrophic layer affected by the wind? The answer is vortex  
 1307 stretching contained within the  $z$ -dependent vorticity equation, (20), but not in the integrated Sverdrup  
 1308 relation. Just to be specific, consider the subtropical gyre where the wind stress curl is negative, and so

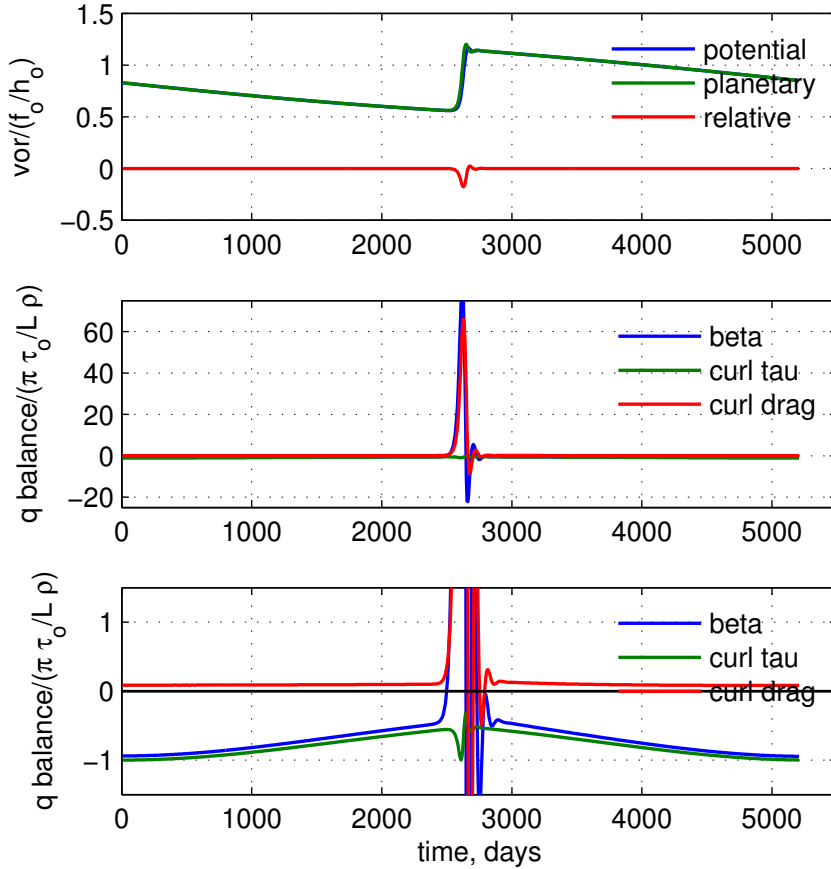


Figure 25: Potential vorticity along the trajectory of Fig. (22). **(upper)** The full potential vorticity (blue line), the planetary vorticity (green line) and the relative vorticity (red line). These are normalized by  $f_o/h_o$ . Notice that the relative vorticity is very small except when the parcel is within the western boundary current where it has a maximum magnitude of  $-1/4$  (normalized). **(middle)** Leading terms in the potential vorticity balance, Eqn. (63). These data are normalized by a nominal wind stress curl,  $8 \times 10^{-8} \text{ m sec}^{-2}$ . When plotted at this scale, about all that can be told is that the beta term is approximately balanced by the drag curl term while the parcel is within the western boundary current. **(lower)** Same data as above, but with a clipped ordinate that reveals the interior balance between the beta term and wind stress curl.

1309 that the Ekman layer transport is convergent. The vertical velocity at the base of the Ekman layer due to  
 1310 wind stress curl alone is just  $\frac{1}{f} \nabla \times \tau$  and the beta effect acting upon the meridional component of Ekman  
 1311 transport contributes another  $\frac{\beta}{f} \tau^x$ . The net vertical velocity is then

$$1312 \quad W(-d_{Ek}) = \frac{1}{\rho_o} \nabla \times \left( \frac{\tau}{f} \right).$$

1313 Only the stress at the sea surface appears here, and letting  $d_{Ek} \rightarrow 0$  does not alter the Ekman transport or  
 1314 its divergence. Thus, while it is unphysical, it is not incorrect to imagine that this vertical velocity is  
 1315 present at the sea surface (though in practice it is largest at the base of the Ekman layer). This  
 1316 Ekman-induced vortex stretching is expected to accompany a meridional, geostrophic transport,

$$1317 \quad \beta \int_{-d}^0 V_{geo} dz = f W(-d_{Ek}) = \frac{f}{\rho_o} \nabla \times \left( \frac{\tau}{f} \right), \quad (72)$$

1318 which is the same as Eqn. (24).

1319 There is an important distinction between the shallow water version of Sverdrup transport and the  
 1320 vortex stretching induced transport described above insofar as in the former, all of the water in the  
 1321 Sverdrup layer follows a forced  $q$  balance,  $dq/dt = \nabla \times \tau / \rho_o$ . In that event, all of the water that  
 1322 participates in the Sverdrup transport must go through the western boundary current in order to reset  $q$   
 1323 (this is a Lagrangian description so we use  $q$  vs.  $Q$ ). In the vortex-stretching case, the water that makes  
 1324 up the geostrophic Sverdrup transport follows the linearized  $q$  conservation, i.e.,  $dq/dt = 0$ , or in the  
 1325  $z$ -dependent case,  $\beta v = f \partial w / \partial z$ . In that event, the water that circulates within the gyre need not go  
 1326 through the western boundary current to reset  $q$  to larger values, since  $q$  is not changed by the wind stress.  
 1327 The real ocean is somewhere between these two extremes: some fraction of the water that participates in  
 1328 the Sverdrup transport is directly wind-forced, but not all, or even most.<sup>16</sup>

#### 1329 4.4 Another way to view the Sverdrup relation

1330 The Sverdrup relation implies or requires a steady state not only of potential vorticity but also of  
 1331 momentum, energy, and of the stratification (layer thickness). Consideration of this latter yields what I  
 1332 believe is the most insightful view of the Sverdrup relation.

1333 The east-west tilt of SSH over the subtropical gyre interior implies a meridional geostrophic current  
 1334 that is equatorward and that is divergent (thinning) on account of the beta effect (Sec. 1.3),

$$1335 \quad \frac{\partial h_{geo}}{\partial t} = \frac{\beta h}{f} V_{geo} < 0.$$

1336 Thus a meridional geostrophic current on a beta plane can not, by itself, be steady. Something more must  
 1337 be present, and of course we know that that could be a wind stress and an associated, convergent Ekman  
 1338 transport,

$$1339 \quad \frac{\partial h_{Ek}}{\partial t} = - \left( \frac{\partial h_{U_{Ek}}}{\partial x} + \frac{\partial h_{V_{Ek}}}{\partial y} \right) = \nabla \times \left( \frac{\tau_o}{\rho_o f(y)} \right) > 0.$$

1340 Assuming that the current is the sum of geostrophic and Ekman currents only, then

$$1341 \quad \frac{\partial h}{\partial t} = \frac{\partial h_{geo}}{\partial t} + \frac{\partial h_{Ek}}{\partial t}$$

---

<sup>16</sup>To follow up on this requires a depth-dependent model and some means to specify the depth of the Ekman layer,  $d_{Ek}$ . These are outside the present scope, but note that a landmark advance on the theory of wind-driven circulation was developed along this line by Jim Luyten, Joe Pedlosky and Hank Stommel, 'The ventilated thermocline', J. Phys. Oceanogr., Feb. 1983, [https://doi.org/10.1175/1520-0485\(1983\)013;0292:TVT;2.0.CO;2](https://doi.org/10.1175/1520-0485(1983)013;0292:TVT;2.0.CO;2).

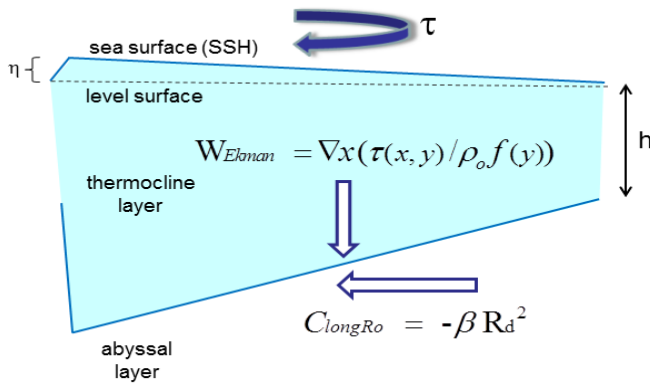


Figure 26: A schematic cross section of the North Atlantic subtropical thermocline, sliced east-west and viewed looking toward the north as in Fig. (1). The wind stress over the subtropical gyre produces an Ekman transport that is convergent and that would tend to thicken the thermocline layer. The Sverdrup relation may be viewed as a steady balance between this positive thickness tendency and the negative thickness tendency associated with the beta effect acting upon the equatorward geostrophic flow.

1342 and a little rearranging gives

$$1343 \quad \frac{\partial h}{\partial t} = \frac{\beta h}{f}(V_{geo} + V_{Ek}) - \frac{1}{\rho_o f} \nabla \times \tau.$$

1344 This is the wind-forced version of the first order wave equation (13) that contains both the Rossby wave  
 1345 propagation mechanism, a balance of the left side and the first term on the right side, and the Sverdrup  
 1346 relation, if the layer thickness is steady.

1347 The large scale thickness field of the subtropical gyre interior may thus be viewed as an arrested,  
 1348 long Rossby wave. The westward translation expected from the  $\beta$ -effect and the first order wave equation  
 1349 is balanced by a wind stress-induced convergence of the Ekman transport. Wind-driven gyres and  
 1350 mesoscale eddies are closely related in as much as they have the same  $\beta$ -effect acting upon meridional  
 1351 flows (this seems obviously true), the difference is that wind stress does not vary appreciably on the  
 1352 horizontal scale of a mesoscale eddy and hence the westward propagation.

## 1353 5 Experiments with other wind fields and basin configurations

1354 The idealized, steady, zonal wind field considered up to here is, of course, just one possibility. In this  
 1355 section we will consider briefly some other, equally idealized wind fields and basin configurations that  
 1356 help reveal several important aspects of the wind-driven circulation.

## 1357 5.1 Annually-varying winds and circulation

1358 The model experiments of Sections 3, 4 and 5 assumed that the wind field was steady, once switched on.  
 1359 That is a reasonable starting point for a study of the wind-driven circulation. However, almost everyone  
 1360 with experience living in a coastal region will attest that the wind over the ocean varies with the seasons,  
 1361 and in some regions it varies quite a lot. For example, the annual variation of the westerlies over the  
 1362 northern North Atlantic is very roughly  $\pm 50\%$  of the annual mean, with the highest winds during winter.  
 1363 The annual variation of easterly wind magnitude is somewhat less, though the annual migration of the  
 1364 Inter-Tropical Convergence Zone (furthest north in summer) produces a large annual variation in the  
 1365 local wind stress curl.<sup>3,11</sup> Meridional winds (not included in this study) show an especially marked  
 1366 annual variation that also contributes significantly to the annual variation of stress curl. Given this large  
 1367 amplitude annual variation, and the day-to-day variation of winds with weather, one might argue that the  
 1368 time-mean wind scarcely exists, outside of our climatologies. This raises an obvious question — what  
 1369 have we missed by considering only the long-term average winds?

1370 Given what we have learned about the response time of the western boundary current, we might  
 1371 guess that an annually varying wind will not have a large effect on at least the western boundary current  
 1372 of the subtropical gyre. But to find out more, let's calculate the solution for an idealized,  
 1373 annually-varying wind stress,

$$1374 \quad \tau^x(x, y, t) = (0.1 + 0.05 \sin(2\pi t/365)) \sin(\pi y/L),$$

1375 where  $t$  is the time in days. Note that this wind stress amplitude varies quite a lot, between 0.05 and 0.15  
 1376 Pa. This annually-varying wind was applied from the start of an integration that was continued past  
 1377 10,000 days. The solution never comes to a steady state, but the annual cycle in the ocean circulation  
 1378 becomes stationary in the sense that it repeats from one year to the next and so the startup transient has  
 1379 been minimized by 10,000 days.

1380 Snapshots of the resulting circulation at times that are near the minimum and maximum response in  
 1381 the tropical gyre are in Fig. (27), and a series of slices through the center of the gyres shows the (inferred)  
 1382  $\eta$  (Fig. 28). The  $\eta(x)$  from the steady wind experiment (red dashed line) runs through the center of the  
 1383 envelope of the time-varying  $\eta(x, t)$ , indicating that the dynamics are effectively linear, i.e., the  
 1384 time-mean of the solution computed with an oscillating wind stress is very nearly the same as the  
 1385 solution computed with the time-mean of the wind stress. The first result of this experiment is that if the  
 1386 steady or long time-mean of the ocean circulation was the only thing of interest, then we would not have  
 1387 to be concerned with resolving explicitly the annual variation of the wind; the long term (yearly or more)  
 1388 time-mean of the wind stress would evidently suffice, at least for this model.

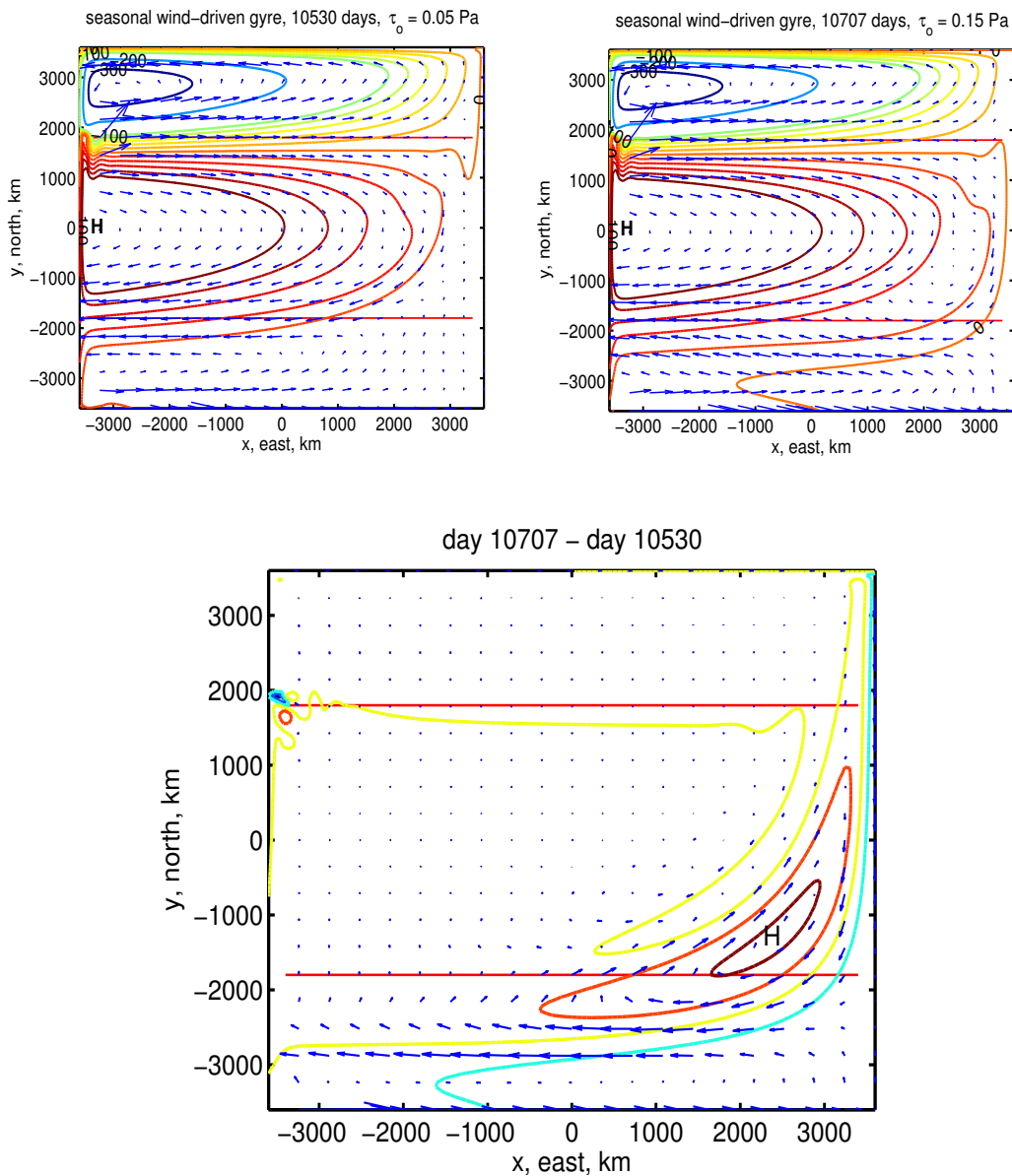


Figure 27: **(upper)** Two snapshots of the circulation taken 180 days apart and near a minimum (left) and maximum (right) of the tropical circulation. The latter occurs about one month after the maximum of the annually-varying wind stress amplitude. An animation of these data is available from [www.whoi.edu/jpweb/seasonal-gyres.mp4](http://www.whoi.edu/jpweb/seasonal-gyres.mp4) **(lower)** The difference of the two snapshots, showing the pattern of the annual cycle. Notice the small, intense eddies near the western boundary at about  $y = 1800$  km, the confluence of the subpolar and subtropical western boundary currents. This kind of time-dependent eddy variability is present even with a steady wind stress.

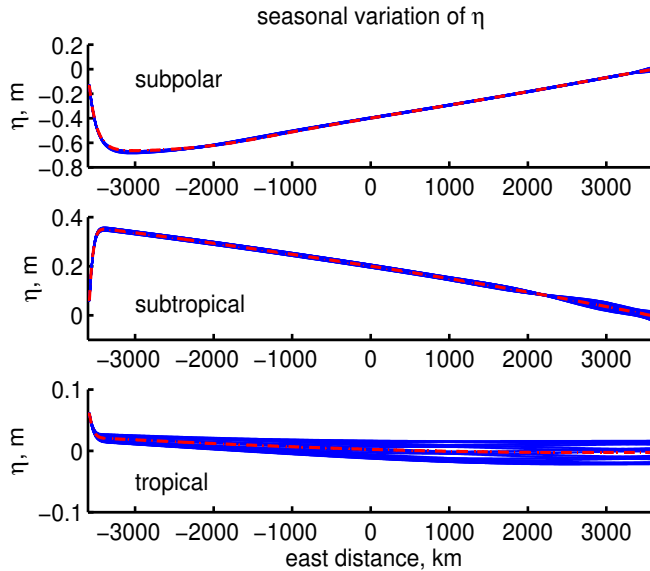


Figure 28: Zonal profiles of SSH,  $\eta(x)$ , from the annually-varying winds experiment. These profiles were taken through the centers of the three gyres noted. The blue lines were taken at 40 day intervals after time = 10,000 days when the solution appeared to be in a statistically steady state. The single red dashed line is a slice through the base case solution having steady winds, and notice that it goes through the center of the envelope of blue lines. Notice too that the  $\eta$  scale differs considerably between the three panels, consistent with the considerably larger  $\eta$  in the subpolar gyre.

1389 A second important result of this experiment is that the amplitude of the annual variation in the  
 1390 ocean varies greatly with latitude. Specifically, the tropical gyre responds much more vigorously to the  
 1391 annually-changing wind than does either the subtropical or especially the subpolar gyre. This is what we  
 1392 should have expected from the start up experiment, which showed a much faster rise of the tropical gyre  
 1393 vs. the subpolar gyre. The amplitude of the annual variation in the ocean depends very much upon the  
 1394 variable of interest. For example, the zonal current sampled on the north side of the middle of the tropical  
 1395 gyre (Fig. 29, solid red line) varies by  $\pm 50\%$  in this experiment, or the same as the wind stress. The  
 1396 explanation for this vigorous low-latitude response appears to be as simple and direct as the  $\propto 1/f^2$   
 1397 dependence of the local, wind-induced (Stage 2) geostrophic current, Eqn. (48). The observed annual  
 1398 variation of zonal currents in the tropics is likely of this sort.<sup>3</sup> There is also an annual period eastern  
 1399 boundary wave that has an appreciable amplitude in the lower subtropics. This wave penetrates only  
 1400 about one wavelength into the interior.

1401 Wbc transport is one measure of the gyre circulation (Rossby et al., 2010, footnote 2): in the  
 1402 subpolar gyre, the wbc transport varies by about  $\pm 0.3$  Sv, in the subtropical gyre by about  $\pm 0.7$  Sv, and  
 1403 in the tropical gyre, by about  $\pm 1.2$  Sv or only about  $\pm 8\%$  (Fig. 30). The latter is much less than the  
 1404 response of zonal current just noted. The western boundary current transport is a bulk property of a gyre,  
 1405 and responds on the time scale of the basin-wide meridional (Sverdrup) flow,  $2L/C_{longRo}$ , Eqn. (51). The  
 1406 long Rossby wave speed is  $\propto 1/f^2$  and much faster within the tropical gyre, but nevertheless, the rise  
 1407 time of the wbc transport of the tropical gyre is many hundreds of days (Fig. 16) and fairly long  
 1408 compared to the time scale of the annually-varying wind, a few months. The response time of the  
 1409 subtropical and subpolar gyres is much longer still, a thousand to many thousands of days, and hence the

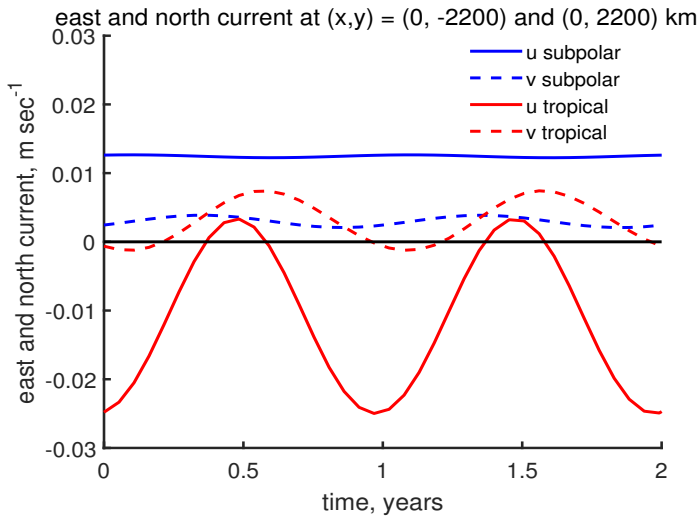


Figure 29: East and north component of the current from the annually-varying wind experiment. The current was sampled at two sites, on the south side of the subpolar gyre (blue lines) and the north side of the tropical gyre (red lines). The current at the high latitude site is almost constant in time despite the annually-varying wind stress. The current at the low latitude site oscillates by about  $\pm 50\%$  around a mean which is very close to the steady state current found in the steady wind stress experiment of Sec. 3.

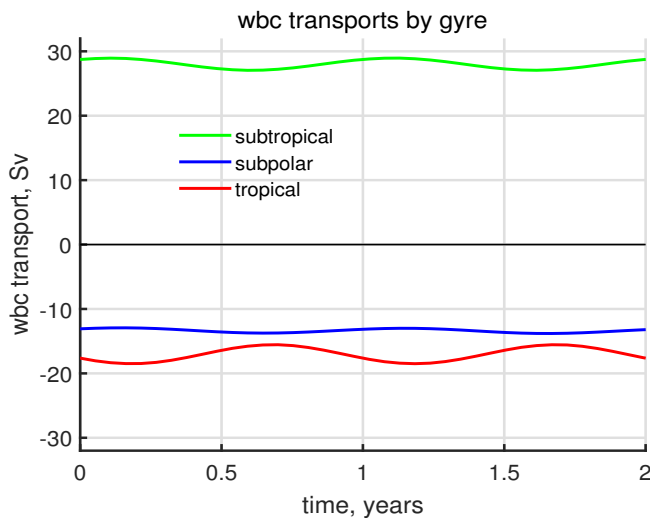


Figure 30: Transports of the western boundary current in each of the gyres from the annually-varying wind experiment. Colors are as in Fig. (16). Notice that the annual variation of the wbc transport in the tropical gyre (red line) is modest when compared to the very large annual variation of especially the zonal current in the interior of that gyre, cf. the red, solid line of Fig. (29).

1410 wbc transport of higher latitude gyres varies even less in response to annually-varying wind.

## 1411 5.2 A stress field with no curl\*

1412 The discussion of wind stress has emphasized importance of the curl of the wind stress curl, rather than  
 1413 the stress itself. And yet, the Ekman transport depends only upon the stress, and the Stage 2 response

1414 includes a term proportional to the  $\beta$ -induced divergence of the Ekman transport, and thus the stress.  
 1415 This raises the question, can there be a steady circulation driven by wind stress alone, that is, by a stress  
 1416 field with no curl?

1417 To find out we can conduct an experiment in which a spatially uniform stress is imposed over the  
 1418 ocean basin. To avoid troublesome instances of vanishing layer thickness near boundaries, the stress is  
 1419 made very small,  $0.01 \text{ N m}^{-2}$ . The amplitude of the resulting currents and layer thickness are also very  
 1420 small, but our interest will be the structure of the response, rather than it's amplitude.

1421 If the spatially uniform stress is eastward, say, then the Ekman transport is southward throughout the  
 1422 basin, and divergent, Eqn. (45). For short times,  $t \leq 1000$  days, this produces a thinning of the active  
 1423 layer (low pressure) that is most pronounced at lower latitudes, while also causing a pileup of water near  
 1424 the equatorial boundary where there is a growing high pressure. The resulting zonal current near the  
 1425 equatorial boundary is thus eastward, and there is a weaker, more distributed westward flow at higher  
 1426 latitudes, evident at  $y > -2000$  km in Fig. (31) (upper and middle).

1427 Just as we have seen before, these zonal currents are necessarily turned into the meridional direction  
 1428 along the eastern boundary, and the result is to initiate a long Rossby wave-like front that propagates  
 1429 westward across the basin. This eastern boundary Rossby wave signals the adjustment toward a steady  
 1430 state, and not too long after the Rossby wave passage the stratification (layer thickness) and flow are  
 1431 indeed quasi-steady. The steady state sea surface (inferred from the layer thickness) slopes up toward the  
 1432 east so that a zonal pressure gradient opposes the wind stress. Most notably, the current in the adjusted  
 1433 steady state vanishes. Absent a curl of the wind stress, there is a vanishing meridional flow in the interior,  
 1434 which comes as no surprise if we have already accepted the Sverdrup relation. Since this applies within a  
 1435 closed basin, neither can there be a steady zonal flow. (see Sec. 7.2, 13)

### 1436 **5.3 Meridional winds over a basin without sidewalls (a channel)\***

1437 One last experiment: consider a basin with dimensions as before, but now replace the no normal flow  
 1438 boundary condition on the eastern and western boundaries with a reentrant boundary condition, i.e., for  
 1439 the zonal velocity,

$$1440 \quad u(x = -L) = u(x = L),$$

1441 as if the basin was a channel that wrapped all the way around a cylinder. Similar boundary conditions are  
 1442 applied to  $h$  and  $v$ . We have had occasion to think about a zonal wind stress acting on a channel of this

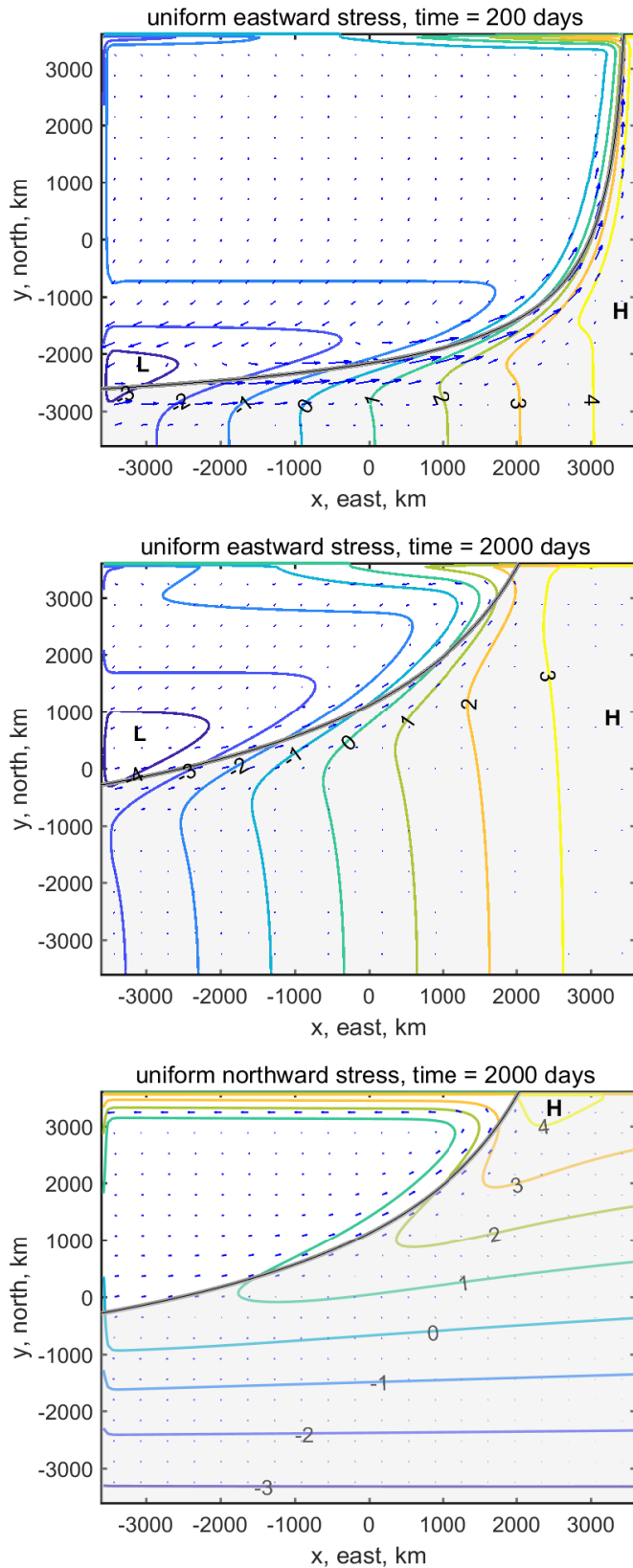


Figure 31: **(upper)** and **(middle)** Two snapshots from a wind-driven experiment in which the wind stress was spatially uniform and eastward at a very small value,  $0.01 \text{ N m}^{-2}$ . The times were 200 and 2000 days after the stress was switched on. The contours are of the anomaly of layer thickness, in meters. The blue arrows are the current, though with the comparatively very large currents within boundary currents omitted. The gray shading extends westward from the eastern boundary at the y-dependent speed of a long Rossby wave. **(lower)** A snapshot at 2000 days from an experiment in which the wind stress was spatially uniform and northward.

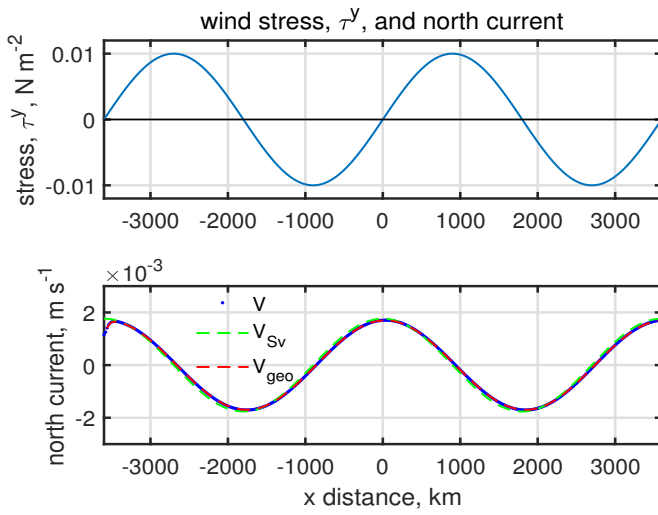


Figure 32: **(upper)** The  $x$  profile of the northward wind stress field applied in the channel experiment. The stress was independent of  $y$ . **(lower)** The north component of current across  $y = 0$  at time = 10,000 days (blue dotted line) along with the expected Sverdrup current (green dashed line) and the meridional, geostrophic current estimated from the thickness field (red dashed line). These are almost identical, and hence the steady meridional flow in this experiment is both geostrophic and Sverdrup, there being no meridional Ekman flow.

1443 sort (Sec. 3.3) and so for this experiment the wind stress is presumed to be in the *meridional* direction.  
 1444 To be consistent with the channel configuration and the reentrant boundary conditions,

$$1445 \quad \tau^y(x) = \tau_0 \sin(2\pi x/L), \quad (73)$$

1446 (Fig. 32, upper) so that  $\tau^y(-L) = \tau^y(L)$  and independent of  $y$ . The stress amplitude is made very small,  
 1447  $\tau_0 = 0.01 \text{ N m}^{-2}$ , to avoid vanishing layer thickness in boundary currents. Meridional winds certainly do  
 1448 occur over the oceans, especially near boundaries, but a basin-wide, meridional wind stress field of this  
 1449 sort is not realistic of any wind stress field observed in nature. Regardless, it does help to make an  
 1450 important point regarding the role of an eastern boundary vis-à-vis the Sverdrup relation. Given the  
 1451 boundary condition (73) the zonal length scale of the stress field will be written

$$1452 \quad L_\tau^x = 2\pi/L,$$

1453 to distinguish from the distance to the eastern boundary that plays such a prominent role in the closed  
 1454 basin cases considered to now.

1455 The Ekman transport that accompanies this meridional wind stress is zonal, and is divergent. The  
 1456 resulting Stage 2 thickness anomaly grows linearly with time as

$$1457 \quad h_{S2} = \frac{\tau_0}{\rho_o f L_\tau^x} \cos(2\pi x/L) t,$$

1458 and forms alternate highs and lows, Fig. (33). The Stage 2 meridional geostrophic current is

$$1459 \quad v_{S2} = \frac{\tau_0 g'}{\rho_o f^2 L_\tau^{x2}} \sin(2\pi x/L) t$$

1460 where  $f$  is  $f(y)$ , and so  $v_{S2}$  is much bigger at lower latitudes (smaller  $y$ ) as we have seen before. Like the  
 1461 Stage 2 response of the closed basin cases, this steadily accelerating current persists for only a finite time,  
 1462 hundreds or thousands of days depending upon  $y$ , after which it is supplanted by a steady or nearly steady  
 1463 Sverdrup balance,

$$1464 \quad v_{Sv} = \frac{\tau_o}{\rho_o L_\tau^x \beta H} \cos(2\pi x/L).$$

1465 In this experiment, where there is no eastern boundary, the near-steady Sverdrup balance develops  
 1466 first at low latitude, and then spreads northward. At a given  $y$ , the adjustment occurs in the time required  
 1467 for a long Rossby wave to propagate westward over the distance  $L_\tau^x$ , the length scale of the wind stress.  
 1468 The northward extent of the adjusted region is then estimated by

$$1469 \quad L_\tau^x = \frac{\beta C^2}{f^2} t, \quad (74)$$

1470 where  $f$  is  $f(y)$ . Using the beta-plane representation of  $f(y)$  and solving for the northward extent of the  
 1471 adjusted region,  $Y$ , gives

$$1472 \quad Y = \sqrt{\frac{C^2}{\beta L_\tau^x}} t^{1/2}, \quad (75)$$

1473 which is used to define the gray shading of Fig. (33). This makes a plausible estimate of the  $y$  that  
 1474 separates the Stage 2 response to the north from the quasi-steady Sverdrup regime to the south. Of course,  
 1475  $L_\tau^x$  is proportional to the basin scale, and so this one case is not completely convincing. The test is that  
 1476 when the east-west scale of the wind stress is made smaller, say  $L_\tau^x = L/4\pi$  and thus  
 1477  $\tau^y(x) \propto \sin(4\pi x/L)$ , while holding the basin width  $L$  constant, the adjustment to Sverdrup balance at a  
 1478 given  $y$  occurs in half the time seen in this case. Thus the relevant east-west scale for adjustment to  
 1479 Sverdrup balance is the zonal scale that is imposed on the meridional flow. In the case of a closed basin  
 1480 with zonal winds that are independent of  $x$ , that scale is the distance to the eastern boundary; in the  
 1481 present experiment, this zonal scale comes directly from the wind field itself.

## 1482 **6 Summary and closing remarks**

### 1483 **6.1 O1: East-west asymmetry of the subtropical and subpolar gyres**

1484 The basin-scale, horizontal structure of the wind-driven ocean circulation, including western  
 1485 intensification and several of the qualitative differences between tropical, subtropical and subpolar gyres,

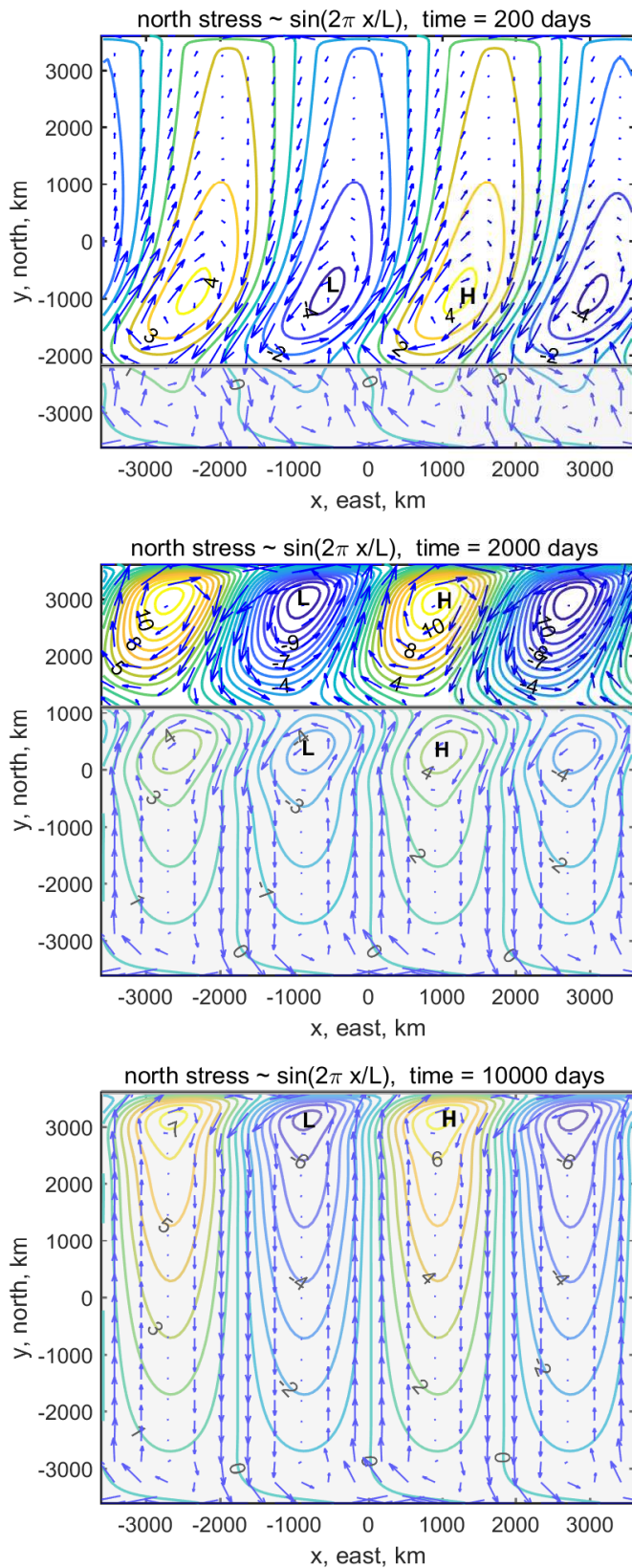


Figure 33: Snapshots from a wind-driven experiment in which the basin is a channel, and the wind stress was northward and  $x$ -dependent (Fig. 32, upper). The stress was set to a very small value,  $0.01 \text{ N m}^{-2}$ . Times were 200, 1000 and 10000 days (upper, middle, lower) after the stress was switched on. The contours are the anomaly of layer thickness in meters and the blue arrows are the current, though with boundary currents omitted. The gray shading extends northward from the southern boundary to a distance  $Y$  determined by the time, the  $y$ -dependent long Rossby wave speed and the zonal scale of the wind,  $L_\tau$ , via Eqn. (75). Poleward of  $Y$  the flow is in Stage 2. Notice that there is clear evidence of westward propagation in especially the southern part of this region. Equatorward of  $Y$  the flow is adjusted to a near steady state Sverdrup balance (Fig. 32, lower). At a given  $y$ , the progression from Stage 2 to Sverdrup flow occurs at the same time across the entire channel (independent of  $x$ ).

1486 have a plausible analog in solutions of the shallow water model. Over the subtropical North Atlantic,  
 1487 where the wind stress curl is negative, the interior meridional flow is southward; the stress curl and  
 1488 interior circulation are reversed in tropical and subpolar gyres, just as expected from the Sverdrup  
 1489 relation. This general result — that the Sverdrup relation provides a plausible and useful explanation of  
 1490 the major wind-driven gyres — has been accepted since at least the 1950s, and has been tested and  
 1491 validated quantitatively in field data-based studies (footnote 5).

1492 The Sverdrup relation is expected to be valid provided that the dominant processes of the potential  
 1493 vorticity balance are just two: the beta effect acting upon a very gentle and thus linear meridional current  
 1494 balanced by the curl (torque) of the wind stress. In practice, this holds in interior regions, well away from  
 1495 zonal or meridional boundaries. In the shallow water model studied here, the north-south extent of the  
 1496 affected zonal boundary regions is rather wide,  $O(1000 \text{ km})$ . This includes a significant part of the  
 1497 subpolar gyre interior, with the result that the meridional and zonal Sverdrup flow of the subpolar region  
 1498 is somewhat less than would otherwise be expected in the absence of the zonal boundary.

1499 In a steady circulation (constant stratification), the meridional Sverdrup transport across every zonal,  
 1500 cross-basin section must be returned in the opposite direction by some other process. In the shallow water  
 1501 model and in the real ocean, this return flow occurs in a comparatively narrow and thus very intense  
 1502 western boundary current (wbc). The wbc is northward in the subtropical gyre where the Sverdrup  
 1503 transport is southward, and reversed in the subpolar and tropical gyres. The width of the western  
 1504 boundary region is observed to be very narrow,  $O(100 \text{ km})$ . In the present shallow water model, the width  
 1505 of the wbc is the baroclinic radius of deformation, the natural length scale of a shallow water model. The  
 1506 inviscid, linear Sverdrup interior fills the rest of the basin, and hence the westward intensification  
 1507 (east-west asymmetry) of the major ocean gyres is very pronounced.

## 1508 6.2 O2: Time scales of the wind-driven circulation

1509 A wind-driven, start-up experiment shows that the circulation at a given point in the interior reaches an  
 1510 approximate, steady, Sverdrup flow some time after the passage of what amounts to a long Rossby wave  
 1511 starting from the eastern boundary. The long Rossby wave speed,  $\beta C^2 / f^2$ , which has a strong  
 1512 dependence upon latitude, is thus a crucial parameter in the time-dependent response of a wind-driven  
 1513 gyre. For a North Atlantic-sized basin, the elapsed time required to reach full steady state is about thirty  
 1514 years at a subpolar latitude, about five years in the subtropics, and much less, about a year, in the tropics.

1515 This marked latitudinal variation in the rise time of the wind-driven circulation is relevant to  
1516 understanding the response to an annually-varying wind stress. Model experiments that assumed a  $\pm 50\%$   
1517 annual period variation of the wind stress find that the subpolar circulation varies almost not at all, the  
1518 subtropical gyre varies only a little, while some aspects of the tropical circulation vary quite a lot. The  
1519 transport of the tropical wbc varies by only about  $\pm 10\%$ , but the zonal flow in the eastern half of the  
1520 tropical gyre varies by  $\pm 50\%$ . This latter variation is partly a response to the local stress curl, and partly  
1521 a Sverdrup flow. Thus a seasonally varying wind stress that will have almost no effect on the subpolar or  
1522 subtropical circulation (interior or wbc) will produce a fairly pronounced response of especially the zonal,  
1523 open ocean SSH and currents in the tropics.

### 1524 6.3 What's gone missing?

1525 This essay has emphasized the basin-scale horizontal structure and the time scales of the wind-driven  
1526 circulation in no small part because that is what the shallow water model can do without misleading us.  
1527 What does the shallow water model miss?

1528 **Amplitude and vertical structure.** The amplitude of the circulation is very important too, of course,  
1529 and here the assessment of the Sverdrup relation in the present idealized solutions is problematic. The  
1530 SSH anomaly in the numerical subtropical gyre (Fig. 11) is about 0.4 m, while the SSH anomaly of the  
1531 North Atlantic subtropical gyre Fig. (1) is considerably greater, more like 1.1 m. The underestimate  
1532 made by the shallow water model is likely contributed by several sources. In the first place, the shallow  
1533 water model gives the meridional volume transport and not SSH *per se*. The gradient of SSH is  
1534 diagnostic of the surface geostrophic velocity, not the water column integral that is volume transport. The  
1535 transport in the numerical model is not sensitive to the stratification. Thus if the model's layer thickness  
1536 is made smaller, say  $h_o = 250$  m, then the current speed is roughly doubled, as is the predicted SSH  
1537 anomaly and slope. The comparatively large initial value of  $h_o$  used here, 500 m, was necessitated by the  
1538 numerical (non-physical) requirement that  $h$  could not be allowed to vanish anywhere in the model  
1539 domain. This is especially at issue for the subpolar gyre where the change in layer thickness was very  
1540 large. This need for a large  $h_o$  is a kluge that betrays a physical deficiency of the present shallow water  
1541 model: a more complete and realistic model physics should include multiple layers in the vertical, as well  
1542 as a vertical mixing process that would serve to keep the directly wind-driven surface layer of the ocean  
1543 finite and realistic no matter what the upwelling might be.

1544 **The overturning circulation and eddy variability.** The discrepancy in SSH amplitude involves much  
1545 more than just a detail of the vertical structure. There is known to be considerably larger transport in the

1546 observed Gulf Stream than is predicted by the Sverdrup relation in numerical ocean models that have  
1547 much better vertical resolution and fully realistic wind fields.<sup>4</sup> The larger-than-Sverdrup western  
1548 boundary current transport in the North Atlantic likely arises from two very different sources. We have  
1549 already had occasion to note that a global scale, meridional overturning circulation contributes about 20  
1550 Sv to the poleward-going, upper ocean transport at the latitude of the subtropical gyre. Deep, cold  
1551 currents, well below the thermocline, provide mass balance across zonal sections. These are completely  
1552 missing from the present shallow water model. As well, the vigorous eddying of the Gulf Stream  
1553 (subtropical western boundary current) is known to produce an intense, and nearly depth-independent  
1554 recirculating gyre which also adds significantly to the poleward transport of the western boundary current  
1555 and so contributes to the large positive SSH anomaly of the observed subtropical gyre. The Sverdrup  
1556 relation applied to the North Atlantic basin certainly isn't wrong, but neither is it the complete story of  
1557 the ocean circulation.

## 1558 **7 Supplemental material**

### 1559 **7.1 Links to models and updated manuscripts**

1560 The code used to solve the wind-drive circulation problems discussed here is very similar to that used in  
1561 the Parts 2 and 3 treatments of geostrophic adjustment and eddy propagation. However, the data required  
1562 to specify the configuration of the wind-driven experiments is sufficiently different that a dedicated  
1563 program was written:

1564 **gyre.for** is a Fortran code that solves the shallow water equations for the wind-driven  
1565 circulation in an enclosed ocean basin. A variety of wind stress forms and time histories may  
1566 be specified. The numerical methods are not highly sophisticated or complex, and the code  
1567 should be fairly amenable to modification. The longest integrations shown here will run in a  
1568 few hours on a fairly capable, PC workstation. Output goes to a Matlab.mat file which may  
1569 be read by a Matlab script,

1570 **gyre\_plot.m** makes several kinds of diagnostic plots from the data generated above.

1571 This model and the most up to date version of these essays may be downloaded from the author's web  
1572 page, <https://www2.who.edu/staff/jprice/>

1573 **7.2 Homework problems**

- 1574 1. At  $30^\circ$  N,  $f = \Omega$ , and the inertial period is  $2\pi/\Omega = 23$  hrs, 56 min, or less than a day by  $\approx 1/365$   
 1575 days. Can you explain where this small difference with a day comes from?
- 1576 2. Starting with Eqns. (5) and (8), eliminate  $v$  to derive the corresponding governing equation for  $h$ . Is  
 1577 it significant that this wave equation is first order vs. the more common second order equation, e.g.,  
 1578 shallow water gravity waves? What is the consequence of the beta effect in the case that the zonal  
 1579 gradient of thickness is positive? Is it relevant that the momentum balance Eqn. (5) is geostrophic?
- 1580 3.
- 1581 4. The steady solution Fig. (6) includes three gyres, tropical, subtropical and subpolar. Contrast the  
 1582 model-computed tropical and subpolar gyres with respect to the magnitude of their currents, layer  
 1583 thickness anomaly, and transports. Compare the solution Fig. (6, lower) with the observed SSH of  
 1584 Fig. (2). Why does the tropical gyre (or region) have a comparatively small SSH anomaly? The  
 1585 subpolar and tropical gyres have roughly comparable anti-clockwise circulations, and yet the wind  
 1586 over the subpolar gyres is westerly, and the wind over the tropical gyre is easterly. But haven't we  
 1587 been saying all along that these gyres are wind-driven?
- 1588 5. Explain the signs and the comparative magnitudes of the current components of Fig. (12). Notice  
 1589 that the Sverdrup meridional flow at the three sites is not identical. Why is there a small but  
 1590 systematic difference?
- 1591 6. The overall pattern of SSH (Fig. 6, lower) and of the transport streamfunction (Fig. 11, left) are  
 1592 similar but not identical. Why is there a difference?
- 1593 7. The potential vorticity derivation of the Sverdrup relation in Sec. 5.1 omitted some important  
 1594 details. 1) Can you show that the drag term in the  $q$ -balance equation for the interior is proportional  
 1595 to the Ekman number times  $L_{Earth}/L_{tau}$ , where  $L_{tau}$  is the horizontal scale of the wind stress field.  
 1596 2) Given speed and space scales of the interior (Sverdrup) flow, show that the relative vorticity of  
 1597 the Sverdrup flow is indeed very, very small compared to planetary vorticity,  $f$ , and so to an  
 1598 excellent approximation the potential vorticity in the interior is given by  $q \approx f/h$ . 3) The advective  
 1599 term of Eqn.(35) may be approximated as Eqn. (13) because the geostrophic flow does not advect  
 1600 layer thickness. What evidence can you find in the steady solution, Fig. (6), that supports this  
 1601 (highly plausible) assertion?
- 1602 8. The real ocean thermocline is continuously stratified in the vertical, and so the best one layer  
 1603 baroclinic model representation of the thermocline will likely have to compromise on something.  
 1604 The values used here,  $H = 500$  m, and  $\delta\rho = 2 \text{ kg m}^{-3}$  are round numbers that give an appropriate

1605 gravity wave speed. What thickness slope is consistent with the Rossby wave view of the  
 1606 subtropical gyre developed in Sec. 4.4, and where is that slope found in the water column of Fig.  
 1607 (1)?

1608 9. Assuming that the boundary current will have a maximum current adjacent to the boundary (and so  
 1609 a single sign of relative vorticity), show that the mode  $\beta = drag$  can obtain also for the case of  
 1610 an equatorward western boundary current as occurs in the tropical and subpolar gyres. Can you  
 1611 envision this balance for an eastern boundary current of either sign?

1612 10. In the discussion of the Stage 3 transient response we noted that the change in the current from  
 1613 Stage 2 zonal flow to meridional Sverdrup flow occurs at a time that is proportional to the transit  
 1614 time of a long Rossby wave starting from the eastern boundary. This suggests an interesting  
 1615 derivation of the Sverdrup relation (albeit for a slightly special wind field) that makes especially  
 1616 clear the crucial role of the eastern boundary in a problem in which there is no other imposed zonal  
 1617 scale. Assume that the wind stress is purely zonal, and is switched on at  $t = 0$  and then held  
 1618 constant, as in the base case. The Stage 2 zonal flow  $u_{S2}$  then grows linearly with time until the  
 1619 arrival of the eastern boundary wave. How does the then extant zonal flow compare with Sverdrup  
 1620 zonal flow? In general, the  $u_{S2}(x, y)$  current is not the same as the steady state Sverdrup zonal flow,  
 1621 since the former depends upon  $\partial^2(\tau/f)/\partial y^2$  and not  $f^{-1}\partial^2\tau/\partial y^2$  as does the Sverdrup zonal  
 1622 current (and see Figs. 10 and 13). To remedy this, suppose that the  $y$  scale of the wind stress field is  
 1623 much less than  $R_E$ . This will result from setting  $n = 6$  in the wind stress Eqn. (27), and thus  
 1624  $\tau^x(y) \propto \sin(6\pi y/L)$ . Can you show that the zonal transport at  $t = T_{ebw}$  is then approximated well  
 1625 by

$$1626 \quad hu_{S2}(t = T_{ebw}) \approx -\frac{(L-x)}{\rho_o\beta} \frac{\partial^2\tau^x}{\partial y^2} = \frac{\partial\Psi_{Sv}}{\partial y},$$

1627 where the last step used Eqn. (61). Why does the zonal transport increases in magnitude in  
 1628 proportion to distance from the eastern boundary,  $L - x$  ?

1629 11. Can you show that the vorticity balance form of the Ekman number appropriate to a western  
 1630 boundary current, Eqn. (66), is related to the usual, momentum balance form  $E = r/f$ , by

$$1631 \quad E_Q = E \frac{L\tau}{R_d}.$$

1632  
 1633 12. Assume a steady, wind-driven circulation. What would you expect to follow if the wind stress  
 1634 suddenly vanished? Check your intuition against [www.whoi.edu/jpweb/wind-off.mp4](http://www.whoi.edu/jpweb/wind-off.mp4)

1635 13. Assume a steady, wind-driven circulation. What would you expect to follow if the wind stress  
 1636 suddenly vanished? Check your intuition against [www.whoi.edu/jpweb/wind-off.mp4](http://www.whoi.edu/jpweb/wind-off.mp4) Now

1637 Imagine an experiment in which the wind stress is spatially uniform over the entire basin, and  
1638 northward. What would you expect for Stage 2 and Stage 3? (Major hint: consider the stress curl.)  
1639 What is the steady response? Once you have formed your answer, take a look at the circulation  
1640 computed from such an experiment shown in Fig. (31, lower).

## Index

- 1641 beta effect, 13
- 1642 eastern boundary
  - 1643 blocking, 38
  - 1644 Rossby wave, 38
- 1645 Ekman currents and transport, 30
- 1646 Ekman pumping and suction, 33
  
- 1647 gyre
  - 1648 exchange, 47
  
- 1649 Rossby wave
  - 1650 arrested, 65
  - 1651 long wave speed, 39
  
- 1652 seasonality
  - 1653 subpolar and subtropical gyres, 7
  - 1654 tropical, 8
- 1655 shallow water model equations, 24
- 1656 Stokes drag, 23
- 1657 streamfunction, 49
- 1658 Sverdrup q balance, 52
- 1659 Sverdrup relation
  - 1660 eastern boundary effect, 79
  - 1661 range of validity, 9
  - 1662 thickness balance, 64
- 1663 Sverdrup transport, 8
- 1664 streamfunction, 50
  
- 1665 thermocline, 1
  
- 1666 western boundary current, 54
  - 1667 width, 55
- 1668 western intensification, 7
- 1669 wind stress, 20
  - 1670 seasonality, 66
  
- 1671 zonal boundary region
  
- 1672 q balance, 56
- 1673 width, 57